What Information on Volatile Organic Compounds Can Be Obtained from the Data of a Single Measurement Site Through the Use of Artificial Intelligence?

Svetlana Stanišić, Mirjana Perišić, Gordana Jovanović, Dimitrije Maletić, Dušan Vudragović, Ana Vranić, and Andreja Stojić

Abstract Increasing air pollutant concentrations over the last few decades have been a focus of contemporary scientific research due to adverse effects on public health, the environment and climate change. In this chapter, we used an innovative integrated methodology for spatio-temporal characterization of sources and concentration forecasts of toxic, mutagenic and carcinogenic representatives of volatile organic species—benzene, toluene, ethylbenzene and xylene, commonly referred to as BTEX. The methodology is based on receptor-oriented air circulation modeling and artificial intelligence implemented through machine learning and explainable artificial intelligence methods. The study covered two years of data obtained from a single monitoring station located at 54a Despota Stefana Boulevard (44°49’68” N, 20°28’04” E). This station was selected from the local and state network for air quality monitoring in the territory of Belgrade. The receptor-oriented modeling was effective for classifying sources of BTEX and the assessment of BTEX concentra-

S. Stanišić (✉)
Environment and Sustainable Development, Singidunum University, Belgrade, Serbia
e-mail: sstanisic@singidunum.ac.rs

M. Perišić · G. Jovanović · D. Maletić · D. Vudragović · A. Vranić · A. Stojić
Institute of Physics Belgrade, National Institute of the Republic of Serbia, Environment and Sustainable Development, Singidunum University, Belgrade, Serbia
e-mail: mirjana.perisic@ipb.ac.rs

G. Jovanović
e-mail: gordana.vukovic@ipb.ac.rs

D. Maletić
e-mail: dimitrije.maletic@ipb.ac.rs

D. Vudragović
e-mail: dusan.vudragovic@ipb.ac.rs

A. Vranić
e-mail: ana.vranic@ipb.ac.rs

A. Stojić
e-mail: andreja.stojic@ipb.ac.rs

E. Pap (ed.), *Artificial Intelligence: Theory and Applications*,
Studies in Computational Intelligence 973,
https://doi.org/10.1007/978-3-030-72711-6_12

tions in the Belgrade urban area surrounding the receptor site that was not regularly monitored. The correlations and ratios between BTEX compounds were used for estimating their interrelationships and presence in the air, which contributed to the identification of their origin. Also, this study evaluated the possibilities of BTEX spatio-temporal forecasts based on the integrated methodology. For this purpose, XGBoost was efficient at forecasting BTEX levels, with estimated errors (6–15%) significantly below the uncertainty obtained by conventional models for the evaluation of average annual pollutant concentrations. The results suggest that temperature, wind speed and wind direction represented the main parameters which explain the spatio-temporal distribution of BTEX, while the impact of other factors showed significant variations depending on the locations of the receptor and the compound.

Keywords BTEX · Volatile organic compounds · Machine learning · Explainable artificial intelligence (xai) · XGBoost

1 Introduction

Growing urban populations, economic development, and transport have a significant impact on environmental pollution. Air pollution constitutes a major underestimated cause of non-communicable diseases, being responsible for 19% of all cardiovascular deaths and 23% of lung cancer deaths globally [19]. Around 91% of the world's population lives in areas where air pollution levels exceed the World Health Organization's recommended values [43]. People often perceive air pollution as an issue that affects people living in middle- and low- income countries or people living in megacities. However, it has been estimated that out of 8.8 million global deaths associated with air pollution in 2015, 8% were citizens of high-income countries, mostly those living in small urban areas where the topography and climate contribute to high air pollutant concentrations [3, 7]. Holgate [17] emphasizes that annually, 40,000 excess deaths in the UK can be attributed to low air quality. Society might be much more aware of this issue if the mortality was a result of drinking polluted water. Air pollution in households has decreased since the 1990's as new fuels such as petroleum gas and renewable sources of energy have replaced biomass. In developing countries, residential combustion of solid fuels for cooking and heating remains a significant source of air pollution and a major concern due to its detrimental health effects, particularly in rural areas [9]. In contrast, in developed countries, indoor air pollution is less important because adverse health effects are associated with exposure to outdoor pollutant concentrations that have decreased over previous decades. However, it has also been estimated that the rapid expansion of metropolises, industrial production, increasing pesticide use, toxic chemicals and motor vehicles will offset the effects of air pollution mitigation measures [13].

Among the air pollutants that are of interest for current and future research due to their detrimental effects on both human health and the environment are volatile organic compounds (VOCs). VOCs are a heterogeneous group of organic species with boiling points $<250\,^{\circ}C$. Their representatives are benzene and its alkylated derivatives toluene, ethylbenzene and xylene, commonly referred to as BTEX. Over the last few decades in developed countries, reducing BTEX levels has been a challenge [26]. This is due to their abundance, their numerous emission sources, their complex atmospheric chemistry, insufficient funds for the establishment and maintenance of monitoring networks, and the fact that abatement programs might have negative impacts on economic output because they are among the most abundantly produced compounds worldwide. They are used as feedstock for several materials and products upon which modern society has become dependent. These compounds are naturally found in crude oil, while in urban and suburban areas they originate from traffic emissions, commercial and industrial uses of petroleum, gasoline, adhesives, coatings, degreasers, solvents, detergents, explosives, pesticides, resins, ink, paints, and varnishes [30, 33, 35]. With the exception of m-/p-xylene, concentrations of BTEX were mostly reported to be higher in indoor air than outdoor air [4].

The health effects of BTEX are wide-ranging. Studies have shown that BTEX can be found in cord blood and the blood of children and adults, particularly adults that are occupationally exposed [18]. Research has shown that long-term exposure to high benzene concentrations increases the risk of developing malignant blood disorders, while long-term exposure to high toluene concentrations causes renal tubular acidosis [42]. Some studies have shown that after benzene concentrations in industrial and urban areas are reduced, lifetime cancer risk decreases by one order of magnitude [20]. In addition, exposure to ambient levels of BTEX, which in many cases were orders of magnitude below the reference concentrations, can be dangerous. This is particularly true during the susceptibility period when exposure can lead to the disruption of endocrine signaling (which is essential for the growth and development), immune responses, reproduction, cardiovascular function and aging. Therefore, populations in highly industrialized areas, the socioeconomically deprived, as well as children, pregnant women and elderly people, appear to be more susceptible to pollution-related morbidity and mortality [5, 32]. While traffic emissions are known to be the main source of outdoor BTEX, converting to alternative renewable energy sources will not reduce demand for consumer products, and the replacement of benzene with safer alternatives, such as toluene and xylene, might ultimately be a poor solution once long-term toluene and xylene exposure scenarios are considered [4]. According to a United States Environmental Protection Agency [40] report, ethylbenzene is sixth on a list of the top 20 chemicals used in children's products, primarily food packaging, toys, sport equipment, arts, crafts and hobby materials. Toluene, on the other hand, is the seventh most used chemical in consumer products, primarily fuels, paints, and coatings. Although toluene and xylenes are less harmful than benzene, it should be kept in mind that the products of photochemical reactions in which BTEX are involved often have more harmful effects on human health than their precursors [14]. It should be also mentioned that limited ventilation in closed premises can often be the reason why indoor BTEX levels are higher than outdoor levels [29].

Apart from their impacts on human health, BTEX and other VOCs are associated with increases in the oxidation capacity of the atmosphere, as well as with the generation of secondary pollutants, such as tropospheric ozone, polycyclic aromatic hydrocarbons and secondary aerosol through photochemical reactions [8, 36]. As regards the impact on global warming, not only do volatile species directly and indirectly contribute to climate change, but their emission and fate are expected to be influenced and increased by global warming.

Despite vast changes in the development and integration of different approaches in the field of environmental science, spatio-temporal air pollution modeling remains a challenge. Two main approaches are typically utilized to forecast air quality and to identify the factors that govern the concentrations of certain pollutants. The first approach relies on atmospheric diffusion models, while the second refers to statistical models that capture the essential relationships between the variables [24]. Multidimensionality and the size of data sets, as well as the complexity of air pollutant processes and interactions, set requirements that exceed the capabilities of conventional statistical methods. For this reason, machine learning (ML) methods and explainable artificial intelligence (XAI), subfields of artificial intelligence (AI) that enable automatized big data analysis and the development of learning algorithms, have been introduced into environmental science research. In this paper, we used an innovative and integrated methodology based on artificial intelligence and implemented through ML ana XAI methods for the modeling of spatio-temporal air pollution and the characterization of BTEX sources in a wider region surrounding the receptor site that was not covered by regular monitoring. The obtained BTEX correlations and ratios were used for estimating the interrelationships between the species in the air, while XGBoost was utilized for efficient spatio-temporal BTEX forecasting. The present paper is an extended version of the study presented at the International Scientific Conference on Information Technology and Data Related Research (Sinteza 2020), Singidunum University [38].

2 Materials and Methods

Nowadays, there are a large number of libraries implemented in different programming languages (R, Python, JS) that deal with interactive display (plotly, leaflet) and spatial data analysis. In addition to various spatial autocorrelation possibilities, the analysis of spatial data patterns, the interpolation of data by statistical methods such as Kriging, Spline or Inverse Distance Weighting, and machine learning methods such as Random Forests are increasingly used. Furthermore, spatial distributions of air pollutant sources can be estimated using general and local hybrid receptors, as well as by analyzing clustered data [9, 33, 34].

Significant improvements to the general hybrid receptor modeling approach have been made in recent decades. Receptor-oriented methods, based on conditional probability and analyzing the residence time of pollutants in an area, have become widely accepted both for studying the dynamic processes and circulation patterns of pollutants in the atmosphere and for investigating the spatial distribution of potential emission sources and their impact on the receptor site without relying on an emission inventory.

The identification of potential emission sources at a local level, as well as their contribution to the measured concentrations of pollutants at the receptor site, can be determined by models analogous to the general hybrid receptor model such as the Potential Source Contribution Function (PSCF), Concentration-Weighted Trajectories (CWT), sQTBA (Simplified Quantitative Transport Bias Analysis) and RTWC (Residence Time Weighted Concentration). The general models, which are based on the analysis of trajectory end points, can be improved by using local wind parameters. This way it is possible to determine pollution circulation patterns very accurately in the area around a given measuring point. A local three-dimensional hybrid receptor model similar to the 3D CWT model was developed for the purposes of this paper [34]. The study involved two-years of regular measurements of BTEX, suspended particles, inorganic gaseous oxides, and meteorological parameters within the Belgrade City Institute for Public Health's automatic monitoring network (44°49'68" N, 20°28'04" E).

Machine learning is an area of artificial intelligence that involves the development of algorithms that can learn based on input data and can thus be trained to predict value variations. Machine learning algorithms are based on the extraction of patterns and the selection of specific attributes from a large number of data, while eliminating irrelevant information. Through identifying most important prediction attributes, machine learning methods acquire knowledge and define the substantial relationships that exist between input and output parameters by focusing on the aspect of the data that is the most useful for efficient forecasting.

Forecasting the concentration dynamics of BTEX in the air was done using the Xtreme Gradient Boosting (XGBoost) method [11], with meteorological data used as predictors. XGBoost is a general-purpose ensemble method of supervised machine learning which combines the results of many decision trees and achieves high accuracy in a wide range of practical applications. It usually outperforms support vector machines, random forests, and deep learning neural networks [31]. The main advantage of the XGBoost method is its obtainment of more precise predictions than those provided by single constitutive decision algorithms. XGBoost is based on a boosting technique that sequentially defines a series of decision trees for classifying input data into two or more attribute-defined classes. Each consecutive decision tree is trained through iterations, taking into account the previously registered classification errors. The datasets from each of the grid cells used for spatio-temporal BTEX forecasting was split into training (80%) and validation (20%) sets. Hyperparameter tuning was implemented using a brute-force grid search and a 10-fold stratified cross-validation. The best performing hyperparameter values were used in the final model.

Methods based on decision trees, such as Gradient Boosting and Random Forests, have been shown to provide inconsistent attribute contributions. This has led to the development of SHAP (SHapley Additive exPlanation), a method that estimates the contribution of each instance of an attribute, which enables interpretation of the model's outputs [15, 21, 31]. To explain the contribution of each feature to the individual XGBoost prediction, the SHAP method was utilized [21]. It is based on coalitional game theory and provides a distribution of each prediction among the features represented as additive attributions. In this study, we used Python SHAP implementation (SHAP Python package). The captured importance of a feature is visually presented as a SHAP summary plot.

3 Results and Discussion

Previous studies have demonstrated strong gradients and pronounced intra-urban spatial variability of pollutant levels. This depends on traffic density, street configuration and prevailing wind direction [41]. In addition to this, Ning et al. [27] emphasized the importance of terrain complexity for air quality because topographic features can, to a certain extent, limit pollutant dispersion under different weather conditions. The results indicate that BTEX concentrations were significantly higher in areas with dense traffic, in the vicinity of busy streets and intersections, where traffic emission sources have a high impact, where local topography limits natural ventilation and vertical dispersion of pollution, and in areas with narrow streets lined by tall buildings and trees.

3.1 BTEX Levels Surrounding the Receptor Site

Benzene concentrations were estimated to range from 1.2 to 2.6 $\mu g\ m^{-3}$, with an average level of 2.6 $\mu g\ m^{-3}$. In a few locations, estimates of pollutant concentrations were extremely high, exceeding the recommended limit of 5 $\mu g\ m^{-3}$. Extreme benzene levels in areas distant from the receptor site should be taken with caution. This is due to a relatively small number of events and therefore limited data produces the calculated values. It has been estimated that the area surrounding the receptor site was mostly influenced by traffic emissions. Other studies have reported that similar average benzene concentrations are sometimes discovered in urban areas where traffic is the predominant source of pollutant emissions [2]. Concentrations of toluene were estimated to range from 0.9 to 8.9 $\mu g\ m^{-3}$ with an average value of 8.7 $\mu g\ m^{-3}$, while the average m/p-xylene concentrations were assessed to be several times higher (8.4 $\mu g\ m^{-3}$) than the concentrations of o-xylene (1.8 $\mu g\ m^{-3}$). Concentrations of ethylbenzene were estimated to range from 0.2 to 2.1 $\mu g\ m^{-3}$ with an average value of 1.8 $\mu g\ m^{-3}$. As predicted, TEX levels were highest in the city center and the north of the city. The assessed TEX levels were also consistent with the reported values for outdoor TEX concentrations in various studies published over the last two decades [1, 10, 16, 23, 25], with somewhat lower levels of toluene than typically expected in an urban area.

3.2 Seasonal and Daily BTEX Variations

While the intensity of BTEX emission sources tend to be higher in winter, evaporations in warmer parts of the year make an important contribution to total pollutant concentrations. On the other hand, the stability of atmospheric conditions and decrease in chemical reactivity of BTEX in winter results in longer retention in ambient air [29]. Furthermore, BTEX are known to exhibit variations on a daily basis. For instance, a previous study that contained a risk assessment of an accidental benzene release in an urban area using an atmospheric dispersion model, showed that benzene spreads over a much larger area during the nighttime due to a stable boundary layer. In contrast, enhanced vertical mixing results in limited dispersion of the pollutant over the study area during the daytime [39]. Similar results were obtained in our study.

3.3 BTEX Forecasting Based on Meteorological Variables as Predictors

As can be seen in Figs. 1 and 2, high correlation coefficients between predicted and observed values (>0,80) were obtained for most of the analyzed data, it can therefore be concluded that XGBoost was a successful and efficient method for forecasting air pollution in an urban area. It should be emphasized that the estimated method errors (6–15%) were significantly lower than the uncertainty (50%) which is required for the evaluation of average annual pollutant concentrations using conventional modeling.

It should be also emphasized that due to the relatively short atmospheric lifetimes of BTEX, the area that can be affected by BTEX emissions is approx. 15–20 km [29], but the consistency of meteorological conditions significantly affects the extent of volatile pollutant dispersion.

The results of this study suggest that low temperatures and weak to moderate wind represent the main parameters which govern the spatio-temporal distribution of benzene in a majority of locations. The impacts of other factors display significant variation depending on the characteristics of the receptor's location (Fig. 1). Namely, one can note that the horizontal axis marked with wind speed is the longest, which means that benzene concentrations were mostly affected by this parameter. Each axis is composed of a series of points that represent the measured values of the predictor. As can be seen in the example for wind speed, extremely high wind speeds, represented by points located on the far right of the axis, have relatively little impact on benzene concentrations in the air. This suggests that benzene concentrations were mostly influenced by weak to moderate wind, which further suggests that emission sources located in the vicinity of the selected receptor site have the highest impact.

Furthermore, the importance of a certain wind direction for pollutant level prediction is related to the position of the emission source which affects the receptor location the most. Namely, in cases where a single pollutant emission source has a

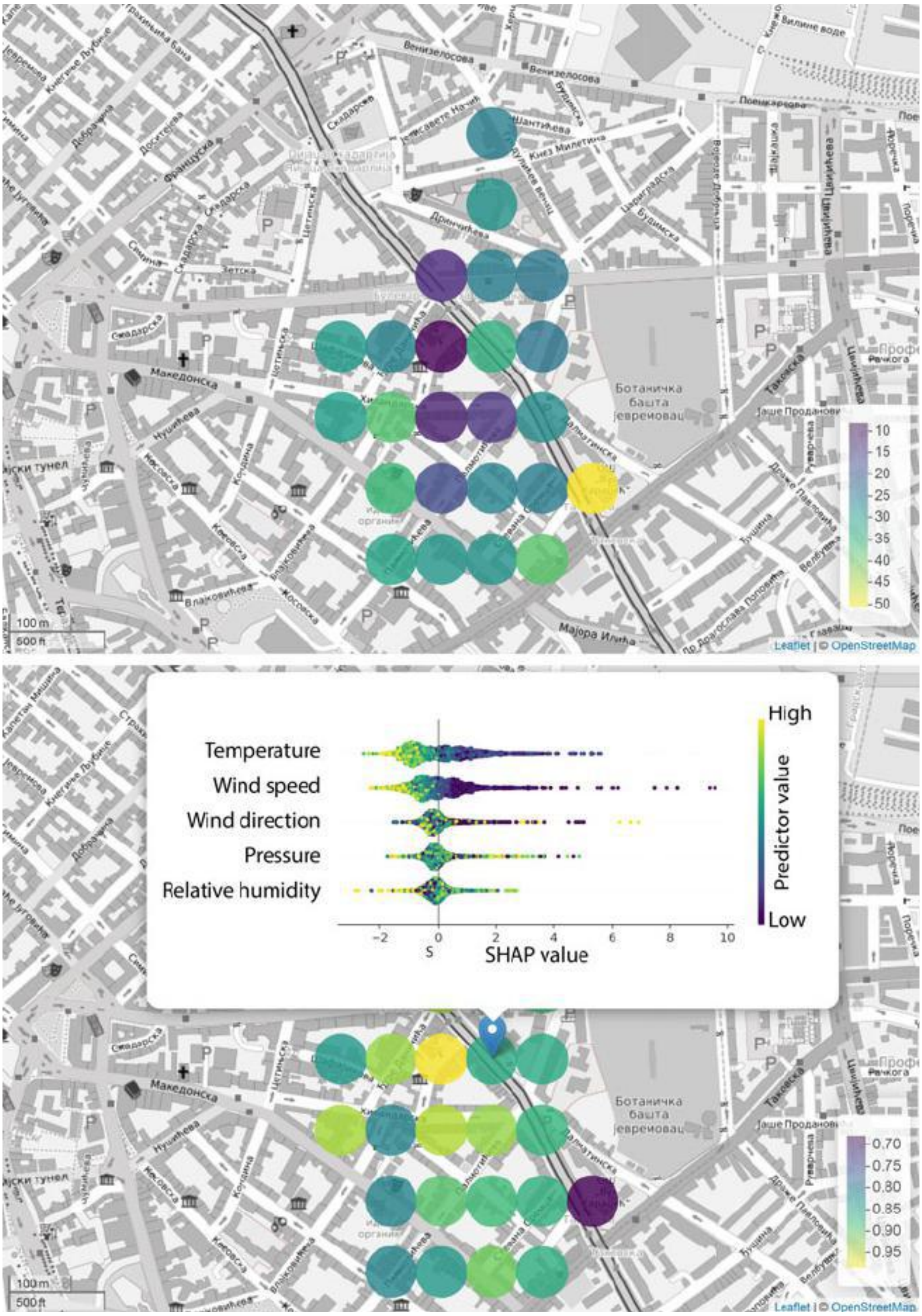

Fig. 1 Benzene forecast based on meteorological parameters—a relative error [%] (top) and SHAP values and predicted/observed correlation coefficients (bottom)

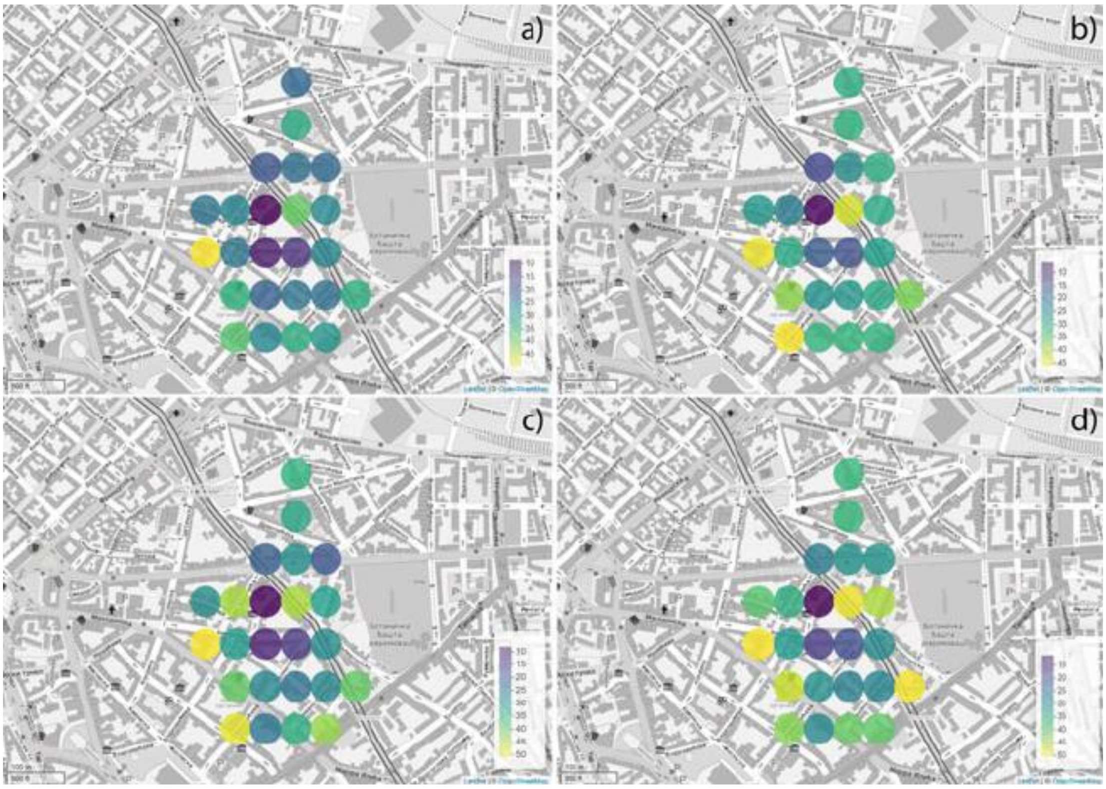

Fig. 2 Toluene (**a**), m,p-xylene (**b**), o-xylene (**c**), and ethylbenzene (**d**) relative error [%] forecasts based on meteorological parameters

major effect on the receptor area, the importance of wind direction as a predicting factor is particularly accentuated. Additionally, the importance of wind direction is evident in situations where tall buildings and trees along the roadside form a corridor that either hinders or assists polluted air masses from the surrounding emission sources, which was the case in this study as well. The importance of relative humidity as predictor for benzene concentrations was predicted to be high in the event of extreme benzene levels. This is because benzene and TEX are partially water-soluble compounds, which suggests that both high and low levels of relative humidity can impact their ambient air levels [28].

The presented figures displaying TEX distributions can be interpreted in the following manner. Atmospheric pressure and wind parameters appear to be the major predictors of TEX behavior in general. The impacts of air temperature and pressure were significantly lower for forecasting toluene levels (Fig. 2) than for forecasting benzene levels, which can be explained by the fact that benzene evaporates at significantly lower temperatures than toluene.

The correlations between the observed and forecasted concentrations of benzene ranged from 0.70 to 0.95, but most often ranged from 0.80 to 0.85. At the location where the correlation was the highest (0.95), benzene concentrations were forecasted with a relative error of 8%, while the most influential SHAP-revealed factor was wind direction. The correlations between the observed and forecasted concentrations of toluene ranged from 0.65 to 0.95, but mostly around 0.80.

At the location where the correlation was the highest (0.95), toluene concentrations were forecasted with a relative error of 9%, while the most influential SHAP-revealed factors were wind speed and direction. The correlations between the observed and forecasted concentrations of m/p-xylenes ranged from 0.65 to 0.95, but averaged approximately 0.75. At the locations where the correlations were highest (0.97 and 0.98), the concentrations of m/p-xylenes were forecasted with relative errors of 6% and 15% respectively, while the most influential SHAP-revealed factors were wind speed, direction, and air pressure. The correlation between the observed and forecasted concentrations of o-xylene ranged from 0.60 to 0.90, with an average of approximately 0.85. At the locations where the correlations were the highest (0.94 and 0.95), o-xylene concentrations were forecasted with relative errors of 12% and 8% respectively, while the most influential SHAP-revealed factors were wind direction and air pressure. The correlations between the observed and forecasted concentrations of ethylbenzene ranged from 0.60 to 0.95, but averaged approximately 0.80. At the location where the correlation was the highest (0.95), ethylbenzene concentrations were forecasted with a relative error of 11%, while the most influential SHAP-revealed factors were wind speed, wind direction, and air pressure.

Although the results demonstrate the capacity of an innovative methodology to identify the importance of certain meteorological factors as predictors of air pollutant concentrations, the fact that variations of meteorological parameters cause changes in other related parameters makes it difficult to distinguish their actual impact on air pollution phenomena. Thus, the impact of meteorological factors should not be observed as the isolated effect of a single parameter and its variations, but as the effect of a certain type of weather. For instance, Liao et al. [22] identified ten typical air circulation types within one of the most polluted areas of China and explored how their synergetic relationship with topography affected the local air quality.

3.4 The Importance of Other Pollutants as Predictors for BTEX Levels

Apart from meteorological parameters, other analyzed factors can be considered important for predicting BTEX concentrations. Namely, for forecasting benzene levels, high CO concentrations appear to be the most important (Fig. 3), with the importance of the other predictors stated here in decreasing order: toluene> ethylbenzene> m/p-xyneles> o-xylene> $PM_{10} > NO_x > NO_2 >$ NO> SO_2.

As regards forecasting toluene levels, high m/p-xylenes, o-xylene and CO concentrations appear be the most important, with the importance of the other predictors stated here in decreasing order: ethylbenzene> benzene> $PM_{10} >$ NO> $NO_x > SO_2 > NO_2$. As regards forecasting m/p-xylenes levels, high toluene, o-xylene, ethylbenzene and CO concentrations appear to be the most important, with the importance of the other predictors stated here in decreasing order: benzene> $NO_2 > NO_x > PM_{10} > SO_2 >$ NO. As regards forecasting o-xylene levels, high m/p-

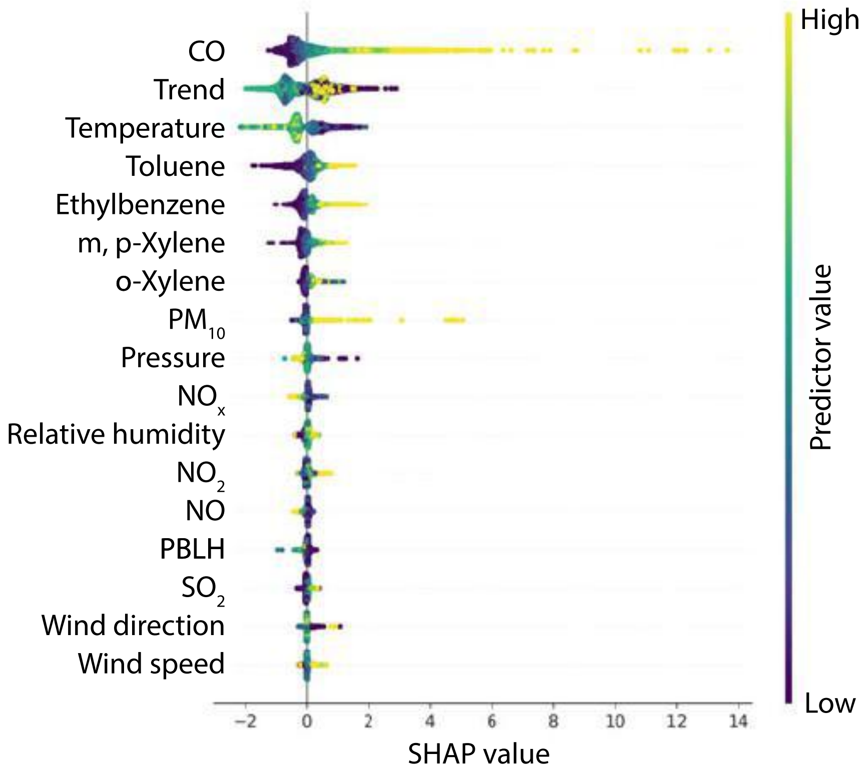

Fig. 3 SHAP summary plot for benzene

xylenes, toluene, ethylbenzene and NO concentrations appear to be the most important, with the importance of the other predictors stated here in decreasing order: NO_x > benzene> CO> PM_{10} > NO_2 > SO_2. As regards forecasting ethylbenzene levels, high m/p-xylenes, o-xylene and benzene concentrations appear to be the most important, with the importance of the other predictors stated here in decreasing order: toluene> NO_2 > SO_2 > CO> PM_{10} > NO> NO_x.

3.5 *The Interdependence of BTEX Level Predictors*

As part of forecasting pollutant concentrations, an examination of the interdependence between individual predicting factors and their combined effect on BTEX concentrations in the air was performed. As shown in the Fig. 4, during the cold part of the year, when temperatures were below 14 °C, concentrations of benzene are better predicted by toluene levels. Conversely, on days when the temperature exceeded 14 °C, benzene and toluene didn't share the same emission sources. Furthermore, during the cold part of the year, benzene concentrations are either significantly higher or lower than average, depending on whether the location is affected by the burning of fossil fuels for heating or not, while during the warmer part of the year benzene concentrations at different locations tended to be more uniform. This is because higher temperatures cause benzene to evaporate at all locations.

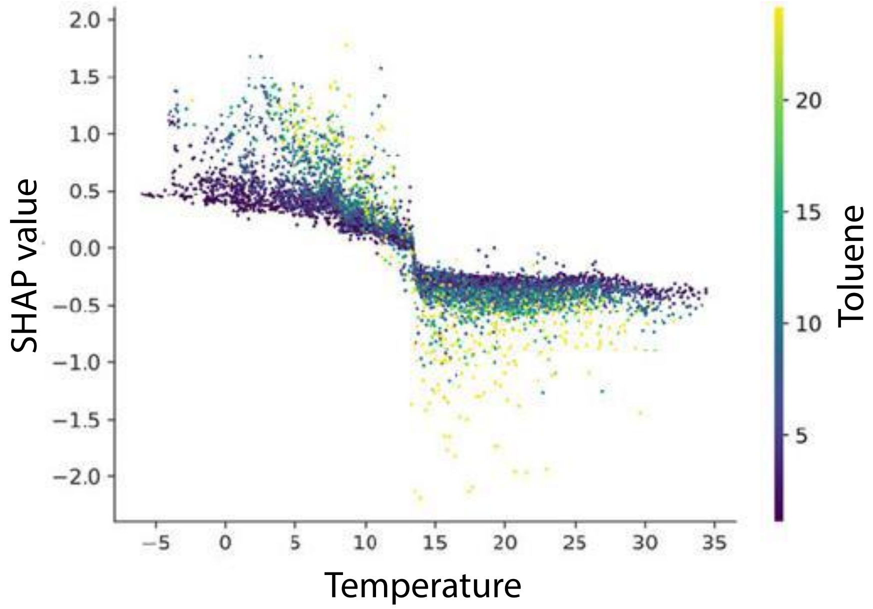

Fig. 4 Benzene SHAP dependency on temperature and toluene

In addition to temperature-toluene interactions, the results suggest that the concentrations of benzene in the ambient air depended on interactions between temperature and carbon monoxide as well. While the effects of interactions between ethylbenzene-m/p-xylenes, ethylbenzene-toluene, ethylbenzene-carbon monoxide and m/p-xylene-carbon monoxide were found to be of minor importance as regards shaping benzene concentrations (Fig. 5).

3.6 Pollutant Correlations and BTEX Origin

The results show moderate correlations between toluene and NO_x and CO concentrations throughout the city. The locations with toluene-NO_x correlations exceeding 0.7 are considered to be affected by burning-related emissions and not by toluene evaporations (Fig. 6).

Relatively high correlations between benzene and carbon monoxide were registered throughout the city, with the notable exception of the south (Fig. 7). The correlations between benzene and SO_2, NO_x and PM_{10} were lower in the eastern, and higher in the western, part of the urban region. These results suggest that benzene in the eastern area of the city is associated with evaporations and emissions from the petrochemical industry such as the Pančevo Oil refinery and the Petrohemija chemical plant. Furthermore, high correlations ($r > 0{,}70$) between benzene and inorganic oxides in the western region of the city may suggest that traffic emissions, as well as remote air pollution sources such as TPP Nikola Tesla A and B in Obrenovac, have a detrimental impact (Fig. 7). The significantly lower correlations between benzene and inorganic oxides, that can be considered indicators of combustion processes in

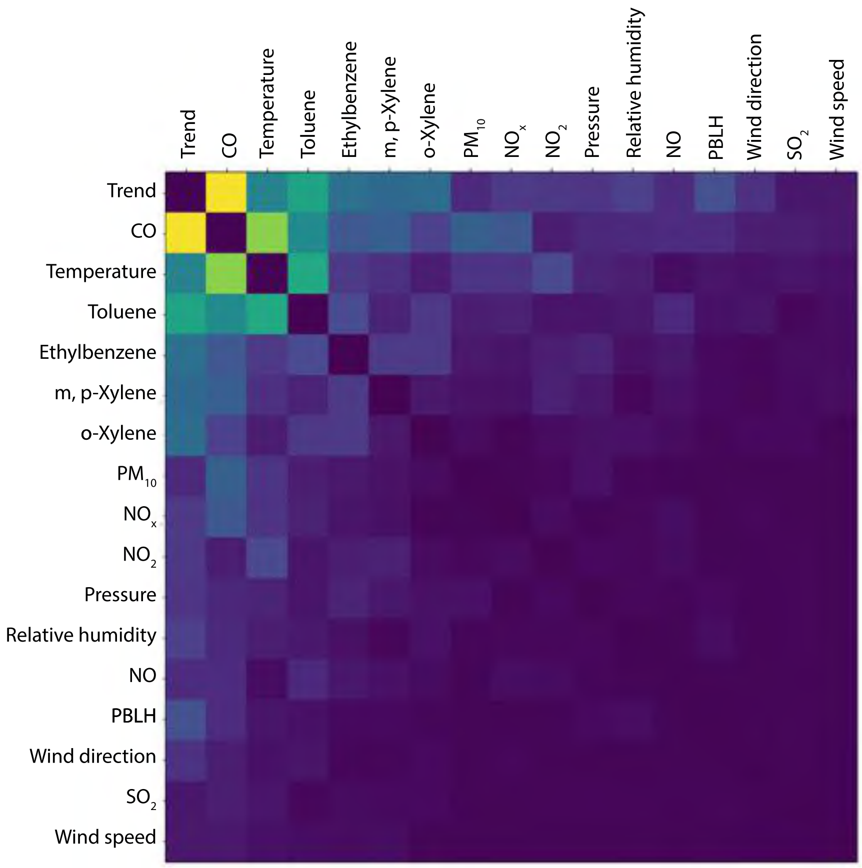

Fig. 5 SHAP interaction plot

the southern part of the city center, probably reflect the impact of gasoline evaporation. This conclusion appears more likely when we take into account that benzene concentrations were assessed to be the lowest in the southern area.

The m/p-xylenes exhibited the highest correlations with NO_x, somewhat lower correlations with CO, while the correlations with SO_2 and PM_{10} tended to be significantly lower throughout the city. A similar calculation was obtained for o-xylene and ethylbenzene.

3.7 BTEX Ratios

The benzene-to-toluene (B/T) ratio is often used as an index for identifying emission sources, while xylenes-to-benzene (X/B) and ethylbenzene-to-benzene (E/B) ratios are generally applied as indices of photochemical reactivity [12]. According to the literature, a B/T ratio below 0.5 suggests that vehicle emissions are the predominant source of BTEX, while X/B and E/B ratios below 1 suggest that sampled air masses are photochemically aged. As the results show, the B/T ratios were approx. 0.3, while the X/B and E/B ratios ranged from 0.7 to 4 with lower ratio values calculated for

Fig. 6 Toluene and NO_x correlations

the central area of the city where narrow streets and tall buildings restrict pollutant dispersion and support the photochemical aging of the emissions. Buczynska et al. [6] showed that B/T ratios ranging from 0.22 to 0.26 for locations that were affected by traffic emissions, while the authors mentioned that ratios below 0.1 reported in previous research suggest additional emission sources of toluene, like industrial emissions, that contribute to high values. It could be concluded from the results that in most locations, BTEX concentrations in ambient air are a result of recent emissions, while traffic emissions might be the major contributor to BTEX concentrations in the analyzed area. Furthermore, BTEX have a similar chemical structure, but there is a difference in the reactivity of these typically unreactive compounds. Namely, benzene is more stable and has a longer atmospheric lifetime [14] which can significantly modify the starting BTEX concentration ratios, and thus another possibility indicated by the B/T ratio is related to aging air masses. Namely, after being emitted from a common source, toluene is about 5 times more reactive than benzene, which is why a high B/T ratio is an indicator of aged air masses. The results suggest that the examined area can be divided diagonally into two segments:

- The north-western and north-eastern area which covers the old city center where the B/T ratio is relatively high. The north-western part is subject to emissions from the industrial area, which includes the petrochemical industry comprised of the Pančevo Oil refinery and the Petrohemija chemical plant. The north-western part is subject to the retention of aged air masses in narrow streets which form an urban

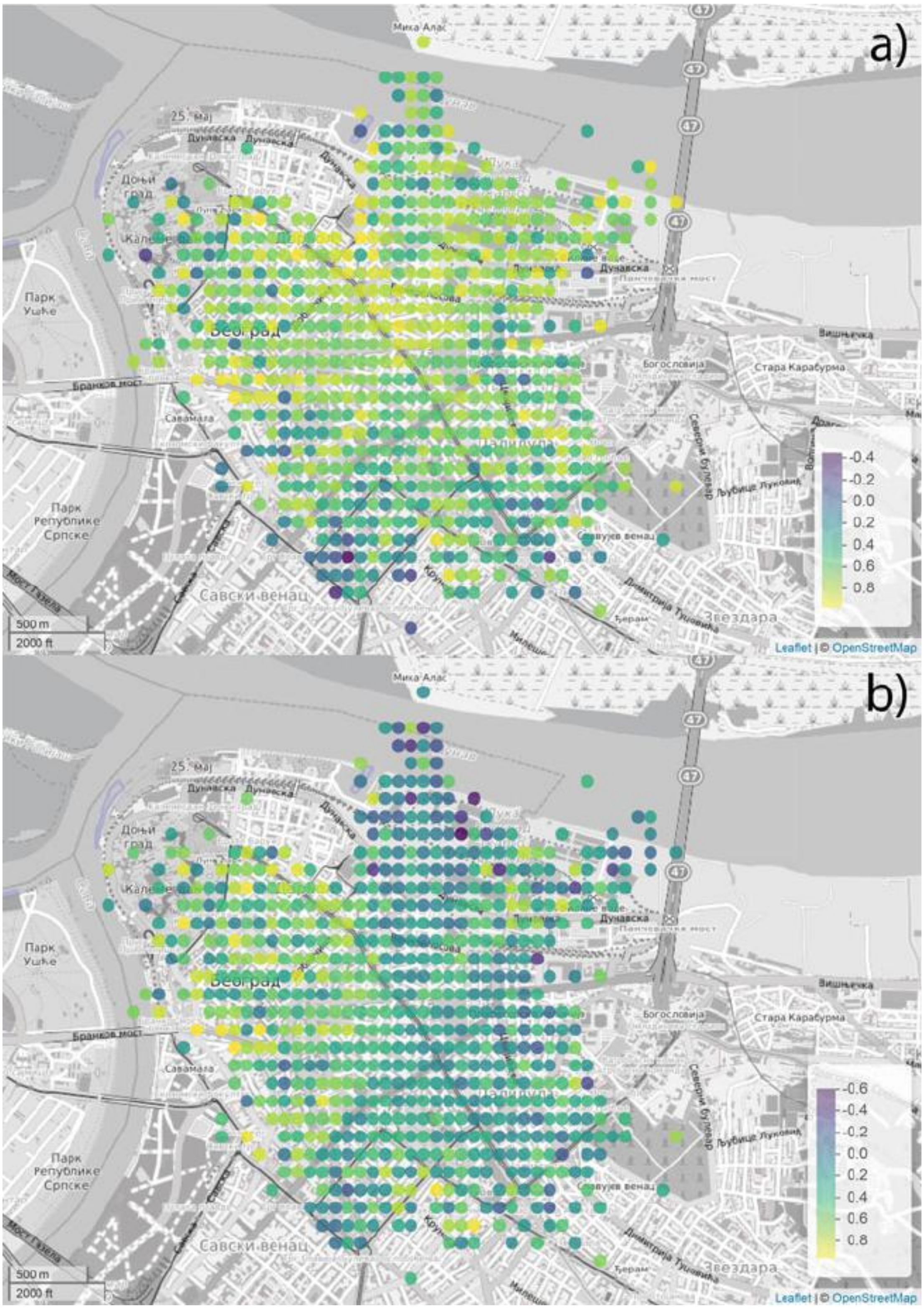

Fig. 7 Benzene correlation coefficients with CO (**a**) and NO_x (**b**)

canyon. The south-western part is subject to the influence of aged air masses from Obrenovac.

- The southern area, covers a large area of the city which displays a relatively low B/T ratio. This indicates the predominant effect of traffic emissions.

Although diagnostic concentration ratios are a commonly used tool for identifying and distinguishing emission sources, they should be used with caution since the calculated values often exhibit seasonal variations and can be susceptible to distortions from a number of environmental factors [37].

4 Conclusions

Identifying pollutant emission sources, investigating the temporal dynamics and spatial distributions of pollutant concentrations, and estimating the contribution of certain emission sources to local air quality are of great importance. They can help to develop an essential understanding of the impact key factors have on processes within natural and anthropogenic ecosystems and their resilience, but are also crucial for defining strategies aimed at improving air quality, resolving environmental issues, and improving human health. While soil and water pollution is mainly of local significance, air pollution can affect very remote areas given meteorological conditions that enable the transportation of pollutants. In addition to this, a number of other factors can contribute to the final effect of meteorological conditions on air pollutant concentrations, including the distribution of pollutant emission sources, local topography, street geometry and the distribution of all elements and surfaces that can be of significance for the air flow regime, pollutant dispersion conditions, their transport pathways and thus, the spatio-temporal variability of their levels. The multidimensionality of modern data, the scope of time series, as well as the complexity of processes and interactions in which air pollutants participate, are too demanding for conventional statistical methods. For this reason, recent decades have seen research conducted to find alternative methods for data analysis. One of the approaches that has proven effective in many professional and scientific fields, including environmental protection, is machine learning which provides the tools for automated analysis of a large amount of data.

As can be concluded, we have demonstrated the use of an efficient methodology for spatio-temporal BTEX concentration modeling in the Belgrade area, based on receptor-oriented air circulation modeling and artificial intelligence implemented through machine learning and explainable artificial intelligence methods. The estimated method errors ranged from 6 to 15%, which is significantly lower than the required uncertainty for conventional models. The presented methodology has the potential to provide a basis for the establishment of a unique and sustainable system for identifying sources of air pollution and enhanced air pollution data coverage that does not require additional investments in monitoring equipment. In the long term, the results of such an approach would provide a solid basis for establishing a sustainable system for improving the management and control of air pollution. As the results show, temperature, pressure, wind speed and wind direction were the main parameters which governed the spatio-temporal distribution of BTEX, while the impact of other factors showed significant variations depending on the characteristics of receptor's location and the compound. In addition, spatial correlations and ratios between different air pollutant concentrations were considered for determining their origin in all the locations covered by our analysis. All examples illustrate how the application of SHAP and other supplemental methods can provide a systematic insight into the impact of emission sources and environmental factors on the presence of BTEX in the air.

Acknowledgements Funding: The authors acknowledge funding provided by the Institute of Physics Belgrade, through a grant by the Ministry of Education, Science and Technological Development of the Republic of Serbia, the Science Fund of the Republic of Serbia #GRANT No. 6524105, AI - ATLAS, and Green Fund of the Ministry of Environmental Protection of the Republic of Serbia (No. 401-00-1219/2018-05).

References

1. Abd Hamid, H., Latif, M.T., Nadzir, M.S.M., Uning, R., Khan, M.F., Kannan, N.: Ambient BTEX levels over urban, suburban and rural areas in Malaysia. Air Qual. Atmos. Health **12**, 341–351 (2019)
2. Baltrėnas, P., Baltrėnaitė, E., Šerevičienė, V., Pereira, P.: Atmospheric BTEX concentrations in the vicinity of the crude oil refinery of the Baltic region. Environ. Monit. Assess. **182**, 115–127 (2011)
3. Behrens, D.A., Koland, O., Leopold-Wildburger, U.: Why local air pollution is more than daily peaks: modelling policies in a city in order to avoid premature deaths. Cent. Eur. J. Oper. Res. **26**, 265–286 (2018)
4. Bolden, A.L., Kwiatkowski, C.F., Colborn, T.: New look at BTEX: are ambient levels a problem? Environ. Sci. Technol. **49**, 5261–5276 (2015)
5. Bose, S., Diette, G.B.: Health disparities related to environmental air quality. In: Health Disparities in Respiratory Medicine, pp. 41–58. Humana Press, Cham (2016)
6. Buczynska, A.J., Krata, A., Stranger, M., Godoi, A.F.L., Kontozova-Deutsch, V., Bencs, L., Naveau, I., Roekens, E., Van Grieken, R.: Atmospheric BTEX-concentrations in an area with intensive street traffic. Atmos. Environ. **43**, 311–318 (2009)
7. Burnett, R., Chen, H., Szyszkowicz, M., Fann, N., Hubbell, B., Pope, C.A., Apte, J.S., Brauer, M., Cohen, A., Weichenthal, S., Coggins, J.: Global estimates of mortality associated with long-term exposure to outdoor fine particulate matter. PNAS USA **115**, 9592–9597 (2018)
8. Campbell, P., Zhang, Y., Yan, F., Lu, Z., Streets, D.: Impacts of transportation sector emissions on future US air quality in a changing climate. Part II: Air quality projections and the interplay between emissions and climate change. Environ. Pollut. **238**, 918–930 (2018)
9. Carter, E., Archer-Nicholls, S., Ni, K., Lai, A.M., Niu, H., Secrest, M.H., Sauer, S.M., Schauer, J.J., Ezzati, M., Wiedinmyer, C., Yang, X.: Seasonal and diurnal air pollution from residential cooking and space heating in the Eastern Tibetan Plateau. Environ. Sci. Technol. **50**, 8353–8361 (2016)
10. Cerón Bretón, J.G., Cerón Bretón, R.M., Martínez Morales, S., Kahl, J.D., Guarnaccia, C., Lara Severino, R.D.C., Rangel Marrón, M., Ramírez Lara, E., Espinosa Fuentes, M.D.L.L., Uc Chi, M.P., Sánchez, G.L.: Health risk assessment of the levels of BTEX in ambient air of one

urban site located in Leon, Guanajuato, Mexico during two climatic seasons. Atmosphere **11**, 165 (2020)
11. Chen, T., Guestrin, C.: Xgboost: a scalable tree boosting system. In: Proceedings of the 22nd ACM SIGKDD International Conference on Knowledge Discovery and Data Mining, pp. 785–794 (2016)
12. Dehghani, M., Fazlzadeh, M., Sorooshian, A., Tabatabaee, H.R., Miri, M., Baghani, A.N., Delikhoon, M., Mahvi, A.H., Rashidi, M.: Characteristics and health effects of BTEX in a hot spot for urban pollution. Ecotoxicol. Environ. Saf. **155**, 133–143 (2018)
13. Fowler, D., Brimblecombe, P., Burrows, J., Heal, M.R., Grennfelt, P., Stevenson, D.S., Jowett, A., Nemitz, E., Coyle, M., Lui, X., Chang, Y.: A chronology of global air quality. Philos. Trans. R. Soc. A **378**, 20190314 (2020)
14. Gallego, E., Roca, F.X., Guardino, X., Rosell, M.G.: Indoor and outdoor BTX levels in Barcelona city metropolitan area and Catalan rural areas. J. Environ. Sci. **20**, 1063–1069 (2008)
15. García, M.V., Aznarte, J.L.: Shapley additive explanations for NO2 forecasting. Ecol. Inform. **56**, (2020)
16. Hajizadeh, Y., Mokhtari, M., Faraji, M., Mohammadi, A., Nemati, S., Ghanbari, R., Abdolahnejad, A., Fard, R.F., Nikoonahad, A., Jafari, N., Miri, M.: Trends of BTEX in the central urban area of Iran: a preliminary study of photochemical ozone pollution and health risk assessment. Atmos. Pollut. Res. **9**, 220–229 (2018)
17. Holgate, S.T.: Every breath we take: the lifelong impact of air pollution-a call for action. Clin. Med. **17**, 8 (2017)
18. Kirman, C.R., Aylward, L.L., Blount, B.C., Pyatt, D.W., Hays, S.M.: Evaluation of NHANES biomonitoring data for volatile organic chemicals in blood: application of chemical-specific screening criteria. J. Expo. Sci. Environ. Epidemiol. **22**, 24–34 (2012)
19. Landrigan, P.J.: Air pollution and health. Lancet Public Health **2**, e4–e5 (2017)
20. Lerner, J.E.C., Kohajda, T., Aguilar, M.E., Massolo, L.A., Sánchez, E.Y., Porta, A.A., Opitz, P., Wichmann, G., Herbarth, O., Mueller, A.: Improvement of health risk factors after reduction of VOC concentrations in industrial and urban area. Environ. Sci. Pollut. Res. **21**, 9676–9688 (2014)
21. Lundberg S., Lee, S.: A unified approach to interpreting model predictions. In: Advances in Neural Information Processing Systems, pp. 4765–4774 (2017)
22. Liao, Z., Gao, M., Sun, J., Fan, S.: The impact of synoptic circulation on air quality and pollution-related human health in the Yangtze River Delta region. Sci. Total Environ. **607**, 838–846 (2017)
23. Liu, A., Hong, N., Zhu, P., Guan, Y.: Understanding benzene series (BTEX) pollutant load characteristics in the urban environment. Sci. Total Environ. **619**, 938–945 (2018)
24. Ly, H.B., Le, L.M., Phi, L.V., Phan, V.H., Tran, V.Q., Pham, B.T., Le, T.T., Derrible, S.: Development of an AI model to measure traffic air pollution from multisensor and weather data. Sensors **19**, 4941 (2019)
25. Marć, M., Namieśnik, J., Zabiegała, B.: BTEX concentration levels in urban air in the area of the Tri-City agglomeration (Gdansk, Gdynia, Sopot), Poland. Air Qual. Atmos. Health **7**, 489–504 (2014)
26. Milazzo, M.J., Gohlke, J.M., Gallagher, D.L., Scott, A.A., Zaitchik, B.F., Marr, L.C.: Potential for city parks to reduce exposure to BTEX in air. Environ. Sci. Process. Impacts **21**, 40–50 (2019)
27. Ning, G., Yim, S.H.L., Wang, S., Duan, B., Nie, C., Yang, X., Wang, J., Shang, K.: Synergistic effects of synoptic weather patterns and topography on air quality: a case of the Sichuan Basin of China. Clim. Dyn. **53**, 6729–6744 (2019)
28. Rattanajongjitrakorn, P., Prueksasit, T.: Temporal variation of BTEX at the area of petrol station in Bangkok, Thailand. APCBEE Procedia **10**, 37–41 (2014)
29. Słomińska, M., Konieczka, P., Namieśnik, J.: The fate of BTEX compounds in ambient air. Crit. Rev. Environ. Sci. Technol. **44**, 455–472 (2014)
30. Stingone, J.A., McVeigh, K.H., Claudio, L.: Early-life exposure to air pollution and greater use of academic support services in childhood: a population-based cohort study of urban children. Environ. Health **16**, 2 (2017)

31. Stojić, A., Stanić, N., Vuković, G., Stanišić, S., Perišić, M., Šoštarić, A., Lazić, L.: Explainable extreme gradient boosting tree-based prediction of toluene, ethylbenzene and xylene wet deposition. Sci. Total Environ. **653**, 140–147 (2019)
32. Stojić, A., Stojić, S.S., Mijić, Z., Šoštarić, A., Rajšić, S.: Spatio-temporal distribution of VOC emissions in urban area based on receptor modelling. Atmos. Environ. **106**, 71–79 (2015b)
33. Stojić, A., Stojić, S.S., Šoštarić, A., Ilić, L., Mijić, Z., Rajšić, S.: Characterization of VOC sources in urban area based on PTR-MS measurements and receptor modelling. Environ. Sci. Pollut. Res. **22**, 13137–13152 (2015a)
34. Stojić, A., Stojić, S.S.: The innovative concept of three-dimensional hybrid receptor modeling. Atmos. Environ. **164**, 216–223 (2017)
35. Šoštarić, A., Stojić, S.S., Vuković, G., Mijić, Z., Stojić, A., Gržetić, I.: Rainwater capacities for BTEX scavenging from ambient air. Atmos. Environ. **168**, 46–54 (2017)
36. Šoštarić, A., Stojić, A., Stojić, S.S., Gržetić, I.: Quantification and mechanisms of BTEX distribution between aqueous and gaseous phase in a dynamic system. Chemosphere **144**, 721–727 (2016)
37. Stanišić, S., Perišić, M., Jovanović, G., Milićević, T., Romanić, S.H., Jovanović, A., Šoštarić, A., Udovičić, V., Stojić, A.: The PM2.5-bound polycyclic aromatic hydrocarbon behavior in indoor and outdoor environments, Part I: emission sources. Environ. Res. 110520 (2020b)
38. Stanišić, S., Perišić, M., Stojić, A.: The use of innovative methodology for the characterization of benzene, toluene, ethylbenzene and xylene sources in the Belgrade area. In: Sinteza International Scientific Conference on Information Technology and Data Related Research, Belgrade, Serbia (2020a)
39. Truong, S.C., Lee, M.I., Kim, G., Kim, D., Park, J.H., Choi, S.D., Cho, G.H.: Accidental benzene release risk assessment in an urban area using an atmospheric dispersion model. Atmos. Environ. **144**, 146–159 (2016)
40. U.S. EPA.: Chemical Data Reporting. United States Environmental Protection Agency, Washington, DC, USA (2016). https://www.epa.gov/sites/production/files/2014-11/documents/2nd_cdr_snapshot_5_19_14.pdf
41. Vardoulakis, S., Solazzo, E., Lumbreras, J.: Intra-urban and street scale variability of BTEX, NO2 and O3 in Birmingham, UK: implications for exposure assessment. Atmos. Environ. **45**, 5069–5078 (2011)
42. Werder, E.J., Engel, L.S., Blair, A., Kwok, R.K., McGrath, J.A., Sandler, D.P.: Blood BTEX levels and neurologic symptoms in Gulf states residents. Environ. Res. **175**, 100–107 (2019)
43. Wright, C.Y., Millar, D.A.: A global statement for air pollution and health. Clean Air J. **29**, 1–2 (2019)

Мнистарство науке, технолошког развоја и иновација
Матични научни одбор за геонауке и астрономију
Датум: 22.10.2024. године
Београд

Институт за физику у Београду
др Душан Вудраговић

11080 Београд
Прегревица 118

Поштовани др Вудраговићу,

Матични научни одбор за геонауке и астрономију је на својој седници од 22. октобра 2024. године, разматрао Ваш захтев за признавање и категорисање публикације:

- Stanišić, S., Perišić, M., Jovanović, G., Maletić, D., Vudragović, D., Vranić, A. & Stojić, A. (2021) What Information on Volatile Organic Compounds Can Be Obtained from the Data of a Single Measurement Site Through the Use of Artificial Intelligence? In: Pap, E. (ed) Artificial Intelligence: Theory and Applications. Studies in Computational Intelligence, vol 973, 207–225. Springer, Cham. https://doi.org/10.1007/978-3-030-72711-6_12.

Одбор је једногласно донео одлуку да се наведена публикација категорише као резултат из категорије **М13** (монографска студија/поглавље у књизи М11 или рад у тематском зборнику водећег међународног значаја) у складу са Правилником о стицању истраживачких и научних звања.

С поштовањем,

Председник Матичног научног одбора
за геонауке и астрономију

др Владимир Срећковић, научни саветник

Computer Physics Communications 326 (2026) 110209

Contents lists available at ScienceDirect

Computer Physics Communications

journal homepage: www.elsevier.com/locate/cpc

New Version Announcement

C+ + CUDA programs for solving the time-dependent dipolar Gross-Pitaevskii equation

Denis Mujo[a], Dušan Vudragović[a,*], Paulsamy Muruganandam[b,c], Sadhan K. Adhikari[d]

[a] Scientific Computing Laboratory, Center for the Study of Complex Systems, Institute of Physics Belgrade, University of Belgrade, Pregrevica 118, Belgrade, 11080, Serbia
[b] Department of Physics, Bharathidasan University, Tiruchirappalli, Tamil Nadu, 620024, India
[c] Department of Medical Physics, Bharathidasan University, Tiruchirappalli, Tamil Nadu, 620024, India
[d] Instituto de Física Teórica, UNESP – Universidade Estadual Paulista, 01.140-70 São Paulo, São Paulo, Brazil

ARTICLE INFO

The review of this paper was arranged by Prof. Dr. J Ballantyne

PACS:
02.60.Cb
02.60.Lj
02.60.Jh
02.60.Cb
03.75.-b
67.85.-d

Keywords:
Bose-Einstein condensate
Gross-Pitaevskii equation
Dipolar atoms
Quantum fluctuations
Quantum droplets
Split-step Crank-Nicolson scheme
Real- and imaginary-time propagation
Partial differential equation
C+ + program
CUDA program
GPU

ABSTRACT

This paper introduces an improved version of our previous CUDA programs [1] for solving the dipolar Gross-Pitaevskii equation in three spatial dimensions, now incorporating a quantum fluctuation term [2–4]. This enhancement is vital for accurately modeling quantum dipolar droplets [5,6] in dipolar Bose-Einstein condensates. Originally developed in C, the code has been transitioned to C+ + to take advantage of its features. Speedup tests were conducted on two types of GPU cards – one commercial and one HPC-optimized – and the results were compared to earlier versions on GPUs and a modern HPC cluster. Both configurations showed an increase in speed.

NEW VERSION PROGRAM SUMMARY

Program title: DBEC-GP-CUDA package, consisting of: (i) imag3d-cuda, (ii) real3d-cuda.
CPC Library link to program files: https://doi.org/10.17632/s858p8zsgp.2
Licensing provisions: CC by 4.0.
Programming language: OpenMP C+ +; CUDA C+ +.
Supplementary material: 10.1016/j.cpc.2026.110209.
Journal reference of previous version: Comput. Phys. Commun. 200 (2016) 406.
Does the new version supersede the previous version?: No.

Nature of problem: These programs are developed to solve the time-dependent nonlinear Gross-Pitaevskii equation (GPE), including contact and dipolar interactions, as well as a quantum fluctuations term [2,3]. within an anisotropic harmonic trap. The package offers programs for solving GPE in three spatial dimensions, capable of computing both stationary and non-stationary solutions through imaginary or real-time propagation.

Solution method: The time-dependent GPE is solved using the same split-step semi-implicit Crank-Nicolson method as before [7,8], enabling the calculation of stationary and non-stationary solutions through propagation in imaginary or real time. The dipolar interaction term is evaluated by applying a Fourier transform to momentum space using the convolution theorem. The quantum fluctuation term has an integral that can be calculated analytically, and therefore, we avoid doing numerical integration for that term.

Reasons for the new version: The development of the new code is motivated by two main reasons. First, the previous version lacked the quantum fluctuation term, which is crucial for accurately modeling stable quantum dipolar droplets. Without it, the code cannot simulate droplet formation, resulting in system collapse at the mean-field level due to predominantly attractive interactions. By adding this term, the system is mechanically stabilized against collapse, allowing the updated code to simulate the process correctly. And considering that the previous Fortran, C, and CUDA programs are widely used in the ultra-cold

* Corresponding author.
E-mail addresses: denis.mujo@ipb.ac.rs (D. Mujo), dusan.vudragovic@ipb.ac.rs (D. Vudragović), anand@bdu.ac.in (P. Muruganandam), adhikari@ift.unesp.br (S.K. Adhikari).

https://doi.org/10.1016/j.cpc.2026.110209
Received 30 March 2026; Received in revised form 27 April 2026; Accepted 5 May 2026
Available online 7 May 2026

atoms community [9–17] and with the discovery of quantum dipolar droplets, we have found it beneficial to have programs that can properly simulate them as well. Second, with modern computers typically equipped with GPUs and HPC clusters with even more powerful GPU cards, we made several improvements and optimizations to better utilize these resources. These enhancements boost performance on modern systems. On the NVIDIA A30 GPU, the speedup over previously published OpenMP/MPI-parallelized programs [18] running on 128 Intel Xeon Gold 6338 CPU cores is 3 or higher. Additionally, we converted the code from C to C+ + to utilize standard library features and adopted an object-oriented approach, enhancing code abstraction and structure.

Summary of revisions: The revised code extends the original dipolar Gross–Pitaevskii programs [1] for solving the dipolar GPE by including the beyond-mean-field quantum fluctuation term needed to describe dipolar quantum droplets, as explained in the supplementary material. This additional contribution follows the formulation of Lima and Pelster [2,3] and is implemented in dimensionless form together with the contact and dipolar interactions.

As described in the supplementary material, this new term is incorporated into the non-derivative part of the propagation scheme through the existing `calcnu` routine. The implementation is validated with simulation examples for ^{164}Dy condensates, including imaginary-time ground-state calculations and real-time evolution after a quench into the dipole-dominated regime, where droplet formation is observed.

In addition to the physics extension, the supplementary material highlights several code improvements. The evolution procedure is simplified into a single main loop, new parameters (NITER, NSNAP, MUEND) improve monitoring and convergence control, and initialization is made more flexible through user-defined Gaussian widths and optional automatic grid-step selection. The revised programs also improve memory management and GPU execution, leading to measurable performance gains over previous CUDA versions and strong speedups compared with earlier implementations.

Additional comments including Restrictions and Unusual features: This package includes two programs: imag3d-cuda for imaginary time propagation and real3d-cuda for real time propagation. Programs are compatible with computers that have NVIDIA GPU cards with Compute Capability 6.0 or higher and require CUDA toolkit versions above 8.0. Because the FFT algorithm in the cuFFT library, our programs may consume varying amounts of memory depending on the grid sizes N_x, N_y, and N_z. For instance, if a grid size is a large prime number, cuFFT will employ an algorithm that requires significantly more memory - often several times more - compared to a grid size that is a power of two. Generally, smaller prime numbers lead to better performance, with the best results achieved when the grid size is a power of two.

CRediT authorship contribution statement

Denis Mujo: Writing – review & editing, Validation, Software, Investigation, Formal analysis; **Dušan Vudragović:** Writing – original draft, Visualization, Validation, Supervision, Software, Investigation, Conceptualization; **Paulsamy Muruganandam:** Writing – review & editing, Validation, Supervision, Software, Investigation, Conceptualization; **Sadhan K. Adhikari:** Writing – review & editing, Visualization, Validation, Supervision, Software, Investigation, Conceptualization.

Data availability

Codes are provided in the Attach Files step.

Declaration of competing interest

The authors declare that they have no known competing financial interests or personal relationships that could have appeared to influence the work reported in this paper.

Acknowledgements

D. M. and D. V. acknowledge support provided by the Institute of Physics Belgrade, through the grant by the Ministry of Science, Technological Development, and Innovations of the Republic of Serbia. The work of P. M. is supported by the Ministry of Education-Rashtriya Uchchatar Shiksha Abhiyan (MoE RUSA 2.0): Bharathidasan University–Physical Sciences. S. K. A. acknowledges support by the Conselho Nacional de Desenvolvimento Cient ífico e Tecnológico (Brazil) grant 303885/2024-6. Numerical simulations were run on the PARADOX supercomputing facility at the Scientific Computing Laboratory, National Center of Excellence for the Study of Complex Systems, Institute of Physics Belgrade.

Supplementary material

Supplementary material associated with this article can be found in the online version at 10.1016/j.cpc.2026.110209.

References

[1] V. Lončar, A. Balaž, A. Bogojević, S. Škrbić, P. Muruganandam, S.K. Adhikari, CUDA programs for solving the time-dependent dipolar Gross-Pitaevskii equation in an anisotropic trap, Comput. Phys. Commun. 200 (2016) 406–410. https://doi.org/10.1016/j.cpc.2015.11.014
[2] A.R.P. Lima, A. Pelster, Beyond mean-field low-lying excitations of dipolar Bose gases, Phys. Rev. A 86 (2012) 063609. https://doi.org/10.1103/PhysRevA.86.063609
[3] A.R.P. Lima, A. Pelster, Quantum fluctuations in dipolar Bose gases, Phys. Rev. A 84 (2011) 041604. https://doi.org/10.1103/PhysRevA.84.041604
[4] F. Wächtler, L. Santos, Quantum filaments in dipolar Bose-Einstein condensates, Phys. Rev. A 93 (2016) 061603. arXiv:1601.04501, https://doi.org/10.1103/PhysRevA.93.061603
[5] H. Kadau, M. Schmitt, M. Wenzel, C. Wink, T. Maier, I. Ferrier-Barbut, T. Pfau, Observing the Rosensweig instability of a quantum ferrofluid, Nature 530 (2016) 194–197. https://doi.org/10.1038/nature16485
[6] I. Ferrier-Barbut, H. Kadau, M. Schmitt, M. Wenzel, T. Pfau, Observation of quantum droplets in a strongly dipolar Bose gas, Phys. Rev. Lett. 116 (2016) 215301. https://doi.org/10.1103/PhysRevLett.116.215301
[7] P. Muruganandam, S.K. Adhikari, Fortran programs for the time-dependent Gross-Pitaevskii equation in a fully anisotropic trap, Comput. Phys. Commun. 180 (2009) 1888–1912. https://doi.org/10.1016/j.cpc.2009.04.015
[8] R.K. Kumar, L.E. Young-S., D. Vudragović, A. Balaž, P. Muruganandam, S.K. Adhikari, Fortran and C programs for the time-dependent dipolar Gross-Pitaevskii equation in an anisotropic trap, Comput. Phys. Commun. 195 (2015) 117–128. arXiv:1506.03283, https://doi.org/10.1016/j.cpc.2015.03.024
[9] S.K. Adhikari, Bright dipolar Bose-Einstein-condensate soliton mobile in a direction perpendicular to polarization, Phys. Rev. A 90 (2014) 055601. arXiv:1410.1369, https://doi.org/10.1103/PhysRevA.90.055601
[10] S.K. Adhikari, Stable matter-wave solitons in the vortex core of a uniform condensate, J. Phys. B At. Mol. Phys. 48 (2015) 165303. arXiv:1506.06367, https://doi.org/10.1088/0953-4075/48/16/165303
[11] S.K. Adhikari, Stable spatial and spatiotemporal optical soliton in the core of an optical vortex, Phys. Rev. E 92 (2015) 042926. arXiv:1510.03663, https://doi.org/10.1103/PhysRevE.92.042926
[12] H. Al-Jibbouri, I. Vidanović, A. Balaž, A. Pelster, Geometric resonances in Bose-Einstein condensates with two- and three-body interactions, J. Phys. B At. Mol. Phys. 46 (2013) 065303. arXiv:1208.0991, https://doi.org/10.1088/0953-4075/46/6/065303
[13] J. Akram, A. Pelster, Sculpting quasi-one-dimensional Bose-Einstein condensate to generate calibrated matter waves, Phys. Rev. A 93 (2016) 023606. arXiv:1509.03826, https://doi.org/10.1103/PhysRevA.93.023606
[14] T. Khellil, A. Balaž, A. Pelster, Analytical and numerical study of dirty bosons in a quasi-one-dimensional harmonic trap, New J. Phys. 18 (2016) 063003. arXiv:1510.04985, https://doi.org/10.1088/1367-2630/18/6/063003
[15] I. Vasić, A. Balaž, Excitation spectra of a Bose-Einstein condensate with an angular spin-orbit coupling, Phys. Rev. A 94 (2016) 033627. arXiv:1602.03538, https://doi.org/10.1103/PhysRevA.94.033627
[16] C.-Y. Lai, C.-C. Chien, Geometry-induced memory effects in isolated quantum systems: cold-atom applications, Phys. Rev. Appl. 5 (2016) 034001. arXiv:1510.08978, https://doi.org/10.1103/PhysRevApplied.5.034001
[17] P. Das, P.K. Panigrahi, Controlled generation of nonlinear resonances through sinusoidal lattice modes in Bose-Einstein condensate, Laser Phys. 25 (2015) 125501. arXiv:1506.00795, https://doi.org/10.1088/1054-660X/25/12/125501
[18] V. Lončar, L.E. Young-S., S. Škrbić, P. Muruganandam, S.K. Adhikari, A. Balaž, OpenMP, OpenMP/MPI, and CUDA/MPI C programs for solving the time-dependent dipolar Gross-Pitaevskii equation, Comput. Phys. Commun. 209 (2016) 190–196. arXiv:1610.05329, https://doi.org/10.1016/j.cpc.2016.07.029

Supplemental material: C++ CUDA programs for solving the time-dependent dipolar Gross-Pitaevskii equation

Denis Mujo[a], Dušan Vudragović[a,*], Paulsamy Muruganandam[b,c], Sadhan K. Adhikari[d]

[a] *Scientific Computing Laboratory, Center for the Study of Complex Systems, Institute of Physics Belgrade, University of Belgrade, Pregrevica 118, 11080 Belgrade, Serbia*
[b] *Department of Physics, Bharathidasan University, Tiruchirappalli 620024, Tamil Nadu, India*
[c] *Department of Medical Physics, Bharathidasan University, Tiruchirappalli 620024, Tamil Nadu, India*
[d] *Instituto de Física Teórica, UNESP – Universidade Estadual Paulista, 01.140-70 São Paulo, São Paulo, Brazil*

In dipolar Bose-Einstein condensates (BEC), mean-field interactions alone are insufficient to describe the emergence and stability of quantum droplets. To capture the crucial role of beyond-mean-field effects, the Gross-Pitaevskii equation (GPE) is extended by an additional term that incorporates the contribution of quantum fluctuations. This leads to the following extended GPE, which incorporates both mean-field dipolar interactions and the beyond-mean-field correction

$$i\frac{\partial\Psi}{\partial t} = \left(-\frac{1}{2}\nabla^2 + U + g|\Psi|^2 + g_{\mathrm{dd}}\int d^3r'\frac{1-3\cos^2\theta}{|\mathbf{r}-\mathbf{r}'|^3}|\Psi|^2 + h_2|\Psi|^3\right)\Psi, \tag{1}$$

where g and g_{dd} are, respectively, the contact and dipole-dipole interaction coupling constants with $g = 4\pi N a_s/\ell$ and $g_{\mathrm{dd}} = 3Na_{\mathrm{dd}}/\ell$, U is the trap potential, N is the number of atoms in the condensate, and h_2 represents the quantum fluctuations term [2, 3]. GPE Eq. (1) is expressed in dimensionless form and integrated into the code accordingly. This is accomplished by selecting a reference frequency ω_r and defining all other physical variables relative to it, i.e., lengths are measured in harmonic oscillator units $\ell = \sqrt{\hbar/(m\omega_r)}$, time in units of $1/\omega_r$, and energy in units of $\hbar\omega_r$. This extended formulation provides a quantitatively accurate description of both the formation and the equilibrium properties of dipolar quantum droplets.

The quantum fluctuation term in the code is derived from Lima and Pelster's research [2, 3], where they first formulated this term for dipolar Bose gases using Bogoliubov-de Gennes (BdG) theory. To extend beyond the mean-field approximation, we decomposed the field operator into the wave function around the condensate wave function, Ψ_c, including a term for quantum fluctuations $\delta\hat{\Psi}$, so that $\hat{\Psi} = \Psi_c + \delta\hat{\Psi}$, retaining terms up to second order in quantum fluctuations. These fluctuations result in a shift in the chemical potential, and BdG theory supplies the term to model this shift

$$h_2 = \frac{128\sqrt{\pi}}{3}\left(\frac{a_s}{\ell}\right)^{5/2} N^{3/2}Q_5,\; Q_5(\epsilon_{\mathrm{dd}}) = \int_0^1 du\left(1-\epsilon_{\mathrm{dd}}+3u^2\epsilon_{\mathrm{dd}}\right)^{5/2}, \tag{2}$$

where $\epsilon_{\mathrm{dd}} = a_{\mathrm{dd}}/a_s$ represents the relative interaction strength. The Q_5 term has an analytical expression, eliminating the need for numerical integration in our codes. For $\epsilon_{\mathrm{dd}} > 1$, which is the section where quantum droplets may form, the Q_5 term gains an imaginary component as well. However, this imaginary part is significantly smaller than the real part, as illustrated in Figure 1, and can be neglected [19, 20]. As seen in Eq. (1), the quantum fluctuation term does not depend on spatial derivatives. Therefore, it is incorporated into our program as an additional term within the `calcnu` function, which handles time propagation for the Hamiltonian component without spatial derivatives.

Figure 2 presents the simulation results based on the input parameters from the experimental setup [5] to demonstrate the code's functionality. On the left, the figure shows the ground-state condensate density $n(x,y) = \int dz|\Psi(x,y,z)|^2$, resulting from the imaginary-time propagation of $N = 20000$ ^{164}Dy atoms, with the contact and dipole-dipole interaction strengths set to $a_s = a_{\mathrm{dd}} = 132\,a_0$ (where a_0 is Bohr radius), which aligns with the experimental conditions. The system's real-time dynamics are simulated by applying a quench to the contact interaction strength, reducing it to $a_s = 80\,a_0$. This moves the system into the dipole-dominated regime $\epsilon_{\mathrm{dd}} > 1$, which is essential for quantum droplet formation. The right side of the Figure 2 shows the condensate density after 110 ms, where droplet formation is clearly visible.

*Corresponding author.
Email addresses: `denis.mujo@ipb.ac.rs` (Denis Mujo), `dusan.vudragovic@ipb.ac.rs` (Dušan Vudragović), `anand@bdu.ac.in` (Paulsamy Muruganandam), `adhikari@ift.unesp.br` (Sadhan K. Adhikari)

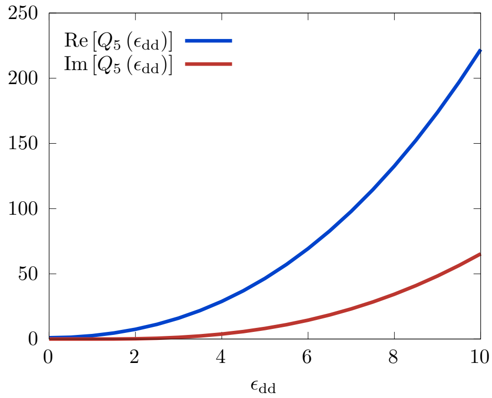

Figure 1: Real and imaginary parts of Q_5 integral as functions of the relative interaction strength, $\epsilon_{\rm dd}$. Notably, the imaginary part is much smaller than the real part, highlighting the dominance of the real component for different $\epsilon_{\rm dd}$ values.

When initialized in a droplet configuration, the condensate preserves its structure during real-time evolution if the state corresponds to a stable solution of the extended GPE. In such cases, the density profile remains essentially unchanged, apart from minor numerical fluctuations or weak collective excitations, confirming that the droplet arrangement represents a stationary or long-lived metastable state. This behavior is illustrated in Figure 3, where the droplet pattern obtained via imaginary-time propagation (a) is used as the initial condition for real-time evolution. As shown in Figure 3 (b), the integrated quasi-2D density at $t = 10\,\mathrm{ms}$ retains the same spatial structure, demonstrating the dynamical stability of the droplet configuration for the chosen parameters ($N = 80000$, $a = 85\,a_0$, $a_{\rm dd} = 130.8\,a_0$).
In the updated code, we've also revised the main evolution loop. Previously, the program used three separate conditional loops—one to introduce the nonlinearities for contact and dipolar interaction, the second to run with fixed nonlinearities, and the third for the final run with fixed nonlinearities. The updated version features a single loop that includes fixed nonlinearities.
The updated code enhances simulation progress monitoring. Unlike the previous version, where physical quantities were calculated only after each main loop, the new version introduces configurable options using the NITER and NSNAP variables. NITER sets the total number of iterations, while NSNAP determines how many snapshots are taken, i.e., how often the physical quantities are calculated during the NITER iterations. To remain compatible with the outputs of the previous code version, one can set NSNAP to 1 to produce the same output.
The updated code now terminates the simulation conditionally once the chemical potential reaches stability. A new optional configuration parameter, MUEND, has been introduced to specify the permissible relative deviation of the chemical potential between two consecutive time steps. When MUEND is set, the simulation will run until the condition $|\mu_{i-1} - \mu_i|/\mu_i > \mathrm{MUEND}$ is satisfied, where μ_{i-1} and μ_i are

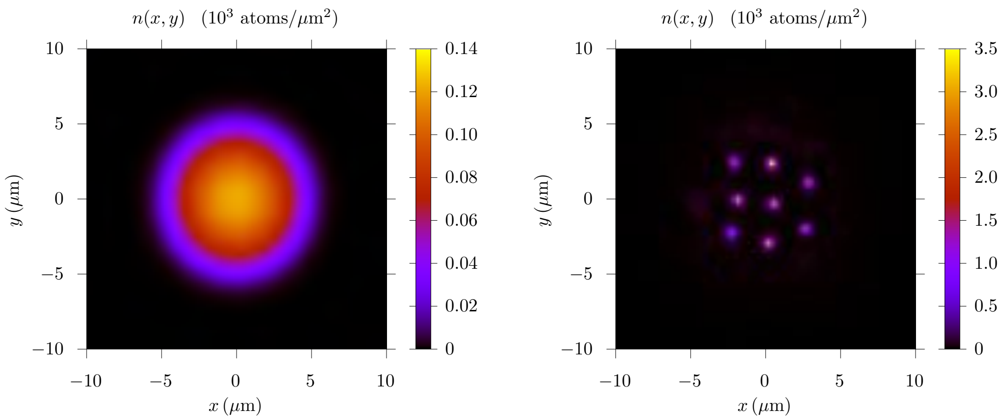

Figure 2: Ground-state condensate densities $n(x, y)$ are shown after imaginary-time propagation (left) and after 110 ms of real-time propagation (right), following a quench in contact interaction strength from $a_s = 132\,a_0$ to $a_s = 80\,a_0$.

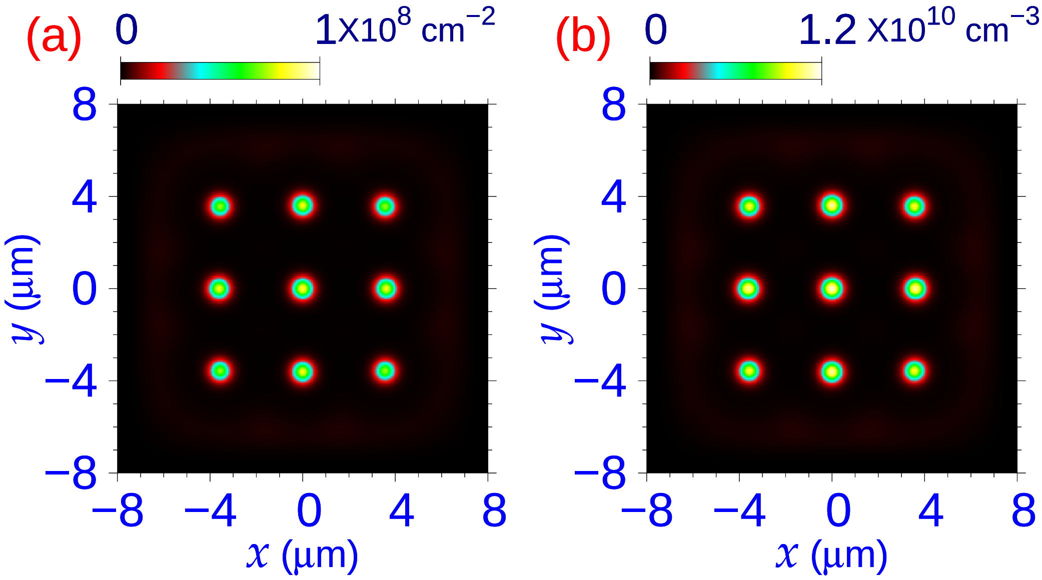

Figure 3: (a) Contour plot of integrated quasi-2D density $n(x, y)$ of a dipolar BEC of $N = 80000$ ^{164}Dy atoms in a trap of angular frequencies $\{\omega_x, \omega_y, \omega_z\} = 2\pi\{33, 33, 167\}$ Hz obrained by imaginary-time propagation. (b) The same by real-time propagation at time $t = 10$ ms, using the converged imaginary-time wave function as the initial state. Atomic scattering (dipolar) length $a = 85a_0$ ($a_{\rm dd} = 130.8a_0$).

the chemical potential values from the current and previous steps.

In the previous programs, initial wave function was initialized as a Gaussian whose values were determined from trap potentials $\gamma = \frac{\omega_x}{\omega_r}$, $\lambda = \frac{\omega_y}{\omega_r}$, $\nu = \frac{\omega_z}{\omega_r}$ with $\psi(x, y, z) \propto \exp\left(-0.5\left(\gamma x^2 + \lambda y^2 + \nu z^2\right)\right)$. In our case, since for the existence of the quantum droplet, potential trap is not necessary, we have added specific, user given, values s_x, s_y and s_z so that the wave function is $\psi(x, y, z) \propto \exp\left(-0.25\left(\frac{x^2}{s_x^2} + \frac{y^2}{s_y^2} + \frac{z^2}{s_z^2}\right)\right)$.

What is also changed compared to the previous programs is the way discretization steps dx, dy, dz and dt are initialized. In previous programs they needed to be initialized directly, and in our programs, if they are not initialized, they will be calculated based on the number of points N_x, N_y and N_z and Gaussian variables s_x, s_y and s_z as

$$di = \frac{2s_i m_i}{Ni}, \; dt = \frac{dj^2}{m_t}, \tag{3}$$

where $i \in \{x, y, z\}$, j corresponds to the index of the smallest value between dx, dy or dz and mx, my, mz are also user given variables that determine how big the condensate should be compared to the simulation box (for example, $m_x = m_y = m_z = 10$ menas that the condensate will be 10 times smaller then the simulation box), and m_t determines the time step.

The new programs keep the same names as in previous C CUDA versions: "imag3d-cuda" for imaginary time propagation and "real3d-cuda" for real-time propagation. The program structure, including method names, remains unchanged. The array initialization has been modified to utilize the C++ standard *vector* library, which automatically manages memory, removing the need for manual deallocation.

In the previous programs, the POTMEM setting was used to optimize GPU memory usage. This setting either allocated two tensors for the trap and dipolar potentials or a single tensor with asynchronous copying from main memory when needed. Now, we have introduced a new setting INITIALIZE_POT which has values 0 or 1, where if the first value is chosen, the program will compute trap potential values on-the-fly on the GPU, and if the second value is chosen, the program will create a 3D tensor which it will use to store precomputed values of the trap potential on the GPU. In the FFT section where the CUDA cuFFT library [21] is used, a single tensor contains both the squared wave function and the FFT result. Methods like calcnu, calclux, calcluy, calcluz, and calcnorm all reuse the same temporary array during calculations. Once data is transferred to the GPU, it remains there, and during each time step, physical quantities such as the wave function and densities are copied back to the CPU for display. Additionally, we used the OpenMP library to parallelize loops during the initialization of the wave function, trap potential, and dipolar potential to further enhance performance.

The code's performance was assessed using two GPUs: the consumer-level NVIDIA GTX 1660s and the HPC-optimized NVIDIA A30. Figure 4 displays the speedup in execution time relative to the previous program versions. Tests were conducted on linear grid sizes ranging from 128^3 up to the grid sizes that are close to the maximum that could fit into each GPU's memory - 416^3 for the GTX 1660s with 6 GB and 704^3 for the A30 with 24 GB. Solid lines indicate the average speedup, which is 1.6 for the GTX 1660s and 1.3 for the A30, observed in both the imag3d-cuda (Figure 4a) and relas3d-cuda (Figure 4b) programs.

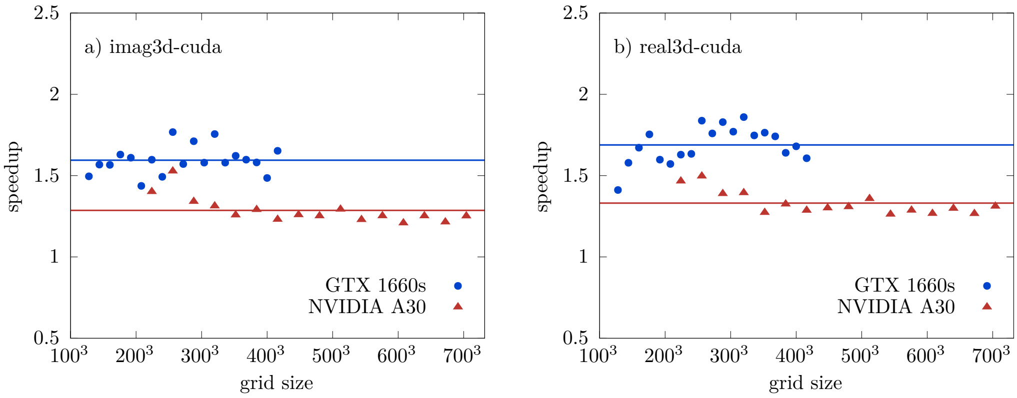

Figure 4: Speedup in execution times of imag3d-cuda and real3d-cuda compared to earlier versions of the programs on NVIDIA GTX 1660 Super and A30 cards. Solid lines show the average speedup achieved. We tested linear grid sizes starting from 128^3 up to the grid sizes that are close to the maximum that could fit into each GPU's memory, which was 416^3 for the GTX 1660 Super and 704^3 for the A30.

The performance of the programs is also evaluated by comparing them to previously published OpenMP/MPI-parallelized programs running on 128 Intel Xeon Gold 6338 CPUs with 128 GB of RAM. The main purpose of this comparison was to assess the potential performance gains from a single GPU card versus an HPC cluster environment. Figure 5 illustrates the speedup of imag3d-cuda and real3d-cuda when run on an NVIDIA A30 card and in a cluster environment. As shown, depending on the grid size, the speedup for imag3d-cuda is three or higher, while for real3d-cuda, it is five or higher.

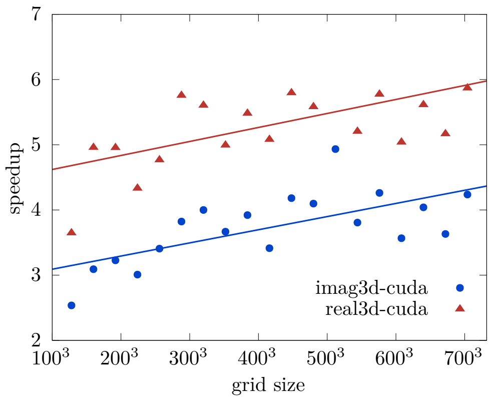

Figure 5: Speedup in execution times of imag3d-cuda and real3d-cuda on NVIDIA A30 card compared to the equivalent MPI/OpenMP parallelized versions of the programs on 128 Intel Xeon Gold 6338 CPUs with 128 GB of RAM. Solid lines show the average speedup achieved.

References

[1] V. Lončar, A. Balaž, A. Bogojević, S. Škrbić, P. Muruganandam, S. K. Adhikari, CUDA programs for solving the time-dependent dipolar Gross-Pitaevskii equation in an anisotropic trap, Computer Physics Communications **200** (2016) 406–410. doi:10.1016/j.cpc.2015.11.014.

[2] A. R. P. Lima, A. Pelster, Beyond mean-field low-lying excitations of dipolar Bose gases, Physical Review A **86** (2012) 063609. doi:10.1103/PhysRevA.86.063609.

[3] A. R. P. Lima, A. Pelster, Quantum fluctuations in dipolar Bose gases, Physical Review A **84** (2011) 041604. doi:10.1103/PhysRevA.84.041604.

[4] F. Wächtler, L. Santos, Quantum filaments in dipolar Bose-Einstein condensates, Physical Review A **93** (2016) 061603. doi:10.1103/PhysRevA.93.061603. arXiv:1601.04501.

[5] H. Kadau, M. Schmitt, M. Wenzel, C. Wink, T. Maier, I. Ferrier-Barbut, T. Pfau, Observing the Rosensweig instability of a quantum ferrofluid, Nature **530** (2016) 194–197. doi:10.1038/nature16485.

[6] I. Ferrier-Barbut, H. Kadau, M. Schmitt, M. Wenzel, T. Pfau, Observation of Quantum Droplets in a Strongly Dipolar Bose Gas, Physical Review Letters **116** (2016) 215301. doi:10.1103/PhysRevLett.116.215301.

[7] P. Muruganandam, S. K. Adhikari, Fortran programs for the time-dependent Gross-Pitaevskii equation in a fully anisotropic trap, Computer Physics Communications **180** (2009) 1888–1912. doi:10.1016/j.cpc.2009.04.015.

[8] R. K. Kumar, L. E. Young-S., D. Vudragović, A. Balaž, P. Muruganandam, S. K. Adhikari, Fortran and C programs for the time-dependent dipolar Gross-Pitaevskii equation in an anisotropic trap, Computer Physics Communications **195** (2015) 117–128. doi:10.1016/j.cpc.2015.03.024. arXiv:1506.03283.

[9] S. K. Adhikari, Bright dipolar Bose-Einstein-condensate soliton mobile in a direction perpendicular to polarization, Physical Review A **90** (2014) 055601. doi:10.1103/PhysRevA.90.055601. arXiv:1410.1369.

[10] S. K. Adhikari, Stable matter-wave solitons in the vortex core of a uniform condensate, Journal of Physics B Atomic Molecular Physics **48** (2015) 165303. doi:10.1088/0953-4075/48/16/165303. arXiv:1506.06367.

[11] S. K. Adhikari, Stable spatial and spatiotemporal optical soliton in the core of an optical vortex, Physical Review E **92** (2015) 042926. doi:10.1103/PhysRevE.92.042926. arXiv:1510.03663.

[12] H. Al-Jibbouri, I. Vidanović, A. Balaž, A. Pelster, Geometric resonances in Bose-Einstein condensates with two- and three-body interactions, Journal of Physics B Atomic Molecular Physics **46** (2013) 065303. doi:10.1088/0953-4075/46/6/065303. arXiv:1208.0991.

[13] J. Akram, A. Pelster, Sculpting quasi-one-dimensional Bose-Einstein condensate to generate calibrated matter waves, Physical Review A **93** (2016) 023606. doi:10.1103/PhysRevA.93.023606. arXiv:1509.03826.

[14] T. Khellil, A. Balaž, A. Pelster, Analytical and numerical study of dirty bosons in a quasi-one-dimensional harmonic trap, New Journal of Physics **18** (2016) 063003. doi:10.1088/1367-2630/18/6/063003. arXiv:1510.04985.

[15] I. Vasić, A. Balaž, Excitation spectra of a Bose-Einstein condensate with an angular spin-orbit coupling, Physical Review A **94** (2016) 033627. doi:10.1103/PhysRevA.94.033627. arXiv:1602.03538.

[16] C.-Y. Lai, C.-C. Chien, Geometry-Induced Memory Effects in Isolated Quantum Systems: Cold-Atom Applications, Physical Review Applied **5** (2016) 034001. doi:10.1103/PhysRevApplied.5.034001. arXiv:1510.08978.

[17] P. Das, P. K. Panigrahi, Controlled generation of nonlinear resonances through sinusoidal lattice modes in Bose-Einstein condensate, Laser Physics **25** (2015) 125501. doi:10.1088/1054-660X/25/12/125501. arXiv:1506.00795.

[18] V. Lončar, L. E. Young-S., S. Škrbić, P. Muruganandam, S. K. Adhikari, A. Balaž, OpenMP, OpenMP/MPI, and CUDA/MPI C programs for solving the time-dependent dipolar Gross-Pitaevskii equation, Computer Physics Communications **209** (2016) 190–196. doi:10.1016/j.cpc.2016.07.029. arXiv:1610.05329.

[19] F. Böttcher, J.-N. Schmidt, J. Hertkorn, K. S. H. Ng, S. D. Graham, M. Guo, T. Langen, T. Pfau, New states of matter with fine-tuned interactions: quantum droplets and dipolar supersolids, Reports on Progress in Physics **84** (2021) 012403. doi:10.1088/1361-6633/abc9ab.

[20] Y. Xiong, L. Yin, Effective single-mode model of a binary boson mixture in the quantum droplet region, Physical Review A **105** (2022) 053305. doi:10.1103/PhysRevA.105.053305.

[21] cuFFT, CUDA API References, CUDA Toolkit Documentation v13.0, 2025. URL: https://docs.nvidia.com/cuda/cufft.

Computer Physics Communications 259 (2021) 107657

Contents lists available at ScienceDirect

Computer Physics Communications

journal homepage: www.elsevier.com/locate/cpc

Spin-1 spin–orbit- and Rabi-coupled Bose–Einstein condensate solver[☆,☆☆]

Rajamanickam Ravisankar[a], Dušan Vudragović[b], Paulsamy Muruganandam[a,c], Antun Balaž[b], Sadhan K. Adhikari[d,*]

[a] Department of Physics, Bharathidasan University, Palkalaiperur Campus, Tiruchirappalli 620024, Tamil Nadu, India
[b] Institute of Physics Belgrade, University of Belgrade, Pregrevica 118, 11080 Belgrade, Serbia
[c] Department of Medical Physics, Bharathidasan University, Palkalaiperur Campus, Tiruchirappalli 620024, Tamil Nadu, India
[d] Instituto de Física Teórica, UNESP – Universidade Estadual Paulista, 01.140-70 São Paulo, São Paulo, Brazil

ARTICLE INFO

Article history:
Received 10 February 2020
Received in revised form 30 August 2020
Accepted 13 September 2020
Available online 5 October 2020

Keywords:
Spinor Bose–Einstein condensate
Spin–orbit coupling
Gross–Pitaevskii equation
Split-step Crank–Nicolson scheme
FORTRAN programs
Partial differential equation

ABSTRACT

We present OpenMP versions of FORTRAN programs for solving the Gross–Pitaevskii equation for a harmonically trapped three-component spin-1 spinor Bose–Einstein condensate (BEC) in one (1D) and two (2D) spatial dimensions with or without spin–orbit (SO) and Rabi couplings. Several different forms of SO coupling are included in the programs. We use the split-step Crank–Nicolson discretization for imaginary- and real-time propagation to calculate stationary states and BEC dynamics, respectively. The imaginary-time propagation programs calculate the lowest-energy stationary state. The real-time propagation programs can be used to study the dynamics. The simulation input parameters are provided at the beginning of each program. The programs propagate the condensate wave function and calculate several relevant physical quantities. Outputs of the programs include the wave function, energy, root-mean-square sizes, different density profiles (linear density for the 1D program, linear and surface densities for the 2D program). The imaginary- or real-time propagation can start with an analytic wave function or a pre-calculated numerical wave function. The imaginary-time propagation usually starts with an analytic wave function, while the real-time propagation is often initiated with the previously calculated converged imaginary-time wave function.

Program summary
Program title: BEC-GP-SPINOR, consisting of: BEC-GP-SPINOR-OMP package, containing programs spin-SO-imre1d-omp.f90 and spin-SO-imre2d-omp.f90, with util.f90.
CPC Library link to program files: https://doi.org/10.17632/j3wr4wn946.1
Licensing provisions: Apache License 2.0
Programming language: OpenMP FORTRAN. The FORTRAN programs are tested with the GNU, Intel, PGI, and Oracle compiler.
Nature of problem: The present Open Multi-Processing (OpenMP) FORTRAN programs solve the time-dependent nonlinear partial differential Gross–Pitaevskii (GP) equation for a trapped spinor Bose–Einstein condensate, with or without spin–orbit coupling, in one and two spatial dimensions.
Solution method: We employ the split-step Crank–Nicolson rule to discretize the time-dependent GP equation in space and time. The discretized equation is then solved by imaginary- or real-time propagation, employing adequately small space and time steps, to yield the solution of stationary and non-stationary problems, respectively.

☆ The review of this paper was arranged by Prof. Stephan Fritzsche.
☆☆ This paper and its associated computer program are available via the Computer Physics Communication homepage on ScienceDirect (http://www.sciencedirect.com/science/journal/00104655).

* Corresponding author.
E-mail addresses: ravicpc2012@bdu.ac.in (R. Ravisankar), dusan@ipb.ac.rs (D. Vudragović), anand@bdu.ac.in (P. Muruganandam), antun@ipb.ac.rs (A. Balaž), sk.adhikari@unesp.br (S.K. Adhikari).

https://doi.org/10.1016/j.cpc.2020.107657

1. Introduction

Previously published FORTRAN [1] and C [2] programs are now popular tools for studying the properties of a Bose–Einstein condensate (BEC) by solving the Gross–Pitaevskii (GP) equation and are enjoying widespread use. These programs have later been extended to the more complex scenario of dipolar atoms [3] and of rotating BECs [4]. The OpenMP [5,6] and CUDA [7–9] version of these programs, designed to make these faster and more efficient in multi-core computers, are also available.

There has been great interest in the studies of spinor BECs using the GP equation after the experimental observation of the same [10,11]. Later, it has been possible to introduce an artificial synthetic spin–orbit (SO) coupling by Raman lasers that coherently couple the spin-component states in a pseudo spin-1/2 [12,13] and spin-1 [14] spinor BEC. In this paper, we present new OpenMP FORTRAN programs to solve the GP equation for a three-component spin-1 spinor quasi-one-dimensional (quasi-1D) and quasi-two-dimensional (quasi-2D) BECs [15] with [16,17] or without [18,19] SO and associated Rabi couplings, based on our earlier programs [5,6]. The GP equation for an SO-coupled three-component spin-1 trapped BEC is conveniently solved by the imaginary- and real-time propagation methods. We provide combined imaginary- and real-time programs in one and two spatial dimensions. The present imaginary-time programs already involve complex variables and are hence combined together with the real-time programs, requiring complex algebra. The choice of the type of propagation (imaginary- or real-time) is made through an input parameter. The imaginary-time approach should be used to solve the GP equation for stationary states. A subsequent study of the non-stationary dynamics of the BEC should be done using the real-time propagation using the imaginary-time wave function as the initial state. We use the split-step Crank–Nicolson scheme for solving the GP equation, as in Refs. [1,2].

In Section 2 we present the GP equation for a spin-1 spinor BEC in a trap. The mean-field model and a general scheme for its numerical solution are considered for both quasi-1D and quasi-2D traps. The details about the computer programs, and their input parameters, output files, etc. are given in Section 3. The numerical method and results are given in Section 4, where we illustrate the results for density and energy by employing the imaginary-time propagation for different interaction strengths (nonlinearities). The stability of the density profiles is demonstrated in real-time propagation using the corresponding converged solution obtained by the imaginary time propagation as the initial state. Finally, a brief summary is given in Section 5. Technical and mathematical details of this investigation are presented in two Appendices. A novel numerical procedure applied in this study is given in Appendix A. Useful analytic variational and Thomas–Fermi (TF) approximations are developed in the Supplementary material.

2. The Gross–Pitaevskii equation for a spin-1 condensate

In the mean-field approximation a quasi-1D or quasi-2D SO and Rabi coupled spin-1 ($F = 1$) BEC is described by the following set of three coupled GP equations, for N atoms of mass $\widetilde{m}$ each, in dimensionless form, for the spin components $F_z = \pm 1, 0$ [18–20]

$$i\partial_t \psi_{\pm 1}(\mathbf{r}) = \left[-\frac{1}{2}\nabla^2 + V(\mathbf{r}) + c_0\rho + c_2\left(\rho_{\pm 1} - \rho_{\mp 1} + \rho_0\right)\right]\psi_{\pm 1}(\mathbf{r}) + \left\{c_2\psi_0^2(\mathbf{r})\psi_{\mp 1}^*(\mathbf{r})\right\} + \frac{\Omega}{\sqrt{2}}\psi_0(\mathbf{r}) + \gamma f_{\pm 1}\,, \tag{1}$$

$$i\partial_t \psi_0(\mathbf{r}) = \left[-\frac{1}{2}\nabla^2 + V(\mathbf{r}) + c_0\rho + c_2\left(\rho_{+1} + \rho_{-1}\right)\right]\psi_0(\mathbf{r}) + \left\{2c_2\psi_{+1}(\mathbf{r})\psi_{-1}(\mathbf{r})\psi_0^*(\mathbf{r})\right\} + \frac{\Omega}{\sqrt{2}}\sum_{j=+1,-1}\psi_j(\mathbf{r}) + \gamma g\,, \tag{2}$$

where $\rho_j = |\psi_j|^2$ are the densities of components $j = \pm 1, 0$, and $\rho(\mathbf{r}) = \sum \rho_j(\mathbf{r})$ is the total density, $V(\mathbf{r})$ is the confining trap, ∂_t ($\partial_{\mathbf{r}} \equiv \{\partial_x, \partial_y, \partial_z\}$) is the partial time (space) derivative, and Ω (γ) is the strength of Rabi (SO) coupling. The SO coupling is a space derivative coupling described by the functions f and g, the details of which are given below. For brevity, the time dependence of the wave functions is not explicitly shown in Eqs. (1) and (2). In 1D, $\mathbf{r} = x$, $\nabla^2 = \partial_x^2 = \partial^2/\partial x^2$, in 2D, $\mathbf{r} = \{x, y\}$, $\nabla^2 = \partial_x^2 + \partial_y^2$, and in 3D, $\mathbf{r} = \{x, y, z\}$, $\nabla^2 = \partial_x^2 + \partial_y^2 + \partial_z^2$. In 3D, distances are expressed in units of the harmonic oscillator length $l \equiv \sqrt{\hbar/\widetilde{m}\omega}$, density ρ_j in units of l^{-3} and time in units of ω^{-1}, where $\omega = \omega_x$ is the x-axis trapping frequency. The potential is $V(\mathbf{r}) = (x^2 + \kappa^2 y^2 + \beta^2 z^2)/2$, where the trap aspect ratios are $\kappa = \omega_y/\omega$ and $\beta = \omega_z/\omega$. The dimensionless nonlinearities are $c_i = 4\pi N \mathcal{A}_i$, $i = 0, 2$, where $\mathcal{A}_0 = (a_0 + 2a_2)/3l$, $\mathcal{A}_2 = (a_2 - a_0)/3l$, with a_0 and a_2 being the scattering lengths in the total spin channels 0 and 2, respectively. For a pancake-shaped trap, with the strong trapping in z direction ($\beta \gg 1, \kappa$), a set of quasi-2D [15] equations can be obtained with $c_i = 2\sqrt{2\pi\beta}N\mathcal{A}_i$, with $V(\mathbf{r}) = (x^2 + \kappa^2 y^2)/2$. For a cigar-shaped trap, with the strong trapping in y and z directions ($\beta, \kappa \gg 1$), a set of quasi-1D [15] equations can be obtained with $c_i = 2\sqrt{\kappa\beta}N\mathcal{A}_i$, where $V(\mathbf{r}) = x^2/2$. In the following we will take $\kappa = 1$ and $V(\mathbf{r}) = \mathbf{r}^2/2$ in both 1D and 2D. In the programs the parameter κ in the potential is set to unity, but a different value can be introduced easily if needed.

In the presence of the SO coupling [16,17], we consider below the SO-coupling contributions $\gamma f_{\pm 1}$ and γg of Eqs. (1) and (2) in different cases. In 1D we consider three possible SO couplings in the Hamiltonian: $\gamma p_x \Sigma_x$, $\gamma p_x \Sigma_y$, and $\gamma p_x \Sigma_z$, where $p_x = -i\partial_x$ is the momentum operator and Σ_x, Σ_y and Σ_z are the irreducible representations of the x, y and z components of the spin-1 matrix Σ, with components

$$\Sigma_x = \frac{1}{\sqrt{2}}\begin{pmatrix} 0 & 1 & 0 \\ 1 & 0 & 1 \\ 0 & 1 & 0 \end{pmatrix}, \quad \Sigma_y = \frac{i}{\sqrt{2}}\begin{pmatrix} 0 & -1 & 0 \\ 1 & 0 & -1 \\ 0 & 1 & 0 \end{pmatrix}, \quad \Sigma_z = \begin{pmatrix} 1 & 0 & 0 \\ 0 & 0 & 0 \\ 0 & 0 & -1 \end{pmatrix}. \tag{3}$$

For the SO coupling $\gamma p_x \Sigma_x$ [21,22] in 1D, the SO coupling terms in Eqs. (1), (2) are $\gamma f_{\pm 1} = -i\widetilde{\gamma}\partial_x \psi_0(\mathbf{r})$ and $\gamma g = -i\widetilde{\gamma}\Big[\partial_x \psi_{+1}(\mathbf{r}) + \partial_x \psi_{-1}(\mathbf{r})\Big]$, respectively, where $\widetilde{\gamma} = \gamma/\sqrt{2}$. For the SO coupling $\gamma p_x \Sigma_y$ they are $\gamma f_{\pm 1} = \mp i\widetilde{\gamma}\partial_x \psi_0(\mathbf{r})$ and $\gamma g = i\widetilde{\gamma}\Big[\partial_x \psi_{+1}(\mathbf{r}) - \partial_x \psi_{-1}(\mathbf{r})\Big]$, respectively. For the SO coupling $\gamma p_x \Sigma_z$ they are [22] $\gamma f_{\pm 1} = \mp i\gamma\partial_x \psi_{\pm 1}(\mathbf{r})$ and $\gamma g = 0$, respectively.

In 2D we consider the general SO coupling term in the form $\gamma(\eta p_y \Sigma_x - p_x \Sigma_y)$, where $\eta = 1, -1$ and 0 for Rashba [23], Dresselhaus [24] and an equal mixture of Rashba and Dresselhaus SO couplings. In Eqs. (1), (2), the Rashba, Dresselhaus and an equal mixture of Rashba and Dresselhaus coupling terms in 2D are $\gamma f_{\pm 1} = -i\widetilde{\gamma}\Big[\eta\partial_y\psi_0(\mathbf{r})\pm i\partial_x\psi_0(\mathbf{r})\Big]$ and $\gamma g = -i\widetilde{\gamma}\Big[-i\partial_x\psi_{+1}(\mathbf{r})+i\partial_x\psi_{-1}(\mathbf{r})+\eta\partial_y\psi_{+1}(\mathbf{r})+\eta\partial_y\psi_{-1}(\mathbf{r})\Big]$.

The normalization and magnetization (m) conditions are given by

$$\int \rho(\mathbf{r})\,d\mathbf{r} = 1\,, \quad \text{and} \quad \int\Big[\rho_{+1}(\mathbf{r})-\rho_{-1}(\mathbf{r})\Big]\,d\mathbf{r} = m\,. \tag{4}$$

Condition (4) is useful to solve the problem for a fixed normalization when magnetization m along z direction is conserved, e.g., when the Hamiltonian commutes with spin-matrix Σ_z. However, in the presence of an SO coupling, that does not commute with Σ_z, magnetization is not conserved due to spin mixing dynamics involving spin-up and down states. In that case, time propagation is performed by imposing only the condition of conservation of normalization without fixing the magnetization during time propagation [25] and it leads to the result for the dynamically stable stationary state with a magnetization determined by the parameters of the model, which could often be zero. In this context, it should be noted that in experiments it is not possible to fix a preassigned value to magnetization, which is not a constant of motion.

The energy functional of the system is [18,19]

$$\begin{aligned} E =& \frac{1}{2}\int d\mathbf{r}\left\{\sum_j |\nabla_{\mathbf{r}}\psi_j|^2 + 2V(\mathbf{r})\rho + c_0\rho^2 \right. \\ &+ c_2\left[\rho_{+1}^2+\rho_{-1}^2+2\left(\rho_{+1}\rho_0+\rho_{-1}\rho_0-\rho_{+1}\rho_{-1}+\psi_{-1}^*\psi_0^2\psi_{+1}^*+\psi_{-1}\psi_0^{*2}\psi_{+1}\right)\right] \\ &\left. + 2\frac{\Omega}{\sqrt{2}}\Big[(\psi_{+1}^*+\psi_{-1}^*)\psi_0+\psi_0^*(\psi_{+1}+\psi_{-1})\Big] + 2\gamma\Big[\psi_{+1}^*f_{+1}+\psi_{-1}^*f_{-1}+\psi_0^*g\Big]\right\}. \end{aligned} \tag{5}$$

3. Details about the programs

We use the split time step Crank–Nicolson discretization rule for solving the GP equations (1) and (2), including the appropriate SO and Rabi couplings with strengths γ and Ω, respectively. This approach has been elaborated in detail in Ref. [1]. An initial (known) wave function at time t is used to calculate the wave function at time $t+\Delta$, after a small time step Δ. The advantage of this approach lies in the fact that different terms on the right-hand-side of Eqs. (1) and (2) can be treated successively. For example, the spatial derivative term involving $\nabla_{\mathbf{r}}$ can be treated independently of the nonlinear interaction terms and also of the SO and Rabi coupling terms. The terms in the square brackets of Eqs. (1) and (2) can be treated in a routined way elaborated in Ref. [1]. The terms in the curly brackets and those proportional to Ω in Eqs. (1) and (2) need special attention and are treated as in Appendix A. Finally, the γ-dependent SO coupling terms only involve first order space derivatives and are treated in a routined fashion.

The presented programs are straightforward modifications of the basic programs published in Refs. [1,2]. The three components of the wave function are accommodated by introducing a new index "L" in addition to the space indices in the corresponding arrays, i.e., the wave-function components are represented by CP(L,I,J) in 2D and CP(L,I) in 1D, where L $=1, 2, 3$ stands for the spin components $j=+1$, 0, and -1, respectively, and I and J denote discretized space points. The time propagation with respect to different terms in Eqs. (1) and (2) are dealt with in different subroutines. The kinetic energy term $(\nabla^2/2)$ is treated using the Crank–Nicolson discretization in subroutines COEF, LUX, and LUY in 2D, and in 1D in subroutines COEF and LU, as in Refs. [1,2]. The potential term and the diagonal part of the nonlinear terms in square brackets, proportional to c_0 and c_2, are treated in the subroutine CALCNU. The off-diagonal part of the nonlinear terms in curly brackets in Eqs. (1) and (2), explicitly considered in Eq. (A.1), is treated in the subroutine HERM, while the different SO coupling terms are treated in the subroutine SO. The conservation of the normalization and magnetization, as defined by Eqs. (A.6) and (A.7), is implemented in the subroutine RENORM. The energies are calculated in the subroutine ENERGY and expectation values of the condensate's cloud sizes are calculated in the subroutine RADIUS in 2D and LENGTH in 1D. The different modules (Subroutines and Functions) of the programs in 1D and 2D and their respective usage are presented in Table 1.

A description of the input parameters together with the output files with description is given in Table 2. Most of the parameters have the same meaning as in our previously published programs and the reader can refer to Ref. [6] for details. For an efficient performance on computers with multiple CPU cores, the programs have been parallelized using the OpenMP library. The number of threads (CPU cores) to be used is declared by the parameter NTHREADS, which should be equal to or less than the total number of available threads. If NTHREADS is set to zero, then all available CPU cores will be used. The parameters NSTP, NPAS, and NRUN denote different numbers of time iterations, the total number of iterations being the sum of these. If NSTP is different from zero, then the program starts the time propagation using an analytic initial function defined in the subroutine INITIALIZE. If NSTP is zero, the program reads an initial wave function for the calculation from input files, i.e., from the previously calculated files named `<code>-wave-fun-fin.txt`. In this way one can perform the imaginary- or real-time propagation with a pre-calculated wave function. The supplied programs use the pre-defined value `NSTP = 10` and use an analytic wave function as the initial state. When using a pre-calculated wave function by setting NSTP to zero, the number of space grid points N (1D) and NX, NY (2D) employed previously should match exactly the number of points used in the current program. The supplied programs assume equal numbers of space step points in both imaginary- and real-time propagation. The parameter OPT_SO selects the type of SO coupling. In 1D, OPT_SO $=1, 2, 3$ uses the SO couplings $\gamma p_x\Sigma_x$, $\gamma p_x\Sigma_y$, and $\gamma p_x\Sigma_z$, respectively. In 2D, OPT_SO $=1, 2, 3$ uses Rashba, Dresselhaus, and an equal mixture of Rashba and Dresselhaus SO couplings, respectively. The choice OPT_SO $=0$ corresponds to no SO coupling. The parameters MAG_0, GAM0 (GAMMA0 in 1D) and OMEGA0 denote magnetization, the strength of SO coupling γ and that of Rabi coupling Ω, respectively. The parameter OPT_PROP selects the type of time propagation: imaginary-time (1) and real-time (2). All input data are conveniently placed at the beginning of each program, as before [5]. After changing the input data in a program a recompilation is required. The output files are conveniently named such that their contents can be easily identified, following the naming convention introduced in Ref. [5]. For example, a file named `<code>-out.txt`, where `<code>` denotes imaginary- (im) or real-time (re) propagation, represents the general output file

Table 1
Different modules of the 1D and 2D programs and their usage.

	Module name	Type	Usage
1D	IMRE1D	MAIN	Main program
	INITIALIZE	Subroutine	Calculates or reads the initial function
	CALC_TRAP	Subroutine	Calculates the confining trap
	COEF	Subroutine	Calculates the coefficients of the Crank–Nicolson method
	SO	Subroutine	Propagates the spin–orbit coupling term in time
	LU	Subroutine	Crank–Nicolson time propagation
	HERM	Subroutine	Propagates the off-diagonal terms of the GP equation and the Rabi coupling term in time
	CALCNU	Subroutine	Propagates the diagonal parts of the GP equation in time
	LENGTH	Subroutine	Calculates the length of the condensate
	RENORM	Subroutine	Fixes the normalization and magnetization
	ENERGY	Subroutine	Calculates the energy of the condensate
	SIMP	Function	Performs integration by Simpson's rule
2D	IMRE2D	MAIN	Main program
	INITIALIZE	Subroutine	Calculates or reads the initial function
	CALC_TRAP	Subroutine	Calculates the confining trap
	COEF	Subroutine	Calculates the coefficients of the Crank–Nicolson method
	SO	Subroutine	Propagates the spin–orbit coupling term in time
	LUX	Subroutine	Crank–Nicolson time propagation in x variable
	LUY	Subroutine	Crank–Nicolson time propagation in y variable
	HERM	Subroutine	Propagates the off-diagonal terms of the GP equation and the Rabi coupling term in time
	CALCNU	Subroutine	Propagates the diagonal parts of the GP equation in time
	INTEGRATE	Function	Performs double integration in x and y
	RADIUS	Subroutine	Calculates the radius of the condensate
	RENORM	Subroutine	Fixes the normalization and magnetization
	ENERGY	Subroutine	Calculates the energy of the condensate
	SIMP	Function	Performs integration by Simpson's rule

Table 2
Name and description of input parameters and output files.

	Name	Description
Input	NSTP, NPAS, NRUN	Number of time iterations, NSTP = 0 reads initial function, NSTP $>$ 0 calculates initial function
	N, NX, NY	Number of space integration points
	NTHREADS	Number of threads used NTHREADS = 0 uses all threads
	C_0, C_2	Nonlinear input parameters (c_0, c_2)
	OPT_SO	Selects the type of SO coupling
	DX, DY	Space discretization steps
	OPT_PROP	Selects the type of time propagation imaginary-time (=1) or real-time (=2)
	OPT_ST	Selects initial function in 2D
	MAG_0	Magnetization (m)
	GAM0	Strength of SO coupling (γ)
	OMEGA0	Strength of Rabi coupling (Ω)
Output	im-out.txt	Input parameters, energy and size
	im-den-<desc>.txt	<desc>=ini initial & =fin final density
	im-phase.txt	phase of a 2D wave function
	im-wave-fun-<desc>.txt	<desc>=ini initial & =fin final wave function
	im-den-rad-<desc>.txt	<desc>=ini initial & =fin final radial density (2D)

containing input data, space and time steps DX, DY and DT, nonlinearity c_0 and c_2, energy, size, etc. The files <code>-den-ini.txt and <code>-den-fin.txt contain the initial and final components and total densities in different columns. In 1D (2D) these densities are functions of one (two) space point(s) placed in the first (and second) column(s) of the respective files. The densities ρ_{+1}, ρ_0, ρ_{-1}, and ρ can be found in the successive columns. The file <code>-den-rad-fin.txt stores the final linear radial densities ρ_{+1}, ρ_0, ρ_{-1}, and ρ for the 2D GP equation in different columns, while the space points are saved in the first column. The file <code>-wave-fun-fin/ini.txt contains the final/initial complex wave functions. For a 2D BEC, the file <code>-phase.txt contains the phases of the component wave functions in different columns, since the phase is important for the study of angular momentum of the respective states. The printing of some of these files, such as the initial density and wave function, is commented out in the programs, so that the supplied programs do not print these.

We provide below the beginning of the 1D program where the parameters are defined so that the reader can easily identify the different statements there. The 2D program is quite similar.

```
! Begin selection of input parameters
MODULE COMM_DATA
! SELECT # OF SPACE POINTS N AND # OF TIME ITERATIONS NSTP, NPAS & NRUN
! USE NSTP = 0 TO READ WAVE FUNCTION FILE FROM STDIN: < im-wave-fun-fin.txt
```

```
  INTEGER, PARAMETER :: N = 640, NX = N-1, NX2 = N/2
  INTEGER, PARAMETER :: NSTP = 10, NPAS = 1000000, NRUN = 100000
! INTEGER, PARAMETER :: NSTP = 0, NPAS = 1000000, NRUN = 100000
! Number of OpenMP threads, less than or equal to the maximum available cores.
  INTEGER, PARAMETER  :: NTHREADS = 0  ! NTHREADS = 0 uses all available cores
  REAL (8), PARAMETER :: Pi = 3.14159265358979D0
 END MODULE COMM_DATA
!****************************************************************
MODULE SPIN_PARS
 USE COMM_DATA, ONLY : PI
!******* SELECT  POLAR (C_2 > 0) OR FERROMAGNETIC (C_2 < 0) BEC ******
! REAL (8), PARAMETER :: C_0 = 241.d0, C_2 =  7.5d0  ! Anti-ferromagnetic
  REAL (8), PARAMETER :: C_0 = 885.d0, C_2 = -4.1d0  ! Ferromagnetic
END MODULE SPIN_PARS
!****************************************************************
MODULE GPE_DATA
 USE COMM_DATA, ONLY : N, Pi
 USE SPIN_PARS, ONLY : C_0, C_2
!*******************************************************************************
!*** SELECT OPTION FOR SO COUPLING AND STRENGTH GAMMA
! INTEGER,PARAMETER :: OPT_SO = 0; REAL (8), PARAMETER :: GAMMA0 = .00D0  ! No SO coupl.
  INTEGER,PARAMETER :: OPT_SO = 1; REAL (8), PARAMETER :: GAMMA0 = .500D0 ! Sigma_x p_x
! INTEGER,PARAMETER :: OPT_SO = 2; REAL (8), PARAMETER :: GAMMA0 = .500D0 ! Sigma_y p_x
! INTEGER,PARAMETER :: OPT_SO = 3; REAL (8), PARAMETER :: GAMMA0 = .500D0 ! Sigma_z p_x
!*******************************************************************************
 REAL (8), PARAMETER :: DX = 0.05D0  !  SELECT SPACE STEP DX
!!SELECT OPTION  FOR  PROPAGATION: IMAGINARY-TIME or REAL-TIME
 INTEGER, PARAMETER :: OPT_PROP = 1; REAL (8), PARAMETER :: DT = DX*DX*0.10D0 ! IMAG
! INTEGER, PARAMETER :: OPT_PROP = 2; REAL (8), PARAMETER :: DT = DX*DX*0.05D0 ! REAL
!!SELECT PARAMETERS OF MODEL
 REAL (8), PARAMETER :: MAG_0 = .400000D0,  ACCUR=1.D-6  ! Magnetization
 REAL (8), PARAMETER :: OMEGA0 = .000D0            ! Rabi and SO coupling
!*******************************************************************************
! End selection of input parameters
```

Below we provide a sample output file re-out.txt for the 2D program for the readers to familiarize.

```
  REAL-TIME PROPAGATION
  # of threads  =       16

  RASHBA SO coupling, GAMMA =  0.500000000000000
  RABI coupling Omega =  0.000000000000000E+000
  Nonlinearity C_0 = 482.000000, C_2 = 15.000000
  OPT_ST =  0.750000000000000

  Space and time steps: DX =  0.10000,  DY =  0.10000, DT =  0.2500E-03
  # of space steps: NX =   161,  NY = 161
  # of time steps:  NSTP = 0, NPAS = 80000, NRUN = 10000

             --------------------------------------------
               RAD(1)   RAD(2)   RAD(3)   Energy    MAG
             --------------------------------------------
NSTP iter.:    3.469    2.194    3.469    8.1969   0.0000
NPAS iter.:    3.468    2.193    3.468    8.1969  -0.0000
NRUN iter.:    3.469    2.195    3.469    8.1969  -0.0000
             --------------------------------------------

 Clock Time:     129 seconds
   CPU Time:    2048 seconds
```

Another crucial aspect for the execution of imaginary-time propagation to find the lowest-energy ground state is a proper choice of initial state with right symmetry property as the final state. Different types of states can be obtained for different sets of parameters. Without SO coupling, the solution is of the Gaussian type and a Gaussian function should be chosen as the initial state. For small Rashba or Dresselhaus SO-coupling strength γ ($\gamma \lessapprox 0.75$), the lowest-energy circularly-symmetric state of the three components of a quasi-2D SO-coupled anti-ferromagnetic (polar) spin-1 BEC is of the $(-1, 0, +1)$ or $(+1, 0, -1)$ type, where the numbers in the parenthesis represent the angular momentum of the vortices in the center of the components $j = +1, 0, -1$, respectively, with the

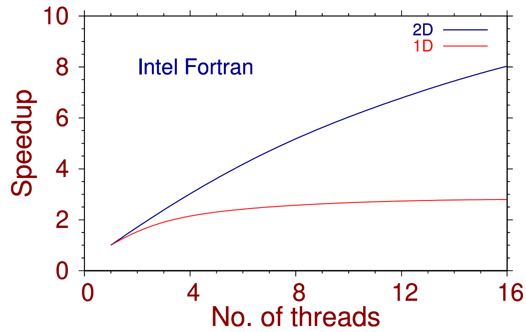

Fig. 1. Speedup of execution on a 20-core machine with two Intel Xeon E5-2650 processors (2 × 10 CPU cores) versus the number of threads used, for a quasi-1D and quasi-2D BEC for a typical run. The size of the space grid in 1D is 1000 and in 2D it is 200×200. The programs were compiled using the Intel Fortran compiler v. 19.0.4.243.

negative sign representing an anti-vortex. For a ferromagnetic spin-1 quasi-2D BEC these states are of the type $(0, \pm 1, \pm 2)$ for Rashba and Dresselhaus SO-couplings, respectively, in agreement with the consideration of Ref. [26]. For an equal mixture of Rashba and Dresselhaus SO couplings, for small γ, the lowest-energy ferromagnetic BEC states are of the Gaussian type without any vortices; the anti-ferromagnetic BEC states are of the stripe type with periodic 1D modulation in density. For an efficient computation, the vortices or anti-vortices are introduced in the initial wave functions when required. The vortex of angular momentum L is imprinted by taking the initial state as a Gaussian multiplied by the factor $(x+iy)^L$, and an anti-vortex by the factor $(x-iy)^L$. For large SO-coupling strength γ ($\gamma \gtrapprox 0.75$), the density of the lowest-energy ground state of the three components of an SO-coupled spinor BEC exhibits different patterns (not considered in this paper). The initial states in the 2D program have to be chosen accordingly. A stripe pattern is generated by multiplying an initial Gaussian state by $\sin(\gamma x)$ and $\cos(\gamma x)$. The user can change the initial state for a SO-coupled BEC by choosing the value of the parameter OPT_ST. For $\gamma <$ OPT_ST the states of type $(\mp 1, 0, \pm 1)$ and $(0, \pm 1, \pm 2)$ are chosen in anti-ferromagnetic and ferromagnetic phases, the upper (lower) sign corresponds to Rashba (Dresselhaus) SO coupling. In the anti-ferromagnetic phase, for $\gamma >$ OPT_ST, the stripe states are chosen as the initial state. However, to reproduce the results reported in this paper there is no need to change the parameter OPT_ST. For an equal mixture of Rashba and Dresselhaus SO couplings Gaussian-type initial states are appropriate for the ferromagnetic phase and stripe states for the anti-ferromagnetic phase.

If the imaginary-time propagation is performed, the programs run either by using an initial analytic input function (if `NSTP` is not set to zero), or by employing a pre-calculated wave function (if `NSTP` is set to zero). The real-time propagation can successfully work only if initialized with a meaningful wave function, usually assuming that `NSTP = 0` is set, and that the program will read a pre-calculated wave function by the earlier performed imaginary-time propagation. The calculation is essentially done within the `NPAS` time iteration loop. Another NSTP time iteration is accommodated to verify if the results converged by comparing the energies and sizes after NPAS and NSTP iterations. The source programs spin-SO-imre1d-omp.f90 (1D) and spin-SO-imre2d-omp.f90 (2D) are located in the directory `src` within the corresponding package directory `BEC-GP-SPINOR-OMP`. A `README.md` file, included in the corresponding root directory, explains the procedure to compile and run the programs in more detail using a makefile. In the beginning of each program the compilation commands are given for GNU, Intel, PGI, and Oracle (former Sun) Fortran compilers. They can be compiled by the `make` command using the provided `makefile` in the corresponding package root directory. Otherwise, they can be compiled by the commands given at the beginning of the programs using Intel, GNU, PGI, and Oracle FORTRAN compilers. The examples of produced output files can be found in the directory `output`, although some large density files are omitted, to reduce the software package size.

We conclude this section demonstrating the efficiency of our OpenMP parallelization scheme using the Intel compiler on a machine with 2×10 CPU cores in Fig. 1, where we plot the speedup versus number of threads. The speedup for n threads is defined as the ratio of clock time for a single thread to that for n threads. From Fig. 1 we find the clock time reduces with the increase of the number of threads, thus making the execution more efficient in a multi-core machine.

4. Numerical results

All calculations reported below were performed with the predefined space and time steps DX and DT in the programs: in 1D DX = 0.05, DT = DX*DX*0.1 (imaginary time) and DT = DX*DX*0.05 (real time); in 2D DX = 0.1, DT = DX*DX*0.1 (imaginary time) and DT = DX*DX*0.025 (real time). To increase the accuracy of calculation, the space step(s) DX and DY should be reduced and the total number of space discretization points N, NX, and NY increased proportionally.

The parameters of the GP equation c_0 and c_2 are taken from the following realistic experimental situations. For the ferromagnetic BEC the quasi-1D trap parameters are $l = 2.41927$ μm, $l_{yz} = 0.54$ μm and we use the following parameters of ^{87}Rb atoms: $N = 10,000$, $a_0 = 101.8a_B$, $a_2 = 100.4a_B$, where a_B is the Bohr radius. Consequently, $c_0 \equiv 2N(a_0 + 2a_2)l/3l_{yz}^2 \approx 885$ and $c_2 \equiv 2N(a_2 - a_0)l/3l_{yz}^2 \approx -4.1$. For the quasi-1D anti-ferromagnetic BEC we use the trap parameters $l = 4.7$ μm, $l_{yz} = 1.05$ μm following parameters of ^{23}Na atoms: $N = 10,000$, $a_0 = 50.00a_B$, $a_2 = 55.01a_B$. Consequently, $c_0 \approx 241$ and $c_2 \approx 7.5$. For the quasi-2D ferromagnetic BEC we use the following parameters of ^{87}Rb atoms: $N = 100{,}000$, $a_0 = 101.8a_B$, $a_2 = 100.4a_B$, [27] $l_z = 2.0157$ μm. Consequently, $c_0 \equiv 2N\sqrt{2\pi}(a_0 + 2a_2)/3l_z \approx 1327.5$ and $c_2 \equiv 2N\sqrt{2\pi}(a_2 - a_0)/3l_z \approx -6.15$. For the quasi-2D anti-ferromagnetic BEC we use the following parameters of ^{23}Na atoms: $N = 100{,}000$, $a_0 = 50.00a_B$, $a_2 = 55.01a_B$, [28] $l_z = 2.9369$ μm. Consequently, $c_0 \approx 482$ and $c_2 \approx 15$.

Although we will calculate the lowest-energy ground state by imaginary-time propagation, it is possible that in some cases for larger values of SO coupling strength γ (not considered in this paper) the imaginary-time approach may converge to a nearby excited state instead of the lowest-energy ground state for certain initial states. The symmetry, such as parity, of the initial state plays a vital role.

Table 3
Convergence of energies of harmonically trapped 1D and 2D spin-1 ferromagnetic (ferro) and anti-ferromagnetic (polar) BECs with change of space steps DX and DY. The parameters in 1D: $c_0 = 885$, $c_2 = -4.1$ (ferro) and $c_0 = 241$, $c_2 = 7.5$ (polar). The parameters in 2D: $c_0 = 1327.5$, $c_2 = -6.15$ (ferro), $c_0 = 482$, $c_2 = 15$ (polar). The SO-coupled results in 1D refer to the coupling $\gamma p_x \Sigma_x$ with $\gamma = 0.5$ and those in 2D correspond to the Rashba coupling with $\gamma = 0.5$. The parameters considered here are appropriate for a Rb and Na BEC with trap parameters of Ref. [25].

DX (=DY)	1D (ferro) energy	1D (ferro) % error	1D (polar) energy	1D (polar) % error	2D (ferro) energy	2D (ferro) % error	2D (polar) energy	2D (polar) % error
0.4	36.01167	0.00058	15.12364	0.00066	13.59737	0.00176	8.19636	0.00660
0.2	36.01146	0	15.12354	0	13.59759	0.00015	8.19687	0.00037
0.1	36.01146	0	15.12354	0	13.59761	0	8.19690	0
< 0.05	36.01146	0	15.12354	0	13.59761	0	8.19690	0

Table 4
Energies of harmonically-trapped spin-1 anti-ferromagnetic (polar) and ferromagnetic (ferro) quasi-1D and quasi-2D BECs for different values of magnetization m. In the quasi-2D case we consider only the circularly-symmetric states. The parameters in 1D: $c_0 = 241$, $c_2 = 7.5$ (polar) and $c_0 = 885$, $c_2 = -4.1$ (ferro), space step DX = 0.05, time step DT = 0.00025. The parameters in 2D: $c_0 = 482$, $c_2 = 15$ (polar) and $c_0 = 1327.5$, $c_2 = -6.15$ (ferro), space steps DX = DY = 0.1, time step DT = 0.0005. The SO-coupled (SO-cpld) results in 1D refer to the coupling $\gamma p_x \Sigma_x$ with $\gamma = 0.5$ and those in 2D correspond to the Rashba or Dresselhaus coupling with $\gamma = 0.5$. For systems with large nonlinearities the numerically obtained energy $E_{\rm num}$ lies between the TF [29] and variational (var) limit: $E_{\rm TF} < E_{\rm num} < E_{\rm var}$. The parameters considered here are appropriate for a Rb and Na BEC with trap parameters of Ref. [25].

	m	1D spinor	1D spinor [25]	1D spinor var	1D spinor TF	1D SO-cpld $\gamma = 0.5$	2D spinor	2D spinor var	2D spinor TF	2D SO-cpld $\gamma = 0.5$
Polar	0	15.2485	15.2485	15.7522	15.2239	15.1235	8.3605	8.8155	8.2577	8.1969
	0.1	15.2514	15.2514				8.3617			
	0.2	15.2599	15.2599				8.3652			
	0.3	15.2743	15.2743				8.3710			
	0.4	15.2945	15.2945				8.3793			
	0.5	15.3209	15.3209				8.3900			
	0.6	15.3537	15.3537				8.4033			
Ferro	0	36.1365	36.1365	37.3574	36.1243	36.0115	13.7420	14.5364	13.6723	
	0.0468	36.1365					13.7420			13.5976
	0.1	36.1365	36.1365				13.7420			
	0.2	36.1365	36.1365				13.7420			
	0.3	36.1365	36.1365				13.7420			
	0.4	36.1365	36.1365				13.7420			
	0.5	36.1365	36.1365				13.7420			
	0.6	36.1365	36.1365				13.7420			

An even-parity (odd-parity) initial state will find the lowest-energy state with even (odd) parity. For small γ there are only a few possibilities of symmetry and this problem does not appear for the results reported in this paper. But for larger γ, and especially in the quasi-2D case, there are states with many possibilities of symmetry and it may not be easy to know, a priori, the symmetry of the lowest-energy state. Hence, for large γ, it is advised to repeat the calculation with different initial states, so as to be sure that the converged state is indeed the lowest-energy ground state. In fact, any numerically computed final wave function, obtained with the same number of space points, can be used as the initial state for a new calculation.

Before we illustrate our results, we now study in Table 3 the convergence of our calculational scheme in 1D and 2D for SO-coupled ferromagnetic and polar BECs employing the above-mentioned parameters in 1D and 2D upon the reduction of space steps DX and (= DY) from 0.4 to 0.05. In this Table we display the energies, viz. Eq. (5), and the respective percentage numerical errors for four different sets of parameters in 1D and 2D. We see that upon a reduction of space step the energy value rapidly converges. The result for energy with space step 0.4 is already very accurate and the result remains unchanged to five significant figures after the decimal point for

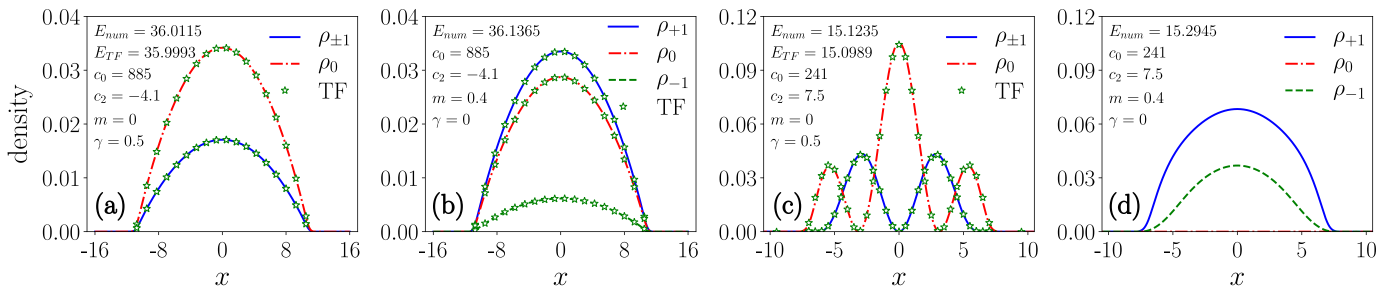

Fig. 2. Numerically calculated component density $\rho_j(x)$ (lines) and energy E of a quasi-1D harmonically trapped SO-coupled ferromagnetic BEC with nonlinearities $c_0 = 885$, $c_2 = -4.1$ and (a) $\gamma = 0.5$ and (b) $m = 0.4$, $\gamma = 0$, compared with the analytic TF result (chain of symbols). The same for an anti-ferromagnetic BEC with nonlinearities $c_0 = 241$, $c_2 = 7.5$ and (c) $\gamma = 0.5$ and (d) $m = 0.4$, $\gamma = 0$. The SO-coupling is $\gamma p_x \Sigma_x$ with $\gamma = 0.5$ in all cases. All densities are calculated by imaginary-time propagation employing Gaussian input functions. All results reported in this paper are in dimensionless units, as outlined in Section 2.

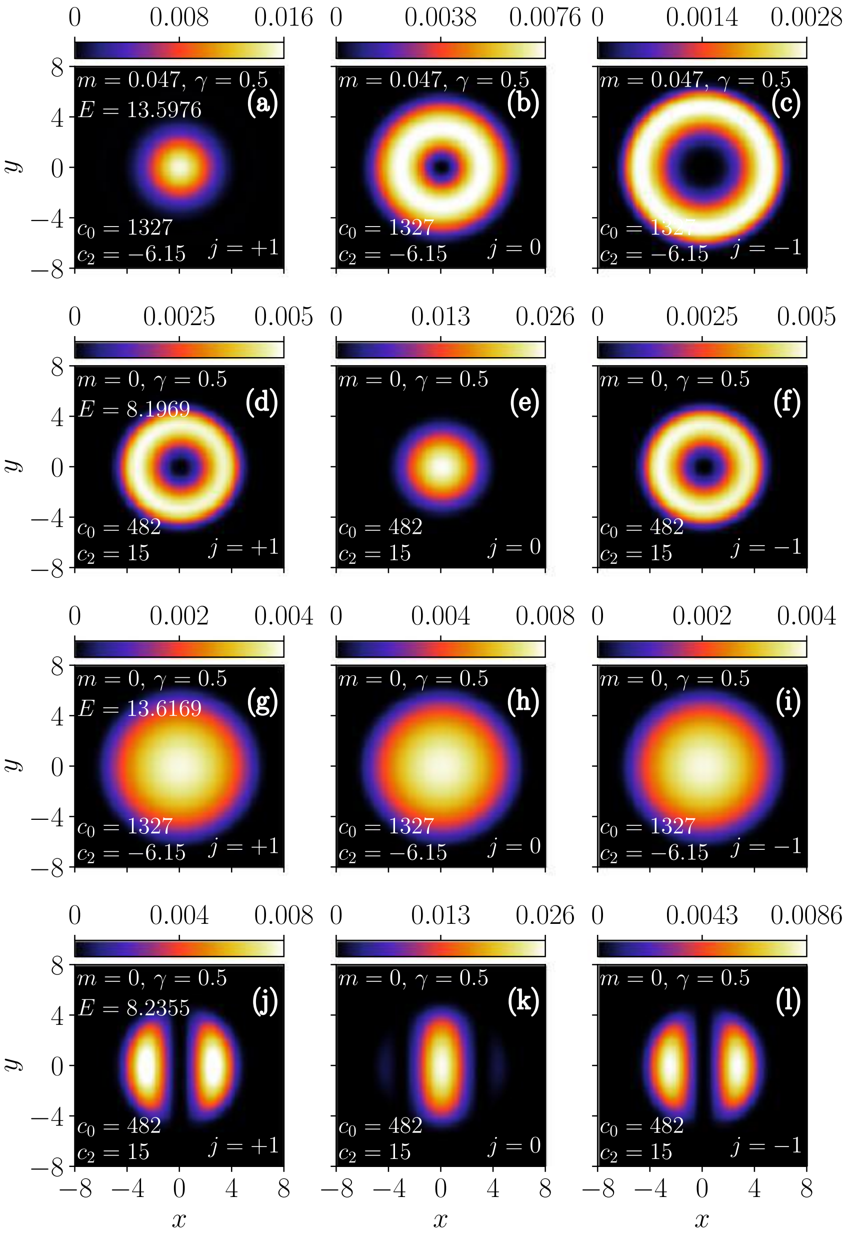

Fig. 3. Contour plots of numerically calculated component densities $\rho_j(x, y)$ for (a) $j = +1$, (b) $j = 0$, and (c) $j = -1$ of a quasi-2D harmonically trapped Rashba or Dresselhaus SO-coupled ferromagnetic BEC with nonlinearities $c_0 = 1327.5$, $c_2 = -6.15$, the SO-coupling strength $\gamma = 0.5$. (d)-(f) A Rashba or Dresselhaus SO-coupled anti-ferromagnetic BEC with nonlinearities $c_0 = 482$, $c_2 = 15$, and $\gamma = 0.5$. (g)-(i) A ferromagnetic BEC with $c_0 = 1327.5$, $c_2 = -6.15$, $\gamma = 0.5$ for an equal mixture of Rashba and Dresselhaus SO couplings. (j)-(l) An anti-ferromagnetic BEC with $c_0 = 482$, $c_2 = 15$, $\gamma = 0.5$ for an equal mixture of Rashba and Dresselhaus SO couplings. The numerical energies are displayed in plots (a), (d), (g), and (j).

space steps 0.1 and 0.05 both in 1D and 2D. In the following we will present results of our study with space steps 0.05 and 0.1 in 1D and 2D, respectively. The accuracy increases as the space-step is reduced, but a reduced value of space step requires a larger number of time iterations for convergence. Hence, it is computationally more economic to use a large space step.

In Table 4 we show the energy, viz. Eq. (1), of an anti-ferromagnetic and a ferromagnetic BEC in quasi-1D and quasi-2D traps for different values of magnetization m. For the quasi-2D trap, we consider only the circularly-symmetric states. In 2D the energies are the same for both Rashba and Dresselhaus SO couplings, although the underlying wave functions are different. The analytic TF and variational energies are also displayed, for comparison, as well as those from Ref. [25]. In the case of a ferromagnetic BEC without SO coupling, the energies are independent of m values, whereas in the anti-ferromagnetic case the dependence on m exists, as can be seen. In both cases the analytic TF and variational energies are independent of m. For condensates with large densities as in Table 4, where the TF results are reliable, the actual energies are larger than the corresponding TF values [29]. On the other hand, the variational energies are always larger than the actual energies. Hence for large nonlinearities, as we see in Table 4, the variational and TF energies define the two bounds for the actual, numerically calculated energy. In Table 4 we also present the numerically calculated energies for the SO-coupled BECs in 1D and 2D for $\gamma = 0.5$.

We show the numerically calculated and the TF component densities $\rho_j(\mathbf{x})$ of a quasi-1D harmonically trapped ferromagnetic SO-coupled BEC for $c_0 = 885$ and $c_2 = -4.1$, with $\gamma = 0.5$ in Fig. 2(a) and $m = 0.4$, $\gamma = 0$ in Fig. 2(b), along with the corresponding

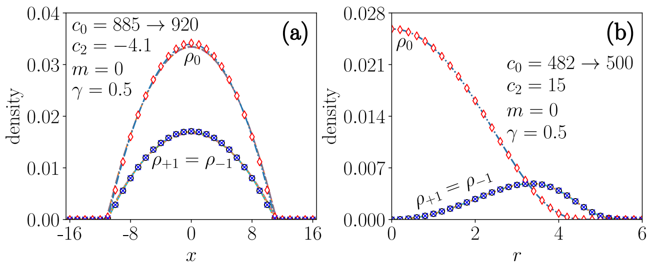

Fig. 4. (a) Numerically calculated component densities of the quasi-1D SO-coupled ferromagnetic BEC of Fig. 2(a) with $c_0 = 885$, $c_2 = -4.1$, $\gamma = 0.5$ during the real-time evolution at times $t = 50, 100, 150, 200$ (full lines), using the imaginary-time wave function as the initial state, compared with the converged imaginary-time densities shown in Fig. 2(a) (chain of symbols). The parameter c_0 was changed from 885 to 920 at $t = 0$. (b) Numerically calculated radial component densities of the quasi-2D anti-ferromagnetic Dresselhaus SO-coupled BEC of Fig. 3(d)–(f) with $c_0 = 482$, $c_2 = 15$, $\gamma = 0.5$ during the real-time evolution at times $t = 50, 100, 150, 200$ (full lines), using the imaginary-time wave function as the initial state, compared with the converged imaginary time densities (chain of symbols). The parameter c_0 was changed from 482 to 500 at $t = 0$.

energy values given by Eq. (5). All the states reported here are the lowest-energy ground states for a given set of parameters, obtained by imaginary-time propagation. The same quantities are shown for an anti-ferromagnetic BEC with $c_0 = 241$ and $c_2 = 7.5$, with $\gamma = 0.5$ in Fig. 2(c) and with $m = 0.4$, $\gamma = 0$ in Fig. 2(d). The SO coupling in both cases is of type $\gamma p_x \Sigma_x$ with $\gamma = 0.5$. These nonlinear parameters c_0 and c_2 were considered previously in Ref. [25]. These states are calculated with the analytic initial functions, included by setting NSTP $\neq 0$.

We now exhibit the density of a Rashba SO-coupled quasi-2D spinor BEC for $\gamma = 0.5$. The BEC components develop distinct angular momentum structure in this case. To illustrate this, we display in Fig. 3(a)–(c) the contour plots of densities of a ferromagnetic Rashba or Dresselhaus SO-coupled BEC. In Fig. 3(d)–(f) the corresponding contour plots of an anti-ferromagnetic Rashba or Dresselhaus SO-coupled BEC are shown, while Fig. 3(g)–(i) displays the same for a ferromagnetic BEC for an equal mixture of Rashba and Dresselhaus couplings. In Fig. 3(j)–(l) the plots are shown for an anti-ferromagnetic BEC, also for an equal mixture of Rashba and Dresselhaus couplings. In all cases the nonlinearities c_0 and c_2 are the same as in Table 3. The components $j = +1, 0$ and -1 in Fig. 3(a)–(c) have angular momentum $0, \pm 1, \pm 2$, respectively, for Rashba and Dresselhaus SO couplings. On the other hand, the components in Fig. 3(d)–(f) have angular momentum $\mp 1, 0, \pm 1$, respectively, for Rashba and Dresselhaus SO couplings. The angular momenta of the spinor components were found from the contour plot of the phases of the corresponding wave functions (not explicitly considered in this paper).

Finally, we demonstrate the dynamical stability of the imaginary-time results using the real-time propagation for a large interval of time. Using the converged imaginary-time wave function as the initial state, the real-time calculation is initiated after introducing a small perturbation, by changing the value of c_0 at $t = 0$ by a small amount. First we consider the quasi-1D SO-coupled ferromagnetic spinor BEC of Fig. 2(a) and perform a real-time simulation for 200 units of time by changing c_0 from 885 to 920. The component densities at times $t = 50, 100, 150$, and 200 are plotted in Fig. 4(a). The imaginary-time converged results (chain of symbols) are also shown, for comparison. Next we consider a quasi-2D anti-ferromagnetic Rashba SO-coupled spinor BEC with $c_0 = 482, c_2 = 15, \gamma = 0.5$, viz. Fig. 3(d)–(f), which is taken as initial state and a real-time propagation is performed for 200 units of time upon changing c_0 from 482 to 500 at $t = 0$. The radial component densities are plotted at times $t = 50, 100, 150$, and 200 in Fig. 4(b) together with the converged imaginary-time density (chain of symbols). The fact that all component densities in Fig. 4(a) and (b) for a quasi-1D and a quasi-2D BEC over a large interval of time are stable during the real-time propagation demonstrates the dynamical stability of the condensate.

5. Summary

We have presented efficient OpenMP FORTRAN programs for solving the GP equation for a three-component spin-1 spinor BEC and used these to calculate the densities and energies for various values of system parameters. Different SO and Rabi coupling terms can be included in the programs. We provide two sets of programs: one for a quasi-1D BEC and the other for a quasi-2D BEC. Each of these programs is capable of executing both the imaginary- and the real-time propagation. The imaginary-time propagation programs yield appropriate results in agreement with variational approximation in all cases [21,30]. We use the split-step Crank-Nicolson discretization to implement time propagation, relying on our earlier OpenMP FORTRAN programs of Ref. [6]. The GP equation can be solved by imaginary- or real-time propagation with an analytic wave function or a pre-calculated numerical wave function as the initial state. We stress that the convergence with one initial state could be much faster than with another initial state, and tailoring the input wave function using an analytic or a previously calculated numerical wave function is always an advantage. We have also presented the results for density and energy of different states and compared these with analytic variational and TF approximate results.

Declaration of competing interest

The authors declare that they have no known competing financial interests or personal relationships that could have appeared to influence the work reported in this paper.

Acknowledgments

We thank Dr. Sandeep Gautam for his kind interest and helpful comments. R.R. acknowledges University Grants Commission (UGC), India for the financial support in the form of UGC-BSR-RFSMS Research Fellowship scheme (2014–15). D.V. and A.B. acknowledge funding provided by the Institute of Physics Belgrade, through the grant by the Ministry of Education, Science, and Technological Development of the Republic of Serbia. The work of P.M. forms parts of sponsored research projects by Council of Scientific and Industrial Research (CSIR), India under Grant No. 03(1422)/18/EMR-II, and Science and Engineering Research Board (SERB), India under Grant No. CRG/2019/004059. S.K.A. acknowledges support by the CNPq (Brazil) grant 301324/2019-0, and by the ICTP-SAIFR-FAPESP (Brazil) grant 2016/01343-7.

Appendix A. Detailed numerical procedure

All terms in Eqs. (1) and (2), except the last terms containing explicit complex conjugation, have the form of a conventional diagonal GP equation for a three-component BEC, whose solution procedure employing the split-step method is well known. The last non-diagonal terms in Eqs. (1) and (2), as well as the Rabi coupling terms proportional to $\widetilde{\Omega}$ require special attention. In explicit matrix notation, the split-step equation that takes into account the last terms of Eqs. (1) and (2), together with the Rabi coupling terms proportional to $\widetilde{\Omega}$, can be written as

$$i\partial_t \begin{pmatrix} \psi_{+1}(\mathbf{r},t) \\ \psi_0(\mathbf{r},t) \\ \psi_{-1}(\mathbf{r},t) \end{pmatrix} = \mathbf{A} \begin{pmatrix} \psi_{+1}(\mathbf{r},t) \\ \psi_0(\mathbf{r},t) \\ \psi_{-1}(\mathbf{r},t) \end{pmatrix}, \quad \text{where} \quad \mathbf{A} = \begin{pmatrix} 0 & a & 0 \\ a^* & 0 & b \\ 0 & b^* & 0 \end{pmatrix}, \tag{A.1}$$

and $a = c_2\psi_-^*\psi_0 + \widetilde{\Omega}$, $b = c_2\psi_0^*\psi_+ + \widetilde{\Omega}$. The real eigenvalues of the Hermitian matrix $\mathbf{A}$ are $\lambda_1 = C = \sqrt{|a|^2 + |b|^2}$, $\lambda_2 = 0$, and $\lambda_3 = -C$, while the corresponding eigenvectors are $v_1 = (v_{11}, v_{12}, v_{13})^T = (a, C, b^*)^T$, $v_2 = (v_{21}, v_{22}, v_{23})^T = (b, 0, -a^*)^T$, and $v_3 = (v_{31}, v_{32}, v_{33})^T = (a, -C, b^*)^T$, respectively. For a sufficiently small time step Δ, the solution of Eq. (A.1) is given by

$$\begin{pmatrix} \psi_{+1}(\mathbf{r},t+\Delta) \\ \psi_0(\mathbf{r},t+\Delta) \\ \psi_{-1}(\mathbf{r},t+\Delta) \end{pmatrix} = \mathbf{V} \begin{pmatrix} e^{-i\Delta\lambda_1} & 0 & 0 \\ 0 & e^{-i\Delta\lambda_2} & 0 \\ 0 & 0 & e^{-i\Delta\lambda_3} \end{pmatrix} \mathbf{V}^{-1} \begin{pmatrix} \psi_{+1}(\mathbf{r},t) \\ \psi_0(\mathbf{r},t) \\ \psi_{-1}(\mathbf{r},t) \end{pmatrix}, \tag{A.2}$$

where

$$\mathbf{V} \equiv \begin{pmatrix} v_{11} & v_{21} & v_{31} \\ v_{12} & v_{22} & v_{32} \\ v_{13} & v_{23} & v_{33} \end{pmatrix} = \begin{pmatrix} a & b & a \\ C & 0 & -C \\ b^* & -a^* & b^* \end{pmatrix}, \qquad \mathbf{V}^{-1} = \frac{1}{2C^2} \begin{pmatrix} a^* & C & b \\ 2b^* & 0 & -2a \\ a^* & -C & b \end{pmatrix}. \tag{A.3}$$

In Eq. (A.2) the right-hand-side is considered known, since it is expressed in terms of the wave-function values at time t, and thus the wave function is easily propagated to time $t + \Delta$. In case of larger spins, if the matrix $\mathbf{A}$ of larger dimension cannot be analytically diagonalized, it can be diagonalized numerically by one of the many available subroutine packages.

When we consider the SO coupling terms proportional to $\widetilde{\gamma}$, they can be also evaluated at time t using the known wave-function values, and the corresponding split-step equations can be solved to propagate the wave functions to time $t + \Delta$. For example, in case of the $\gamma p_x \Sigma_x$ coupling in 1D, these are performed via

$$\psi_{\pm 1}(\mathbf{r},t+\Delta) = \psi_{\pm 1}(\mathbf{r},t) - \Delta\widetilde{\gamma}\partial_x\psi_0(\mathbf{r},t), \tag{A.4}$$

$$\psi_0(\mathbf{r},t+\Delta) = \psi_0(\mathbf{r},t) - \Delta\widetilde{\gamma}\Big[\partial_x\psi_{+1}(\mathbf{r},t) + \partial_x\psi_{-1}(\mathbf{r},t)\Big]. \tag{A.5}$$

In Eqs. (A.4) and (A.5) the right-hand-side at time t is known and hence the wave-function values at time $t + \Delta$ can be obtained from those at time t. All SO coupling terms are treated in the same fashion.

The simultaneous maintenance of the normalization and magnetization m, viz. Eq. (4), during the time propagation, given by Eqs. (4), is done following the procedure of Ref. [31], by rescaling the wave-function components after each time step Δ according to $\psi_j \to d_j\psi_j$, where

$$d_0 = \frac{\sqrt{1-m^2}}{\sqrt{N_0 + \sqrt{4(1-m^2)N_{+1}N_{-1} + m^2N_0^2}}}, \quad d_1 = \frac{\sqrt{1+m-d_0^2N_0}}{\sqrt{2N_{+1}}}, \quad d_{-1} = \frac{\sqrt{1-m-d_0^2N_0}}{\sqrt{2N_{-1}}}, \tag{A.6}$$

and $N_j = \int d\mathbf{r}\, \rho_j(\mathbf{r},t)$. However, when the SO coupling does not commute with Σ_z, we do not impose the condition of conservation of magnetization and the rescaling is done according to

$$d_0 = d_{+1} = d_{-1} = \frac{1}{\sqrt{N_0 + N_{+1} + N_{-1}}}. \tag{A.7}$$

Appendix B. Supplementary data

Supplementary material related to this article can be found online at https://doi.org/10.1016/j.cpc.2020.107657. It contains analytic variational and Thomas-Fermi approximations developed for the calculations presented in this paper.

References

[1] P. Muruganandam, S.K. Adhikari, Comput. Phys. Comm. 180 (2009) 1888.
[2] D. Vudragović, I. Vidanović, A. Balaž, P. Muruganandam, S.K. Adhikari, Comput. Phys. Comm. 183 (2012) 2021.
[3] R. Kishor Kumar, L.E. Young-S, D. Vudragović, A. Balaž, P. Muruganandam, S.K. Adhikari, Comput. Phys. Comm. 195 (2015) 117.
[4] R.K. Kumar, V. Lončar, P. Muruganandam, S.K. Adhikari, A. Balaž, Comput. Phys. Comm. 240 (2019) 74.

[5] L.E. Young-S, D. Vudragović, P. Muruganandam, S.K. Adhikari, A. Balaž, Comput. Phys. Comm. 204 (2016) 209.
[6] L.E. Young-S, P. Muruganandam, S.K. Adhikari, V. Lončar, D. Vudragović, A. Balaž, Comput. Phys. Comm. 220 (2017) 503.
[7] V. Lončar, A. Balaž, A. Bogojević, S. Škrbić, P. Muruganandam, S.K. Adhikari, Comput. Phys. Comm. 200 (2016) 406.
[8] V. Lončar, L.E. Young-S, P. Škrbić, S.K. Adhikari, A. Balaž, Comput. Phys. Comm. 209 (2016) 190.
[9] B. Satarić, V. Slavnić, A. Belić, A. Balaž, P. Muruganandam, S.K. Adhikari, Comput. Phys. Comm. 200 (2016) 411.
[10] D.M. Stamper-Kurn, M.R. Andrews, A.P. Chikkatur, S. Inouye, H.-J. Miesner, J. Stenger, W. Ketterle, Phys. Rev. Lett. 80 (1998) 2027.
[11] J. Stenger, S. Inouye, D.M. Stamper-Kurn, H.-J. Miesner, A.P. Chikkatur, W. Ketterle, Nature 396 (1998) 345.
[12] Y.-J. Lin, K. Jiménez-García, I.B. Spielman, Nature 471 (2011) 83.
[13] V. Galitski, I.B. Spielman, Nature 494 (2013) 49.
[14] D. Campbell, R. Price, A. Putra, A. Valdés-Curiel, D. Trypogeorgos, I.B. Spielman, Nature Commun. 7 (2016) 10897.
[15] L. Salasnich, A. Parola, L. Reatto, Phys. Rev. A 65 (2002) 043614.
[16] J. Dalibard, F. Gerbier, G. Juzeliūnas, P. Öhberg, Rev. Modern Phys. 83 (2011) 1523.
[17] Y. Li, Giovanni I. Martone, S. Stringari, Ann. Rev. Cold At. Mol., Vol. 3, World Scientific, 2015, p. 201 (Ch 5).
[18] Y. Kawaguchi, M. Ueda, Phys. Rep. 520 (2012) 253.
[19] V.I. Yukalov, Laser Phys. 28 (2018) 053001.
[20] S. Gautam, S.K. Adhikari, Phys. Rev. A 92 (2015) 023616.
[21] S. Gautam, S.K. Adhikari, Laser Phys. Lett. 12 (2015) 045501.
[22] S.K. Adhikari, Physica E 118 (2020) 113892.
[23] E.I. Rashba, Fiz. Tverd. Tela 2 (1960) 1224; Sov. Phys. Solid State 2 (1960) 1109, English Transla..
[24] G. Dresselhaus, Phys. Rev. 100 (1955) 580.
[25] W. Bao, F.Y. Lim, SIAM J. Sci. Comput. 30 (2008) 1925.
[26] T. Mizushima, K. Machida, T. Kita, Phys. Rev. A 66 (2002) 053610.
[27] E.G.M. van Kempen, S.J.J.M.F. Kokkelmans, D.J. Heinzen, B.J. Verhaar, Phys. Rev. Lett. 88 (2002) 093201.
[28] A. Crubellier, O. Dulieu, F. Masnou-Seeuws, M. Elbs, H. Knöckel, E. Tiemann, Eur. Phys. J. D 6 (1999) 211.
[29] P. Schuck, X. Viñas, Phys. Rev. A 61 (2000) 043603.
[30] S. Gautam, S.K. Adhikari, Phys. Rev. A 95 (2017) 013608.
[31] F.Y. Lim, W. Bao, Phys. Rev. E 78 (2008) 066704.

Supplementary Material: Spin-1 spin-orbit- and Rabi-coupled Bose-Einstein condensate solver

---

---

1. Variational and Thomas-Fermi approximations

The Gross-Pitaevskii equations (1) and (2) can be derived from the energy functional [1, 2]

$$
\begin{aligned}
E[\psi] = &\frac{1}{2}\int d\mathbf{r}\Bigg\{\sum_j |\nabla_{\mathbf{r}}\psi_j|^2 + 2V(\mathbf{r})\rho + c_0\rho^2 \\
&+ c_2\left[\rho_{+1}^2 + \rho_{-1}^2 + 2\left(\rho_{+1}\rho_0 + \rho_{-1}\rho_0 - \rho_{+1}\rho_{-1} + \psi_{-1}^*\psi_0^2\psi_{+1}^* + \psi_{-1}\psi_0^{*2}\psi_{+1}\right)\right] \\
&+ \frac{\Omega}{\sqrt{2}}\Big[(\psi_{+1}^* + \psi_{-1}^*)\psi_0 + \psi_0^*(\psi_{+1} + \psi_{-1})\Big] + \gamma\psi_{+1}^* f_{+1}(\partial_{\mathbf{r}}\psi_j) + \psi_{-1}^* f_{-1}(\partial_{\mathbf{r}}\psi_j) + \psi_0^* g(\partial_{\mathbf{r}}\psi_j)\Bigg\}. \qquad (1)
\end{aligned}
$$

We describe now two approximation schemes for the solution of the spinor GP equations, i.e., the variational approximation and the TF approximation [3, 4]. For a ferromagnetic BEC ($c_2 < 0$) without SO coupling, the ground-state densities are essentially proportional to each other, such that

$$
\psi_j(\mathbf{r}) = \alpha_j\widetilde{\psi}(\mathbf{r})\,,\ j = \pm 1, 0\,, \qquad (2)
$$

where α_j are complex numbers and the function $\widetilde{\psi}(\mathbf{r})$ is to be determined. If we substitute Eq. (2) into Eqs. (1) and (2), we obtain three equations for the unknown function $\widetilde{\psi}(\mathbf{r})$. For these equations to be consistent, one must have [3]

$$
\mu\widetilde{\psi}(\mathbf{r}) = \left[-\frac{1}{2}\nabla^2 + V(\mathbf{r}) + g\widetilde{\rho}(\mathbf{r})\right]\widetilde{\psi}(\mathbf{r})\,, \quad \widetilde{\rho}(\mathbf{r}) = |\widetilde{\psi}(\mathbf{r})|^2\,, \qquad (3)
$$

with $g = (c_0 + c_2)$ and subject to $\int\widetilde{\rho}(\mathbf{r})\,d\mathbf{r} = 1$, with μ the chemical potential and $|\alpha_{\pm 1}| = (1 \pm m)/2\,,\quad |\alpha_0| = \sqrt{(1 - m^2)/2}$. For the ground state of an anti-ferromagnetic BEC ($c_2 > 0$), the $j = 0$ component is absent, $\psi_0 = 0$. In this case Eq. (2) holds only for $m = 0$, with $|\alpha_{\pm 1}| = 1/\sqrt{2}, \alpha_0 = 0$, while Eq. (3) is again valid with $g = c_0$.

1.1. Variational approximation

Equation (3) can be derived by a minimization of the energy functional

$$
E = \frac{1}{2}\int d\mathbf{r}\left[\left|\nabla\widetilde{\psi}(\mathbf{r})\right|^2 + \mathbf{r}^2\left|\widetilde{\psi}(\mathbf{r})\right|^2 + g\left|\widetilde{\psi}(\mathbf{r})\right|^4\right]. \qquad (4)
$$

We consider the variational ansatz $\widetilde{\psi}(\mathbf{r}) = \left[w\sqrt{\pi}\right]^{-d/2}\exp\left(-\frac{\mathbf{r}^2}{2w^2}\right)$ where $d = 1$ in 1D and $d = 2$ in 2D, and w is a variational parameter. With this ansatz the energy functional becomes

$$
E = \frac{d}{4w^2} + \frac{dw^2}{4} + \frac{g}{2\left(w\sqrt{2\pi}\right)^d}\,. \qquad (5)
$$

The parameter w is obtained by a minimization of this energy.

1.2. Thomas-Fermi approximation

In absence of SO coupling ($\gamma = 0$), for an anti-ferromagnetic ($c_2 > 0$) spin-1 BEC with zero magnetization and for a ferromagnetic ($c_2 < 0$) spin-1 BEC, there are simple analytic solutions based on a decoupled mode TF approximation and we quote the results here. The density of the three components are given by [3]

$$\rho_j(\mathbf{r}) = |\alpha_j|^2 \rho_{\rm TF}(\mathbf{r}) = |\alpha_j|^2 \frac{L_d^2 - \mathbf{r}^2}{2g} \tag{6}$$

where $L_1 = [3g/2]^{1/3}$ in 1D and $L_2 = [4g/\pi]^{1/4}$ in 2D. In 1D this density is the linear density, while in 2D it is the radial density. The TF energy can be evaluated and yield $E_{\rm TF} = 3[3g/2]^{2/3}/10$ in 1D, and $E_{\rm TF} = 2\sqrt{g/\pi}/3$ in 2D.

Some useful analytic results can be obtained for a ferromagnetic BEC in 1D in the absence of magnetization ($m = 0$) for non-zero SO ($\gamma \neq 0$) and Rabi ($\Omega \neq 0$) coupling strengths. The ansatz for the wave function components is taken to be $\alpha_{\pm1} = e^{i\gamma x}/2, \alpha_0 = -e^{i\gamma x}/\sqrt{2}$ in Eq. (2), viz. Eq. (22) of Ref. [5]. For the SO coupling of the form $\gamma p_x \Sigma_x$, the total energy for small values of $\gamma \neq 0$ can be now evaluated to yield $\widetilde{E}_{\rm TF} = E_{\rm TF} - \frac{\gamma^2}{2} - \Omega$, where $E_{\rm TF}$ are the above calculated expressions in 1D or 2D. In this case the TF profile for the density remains unchanged for small γ and Ω. However, the energy gets modified due to the SO and Rabi couplings.

Additional useful analytic results can be obtained for an anti-ferromagnetic BEC in 1D in the absence of magnetization ($m = 0$) for a non-zero SO coupling strength ($\gamma \neq 0$). The ansatz for the wave function components in this case is taken to be $\alpha_{\pm1} = i\sin(\gamma x)/\sqrt{2}, \alpha_0 = -\cos(\gamma x)$ in Eq. (2), viz. Eq. (18) of Ref. [5]. For the SO coupling of the form $\gamma p_x \Sigma_x$, the total TF energy for small values of $\gamma \neq 0$ and $\Omega \neq 0$ can be now evaluated: $\widetilde{E}_{\rm TF} = E_{\rm TF} - \frac{\gamma^2}{2}$. The TF profile for the density remains unchanged for small γ, but the energy gets modified due to the SO coupling.

References

[1] Y. Kawaguchi, M. Ueda, Phys. Rep. 520 (2012) 253.
[2] V. I. Yukalov, Laser Phys. 28 (2018) 053001.
[3] S. Gautam, S. K. Adhikari, Phys. Rev. A 92 (2015) 023616.
[4] P. Schuck, X. Viñas, Phys. Rev. A 61 (2000) 043603.
[5] S. Gautam, S. K. Adhikari, Laser Phys. Lett. 12 (2015) 045501.

EPJ Data Science https://doi.org/10.1140/epjds/s13688-026-00674-x

Article in Press

Towards operational validation of LLM-agent social simulations: a replicated study of a Reddit-like technology forum

Received: 2 February 2026

Accepted: 3 June 2026

Published online: 11 June 2026

Cite this article as: Tomašević, A., Cvetković, D., Major, S. *et al.* Towards operational validation of LLM-agent social simulations: a replicated study of a Reddit-like technology forum. *EPJ Data Science* (2026). https://doi.org/10.1140/epjds/s13688-026-00674-x

Aleksandar Tomašević, Darja Cvetković, Sara Major, Slobodan Maletić, Miroslav Anđelković, Ana Vranić, Boris Stupovski, Dušan Vudragović, Aleksandar Bogojević, Marija Mitrović Dankulov

Towards Operational Validation of LLM-Agent Social Simulations: A Replicated Study of a Reddit-like Technology Forum

Aleksandar Tomašević[1*], Darja Cvetković[1], Sara Major[2], Slobodan Maletić[3], Miroslav Anđelković[3], Ana Vranić[1], Boris Stupovski[1], Dušan Vudragović[1], Aleksandar Bogojević[1], Marija Mitrović Dankulov[1]

[1*]Institute of Physics Belgrade, University of Belgrade, Belgrade, Serbia.
[2]Faculty of Philosophy, University of Novi Sad, Novi Sad, Serbia.
[3]Vinča Institute of Nuclear Sciences, University of Belgrade, Belgrade, Serbia.

*Corresponding author(s). E-mail(s): atomasevic@ipb.ac.rs;

Abstract

Validation of LLM-agent social simulations remains underdeveloped, with most studies relying on subjective assessments or single runs. We address this gap by running 30 independent 30-day simulations of a technology forum modeled on Voat's v/technology, using stateless Dolphin Mistral 24B agents on the Y Social platform, and evaluating operational validity across five dimensions: activity patterns, network structure, toxicity, topical coverage, and stylistic convergence. Against 30 matched, non-overlapping 30-day Voat comparison windows, results show overlapping 99% confidence intervals for unique users, root posts, and daily active users, while comments, average thread length, and mean toxicity remain higher in simulation. Both simulated and empirical networks exhibit core–periphery structure, though simulated cores are larger and more diffuse and repeated interactions are less frequent. Topic alignment is near-complete, but toxicity is misallocated across content layers: simulated root posts are substantially more toxic than real submissions, while simulated comments are less toxic than Voat comments. These findings demonstrate that LLM agents in platform-faithful environments can reproduce familiar online regularities, while systematic divergences—particularly those linked to stateless agent design and content-layer calibration—point to concrete directions for future improvement.

Keywords: Agent-based modeling, LLM Agents, Social simulation, Operational validity, Reddit, Voat, Online social networks

1 Introduction

Online social media is a primary arena for public discourse and collective sense-making, yet it often generates polarization, echo chambers, harassment, and norm violations that co-evolve with moderation and platform design [1–4]. Studying such dynamics *in vivo* is increasingly difficult in the post-API era due to ethical issues, limited access, and reproducibility constraints [5]. Complementary to traditional agent-based models, recent LLM-based simulations embed language-model agents in platform-faithful environments to test whether recognizable online regularities emerge from culturally informed, norm-conditioned interactions [6–8]. However, generating realistic contentious and toxic discourse remains challenging: standard aligned models tend toward politeness and consensus, poorly suited to simulate the disagreements and norm violations that drive real online dynamics. Moreover, generative agent-based modeling faces a central methodological challenge: rigorous validation frameworks remain underdeveloped [8, 9]. Recent reviews find that most studies rely on subjective "believability" assessments rather than quantitative comparison with empirical data, and nearly all report results from single simulation runs, akin to drawing conclusions from a single case study [8]. Newly emerging proposals thus caution against treating LLM outputs as substitutes for human participants without explicit empirical checks [10, 11]. Even when multi-user discussions appear realistic, conversational realism does not guarantee that platform-level structures and distributions match the target system [12–14]. Ground truth for validating that agents act as the persons they simulate is rarely accessible, and the black-box nature of LLMs intensifies interpretability problems [10].

As online platforms begin to mix people and artificial users in the future, human-machine interactions will become an increasingly important subject of social-science research [15]. Understanding what AI agents alone can produce in a social media environment provides a critical baseline for later human-machine studies, where even suspected machine presence may change how people act. The present work presents a first step toward this goal, by studying machine-machine interaction in a Reddit-like forum. We treat LLM agents as carriers of cultural knowledge and conversational norms [16], and ask whether they can share, remix, and react to content in ways that yield familiar social-media patterns, without agents being given a specific aim or over-control of their behavior.

We view LLM agents as cultural technologies rather than payoff-maximizing decision makers. Agents do not optimize utilities for posting, replies, or visibility. Instead, models trained on large conversational corpora encode social norms, roles, and routines. In practice, agents respond by what seems *appropriate* in context—given a topic, a thread position, and a persona—rather than by trying to achieve a specific goal through reward maximization. This lets us test whether compressed cultural knowledge alone can generate familiar online patterns when placed inside a realistic platform setting [7, 16, 17].

Concretely, we simulate Voat's v/technology forum on the Y Social platform using persona-based LLM agents and a fixed catalog of technology URLs drawn from the original forum. To preserve disagreement and the possibility of toxic speech, we use the uncensored Dolphin Mistral 24B model. Voat offers a useful baseline because its Reddit-like architecture and complete lifecycle data enable platform-faithful calibration, while v/technology itself is comparatively mainstream in topic content on the platform, though not necessarily in ideological composition.

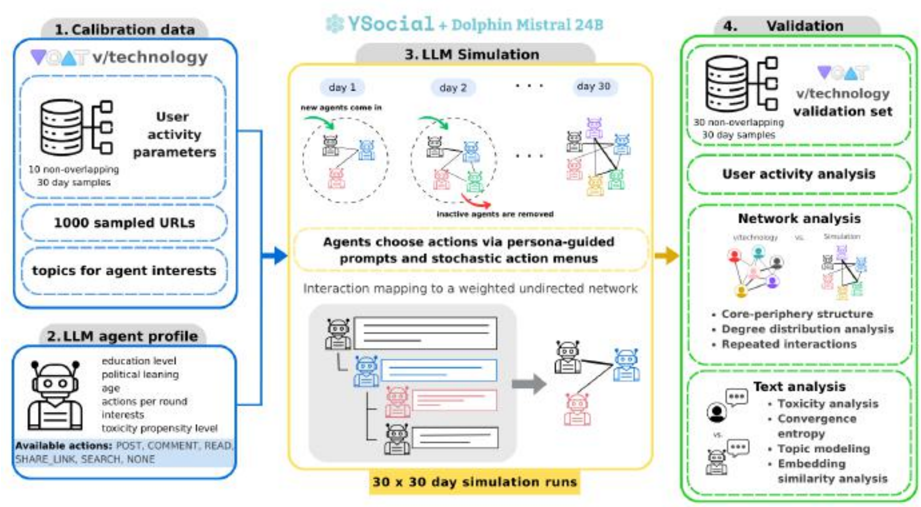

Fig. 1 Visual abstract of the simulation and validation workflow. The study proceeds through four stages. **(1) Calibration data:** we extract user activity parameters from 10 non-overlapping 30-day samples of Voat's v/technology subverse (MADOC dataset). **(2) LLM agent profile:** each agent is assigned a concise persona comprising education level, political leaning, age, per-round action budget, topical interests, and a toxicity propensity level. **(3) LLM simulation:** the Y Social platform runs 30 independent 30-day simulations using Dolphin Mistral 24B; agents enter and exit the population daily according to calibrated growth and churn rates, choose actions via persona-guided prompts and stochastic menus, and their interactions are mapped to a weighted undirected network. **(4) Result validation:** simulation outputs are compared against 30 matched, non-overlapping 30-day Voat windows across five dimensions: user activity patterns, network structure (core-periphery, degree distribution, repeated interactions), and text analysis (toxicity, convergence entropy, topic modeling, embedding similarity).

We calibrate population size, growth, posting and reply likelihoods, and per-round action budgets to Voat's v/technology and run 30-day simulations. We adopt a complex-systems view [6, 8]: can LLM agents, carrying compressed cultural knowledge and operating under realistic platform constraints, reproduce the emergent patterns characteristic of online communities?

We address this question through three validation dimensions, which also structure our contributions:

1. **Activity patterns:** Do simulated posting rates, thread dynamics, and user turnover match empirical distributions? We provide a platform-faithful baseline calibrated to Voat's v/technology with replicated validation across 30 runs.
2. **Network structure:** Does the interaction network exhibit comparable structural properties? We analyze core–periphery organization, degree distributions, and repeated interactions against 30 Voat comparison windows.
3. **Textual convergence:** Do agent outputs converge toward reference community characteristics? We evaluate toxicity distributions, topic alignment via embedding similarity, and linguistic convergence entropy.

Together, these provide an operational-validation framework and a reproducible approach to LLM-based community simulation. Figure 1 provides a visual overview of the complete workflow.

The paper proceeds as follows: we first discuss our view of LLMs as social agents, then outline the simulation approach and design, detail evaluation methods, present results on activity, network structure, toxicity, topics/embeddings, and stylistic convergence, and discuss implications and limitations.

2 LLMs as social agents

Recent work argues that large language models are best understood as cultural and social technologies: systems that reorganize and render usable the information produced by people, just as print, markets, and bureaucracies have historically done [17]. From this perspective, the key question is not whether models can be autonomous minds, but how they moderate access to, and coordination of, cultural repertoires and human knowledge. Much like earlier technologies, LLMs reduce complexity and function as mediators between individual actors and a broader repository of human knowledge and culture, simultaneously being shaped by existing epistemic and symbolic structures and reciprocally influencing them [16]. Their ability to compress and disseminate information and cultural scripts, while continually being refined by external input (primarily through reinforcement learning from human feedback) positions them as potentially central to processes of meaning-making in mediated publics. This implies a broad array of potential applications and risks yet to be fully understood [17].

What makes large models a particularly valuable resource for researchers seeking to understand social patterns is their ability to not only store, reproduce, and transform vast amounts of data, but, with careful prompting, to explicate and simulate the various social perspectives implicit in it [10, 18]. Consider the action space agents must navigate to produce realistic threads in a Reddit-like environment: a single discussion about operating-system updates might involve quoting prior turns, deploying in-group jargon (kernel, distro, drivers, telemetry), using irony ("just use

Arch"), and sustaining disagreement via reply chains, while reactions and feed visibility concentrate attention on the most contested subthreads. Classical ABMs often used parsimonious, deterministic, or rational-choice rules for tractability, but these are poorly suited for such culture-laden, role-dependent interaction [19]. LLM simulations replace payoff optimization with linguistic, norm-guided action selection. This allows them to capture the compression dynamics underlying human social coordination [20], i.e. the patterned reductions that emerge from the ways human groups process and distill cultural and cognitive complexity. Recent work in generative agent-based modeling has demonstrated the potential for language-mediated simulations [7], though our approach more specifically targets social media dynamics.

We adopt this norm-guided approach to LLM simulations, positing that agents' choices are generated via normative role expectations. By "LLM social agent" we mean a language-model-driven (artificial) participant in an online forum that produces context-appropriate posts and replies grounded in shared norms, roles, and routines. Here, the concept of *appropriateness* implies that agent action is grounded in socially agreed-upon rules and understandings about what normal, reasonable, and legitimate behavior is for actors within a given social setting [21]. Instead of pursuing utility or optimization of returns, agents must favor normative fit and try to adhere to the prescribed roles and expectations associated with their community.

Since models are trained on human culture, algorithmic fidelity implies that subpopulation-conditioned agents can inherit group-level beliefs and biases. This means they reproduce the social constructions—cultural codes, conventions, and inclinations—already present in the training data, rather than simulating generic human behavior. At the same time, because their "social cognition" is not experiential, they lack the ability to independently reinterpret norms and negotiate social constructs [17], meaning they can only mirror the objectified realities established by humans through socialization and social interaction [22]. By replicating existing cultural narratives, the inherent biases of agents thus closely resemble the real-world propensities of human actors within a given context [23]. This allows LLMs to act as carriers of established hermeneutic structures and enables concrete computational implementations of social construction [7, 24].

In Reddit-like forums where interaction is language-mediated and governed by explicit rules and tacit norms, we find this framing fits better than homo-economicus assumptions: agents generate choices by appropriateness and role, leveraging background cultural knowledge to ground identities, routines, and sense-making [6, 7, 16]. For instance, under a post about a Windows update and telemetry changes, an open-source/privacy-oriented persona may argue for Linux alternatives (e.g., Fedora/Debian) and emphasize control and transparency, while a gaming-oriented persona may defend Windows on the grounds of driver support and DirectX compatibility.

In line with ABM validation practice simulation succeeds [25–27], if it reproduces the right distributional patterns for the right reasons, not by matching individuals or text. Accordingly, we treat LLM agents as tools for studying norm-guided interactions, not as models of human cognition [7, 28]. Building on prior work, first, we design LLM agents' interactions as stateless micro-dialogues, without long-term chat memory.

Second, we expose content through a reverse chronological feed based on post popularity (ranked by reaction count with recency tie-breaking) within a 96-round visibility window, so engaged items are surfaced while decisions remain grounded in recent context. Third, we enforce a small stochastic action menu with heavy-tailed per-round budgets to induce unequal participation. Fourth, we prioritize mentions so local conversational dependencies propagate within threads even under stateless prompting. Fifth, we seed discussion from a fixed Voat link catalog to anchor topics culturally without external drift.

3 Methods

We implement the study using Y Social, a client–server digital twin of a Reddit-like forum [29]. The platform consists of three main components: (i) a stateful server that maintains users, content, and recommendation logic; (ii) a simulation engine that advances the simulation clock, schedules agents, and orchestrates interactions; and (iii) a stateless LLM (via Ollama) that generates agent actions and drafts text for posts and comments based on constraints provided by the engine. This architecture enables controlling global parameters such as feed design, initial agent population, simulation duration, activity probabilities, and churn or growth dynamics, while keeping the agent model fixed. At the same time, it logs the full system trajectory for evaluation. Implementation details of Y Social are beyond the scope of this paper; we refer readers to [29] for a detailed description.

3.1 Calibration Data

To inform the simulation design, we analyze samples from the MADOC dataset, drawn from real-world Voat data, with a focus on the v/technology subverse. This community centers on technology-related topics (e.g., Big Tech, AI, privacy, and gadgets), in contrast to the more political or conspiratorial content associated with other subverses.

We construct 10 non-overlapping 30-day calibration windows and, for each, compute daily activity, user dynamics, and thread characteristics. Table 1 summarizes the key metrics used to calibrate the simulation (see also Figure 1, panel 1). Validation in Results uses a separate set of 30 matched, non-overlapping comparison windows (each a single 30-day sample).

Taken together, these statistics describe a small and relatively volatile forum: approximately 576 unique users per 30-day window, with around 32 active users per day. Threads are shallow (≈ 1.07 comments per post), and overall activity is low ($\sim$618 posts and $\sim$665 comments per window). Daily inflow of new users is high ($\sim$60%), and churn is also high ($\sim$75%), indicating less persistent engagement. Accordingly, our simulation emulates a smaller, less stable forum with higher turnover and shorter, sparser conversations.

To ensure discussions are oriented toward technological topics, we built a fixed-URL catalog from Voat's v/technology dataset (MADOC). URLs are cleaned (tracking removed, domains normalized), deduplicated, and sampled to create a pool of 1,000 links (Table 2). These are stored locally and used during share-link actions.

Table 1 MADOC calibration samples summary for Voat v/technology (10 windows of 30 days each). Means and standard deviations are across windows.

Metric	Mean	SD	Min–Max
Users per 30 days sample	576.10	111.11	385–721
Active users per day	31.52	5.96	21.50–40.57
New users per day (%)	59.44	2.29	55.69–62.49
Churned users per day (%)	75.13	1.73	71.95–76.80
Comments per post	1.07	0.09	0.96–1.19
Posts per 30 d	618.40	109.69	440–819
Comments per 30 d	664.50	135.36	435–864
Active users on day 1	32.60	15.05	14–66

Table 2 Top calibration domains (from calibration URL list). Examples illustrate the kind of content used to seed/calibrate topics.

Domain	Count	Example (brief description)
`wikipedia.org`	170	Commodore International; Van Eck phreaking (encyclopedic background on legacy computing and security)
`github.com`	62	AdNauseam FAQ (ad tech resistance; extension documentation)
`bitchute.com`	60	Platform videos (alternative video hosting; tech/policy adjacent links)
`twitter.com`	31	Social link (tweet/profile referenced in discussion)
`hooktube.com`	26	Alternative YouTube front end (example video link)
`reddit.com`	21	r/zeronet (discussion hub for decentralized web)
`breitbart.com`	17	Policy/politics piece (tech adjacent regulatory context)
`puri.sm`	14	Librem 5 smartphone (privacy focused hardware product page)
`thepostmillennial.com`	3	Opinion/news piece (tech-adjacent policy/culture coverage)

3.2 LLM user profiles

In the simulation, the client instantiates a population of agents with sampled personas according to Table 3 (see also Figure 1, panel 2). Each agent is assigned a fixed locale (English, U.S.), an education level (from high school to PhD), an age between 18 and 60, and 2–5 topical interests drawn from a 10-category, technology-focused catalog. Agents are also assigned a toxicity propensity level, Absolutely No, No, Moderately, with probabilities (0.80, 0.15, 0.05). Personas generated like this are constructed for face validity rather than demographic representativeness and are not calibrated to Voat's user population.

Table 3 Agent population initialization parameters.

Attribute	**Values / Sampling**
Locale	English (American)
Education level	{high school, bachelor, master, phd}
Political leaning	Religious-Patriot Conservatives, Pro-Business Establishment Right, Anti-Elite Populist Right, Socially Moderate Right
Leaning fractions	0.35, 0.25, 0.25, 0.15
Age	18–60
Actions per activation (round)	1–10
Number of interests	2–5
Interests catalog	Social Media & Online Platforms; Internet Policy & Regulation; Artificial Intelligence; Electric Vehicles & Transportation; Software Development; Clean Energy & Sustainability; Cybersecurity & Privacy; Big Tech; Space Technology; Open Source Projects
Toxicity propensity level	{Absolutely No, No, Moderately}; weights 0.80, 0.15, 0.05

Political leaning is the only benchmark-informed constrained attribute; other persona dimensions are sampled broadly. To reflect the ideological profile of v/technology, agents are sampled from four right-of-center segments listed in Table 3, with fixed proportions (0.35, 0.25, 0.25, 0.15). These segments correspond to Pew's 2021 typology [30] and are intended to approximate the platform's alt-right–skewed environment [31]. The weights are heuristic and used to induce plausible stance variation, not to estimate Voat's true population.

Finally, each agent receives a per-round action budget between 1 and 10 actions, sampled from a truncated Zipf distribution (s=2.5). This produces a heavy-tailed activity pattern, most agents are minimally active, while a small minority contribute disproportionately, consistent with participation inequality observed in online communities [32, 33].

Each agent is able to perform the following actions:

1. **posting** creates a root submission and expands the content inventory;
2. **commenting** deepens a thread and alters its shape and lifetime;
3. **reading** represents lurking behavior and can shift interests based on consumed content;
4. **searching** steers engagement toward topical items (e.g., searching for Linux drivers or AI chips) and contributes to topic–interest alignment;
5. **share-link** propagates existing news posts or ingests fresh articles from the news database, seeding discussion around real-world content and changing the mix of link vs. text submissions.

Interests therefore form a simple feedback loop: they shape exposure and search, are injected into prompts through server-side state, and can themselves shift after engagement.

Agents interact with the platform through short, stateless micro-dialogues between an agent and a handler. The handler, implemented by the simulation engine, prompts the LLM to select actions and generate text. All agent decisions, picking actions from the menu, generating text, and reacting to content, are made by Dolphin Mistral 24B Venice Edition (model details are provided in SI Section S1). Importantly, agents have no internal memory; continuity is maintained via server-side state (e.g., thread history and user interests) passed into each prompt. They are also linked to a server-side recommender that provides content across rounds. The feed is non-personalized and ranked by popularity within a fixed visibility window: posts are ordered by total reactions (likes + dislikes), with ties broken by recency. Agents do not see their own posts, and items older than 96 rounds are excluded. When agents open a thread, the visible reply context is capped at $K = 3$ prior items. This uniform cap is a pragmatic context-window control for the smaller model setup rather than a behavioral claim that all users read equally deep. It keeps conversations grounded in the local thread context and the agent's persona. Variable-depth policies tied to agent activity or empirical thread-depth distributions are a natural future extension.

3.3 LLM simulation

The simulation runs in discrete daily iterations. At $t = 0$, we set the total duration of the simulation and initialize the population with 50 agents generated as described previously. Each day, a subset of agents is activated, and at the end of day t, we update the population using the rates from Table 4. First, a fraction of agents with the longest inactivity is removed (ties broken randomly). Then, new agents are added, sampled using the same initialization procedure, at a rate proportional to the pre-churn population.

The engagement of active agents is defined by weighted likelihoods, Table 4. The agent receives a small stochastic menu of actions, and via a prompt, selects one action at a time until its per-round budget is exhausted. Every turn presents exactly three options: `NONE` and two distinct actions sampled (without replacement) from five options—posting, reading, commenting, searching, and sharing links—according to engagement-likelihood weights. Chosen weights can reproduce the observed comment-to-post ratio, but the mapping from per-turn menus to realized comment volumes is not linear due to reply cascades and thread depth. Passive engagement, such as exposure without content creation, is not directly observable in the calibration data, so the read/search weights must be treated as heuristic. MADOC includes only a static subscriber-count field rather than a time-varying membership series, so it cannot support direct calibration of passive engagement dynamics.

Implementation details (e.g., prompt templates and client modifications) are available in the project repositories.[1]

[1]Upstream client: https://github.com/YSocialTwin/YClientReddit; modified client: https://github.com/atomashevic/YClient-Reddit

Table 4 Parameters for the Voat v/technology simulation.

Simulation setup		*Engagement likelihoods*	
Parameter	**Value**	**Parameter**	**Value**
Duration (days)	30	Post	0.5%
Starting agents	50	Link share	6.0%
New agents per day	30%	Comment	6.0%
Agent removal per day	90%	Read	40.0%
		Search	10.0%

3.4 Validation

Our validation strategy assesses whether the simulation produces realistic social media behavior across multiple dimensions. The simulation creates conversational interaction structures, as illustrated in Figure 2, which we analyze using five complementary methods: (1) *network analysis*, examining interaction topology and core–periphery structure; (2) *toxicity analysis*, quantifying harmful language with a RoBERTa classifier; (3) *semantic similarity*, measuring alignment between simulated and real texts; (4) *topic analysis*, comparing thematic structure via topic modeling; and (5) *convergence entropy*, testing whether agents exhibit stylistic accommodation within threads. To enable statistical inference, we conduct 30 independent simulation runs and compare activity, network, toxicity, and repeated-interaction metrics against 30 matched, non-overlapping 30-day Voat windows from v/technology. For the smaller sensitivity analyses reported in SI Section S10, we use percentile bootstrap 99% confidence intervals. Topic modeling uses a uniform random sample of 10,000 Voat threads drawn from the MADOC v/technology corpus, whereas item-level semantic retrieval uses the full Voat corpus as the reference base; convergence entropy is benchmarked against the external GPT-4o mini reference. Here we outline the methodological approach; SI Sections S6–S13 provide the full benchmark tables, additional network diagnostics, expanded toxicity robustness checks, alternative embedding visualizations, complete topic-match lists, and the benchmark power analysis.

Network analysis. We represent conversational interactions as an undirected, weighted graph to investigate network structure and core–periphery organization. Nodes are users; an edge connects a commenter to the author of the parent item (post or comment). Self-interactions are removed. Repeated exchanges increment an integer edge count that we then normalize to $[0, 1]$ by dividing by the maximum edge count in that graph. On the full graph, we report standard descriptors computed with the NetworkX Python library [34]: nodes, edges, density, mean degree, mean weighted degree (sum of normalized weights), and the weighted clustering coefficient. To identify a dense "core" coupled to a sparse "periphery", we fit a two-class hub–and-spoke stochastic block model (SBM) [35] to the largest connected component (LCC), which assigns each node to the core or periphery while capturing characteristic within- and between-connectivity. For the two tail-shape claims used in the activity and network results, SI Sections S7 and S8.4 report separate discrete fits for root-posts-per-user and positive degree using the Clauset–Shalizi–Newman procedure

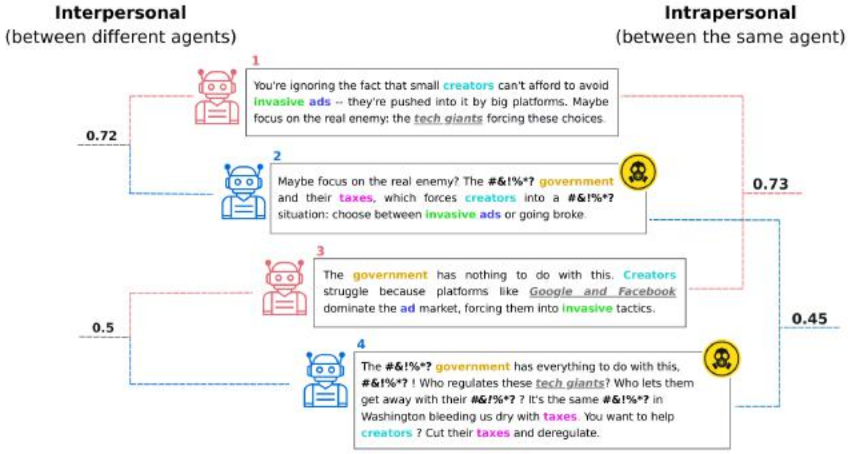

Fig. 2 Illustrative thread showing a discussion between two simulated agents (red and blue) on the topic of content creators and platform economics. Dashed lines on the left indicate *interpersonal* message pairs (between different agents), while those on the right indicate *intrapersonal* pairs (consecutive messages from the same agent), used to compute convergence entropies. Numbers denote cosine similarity scores between paired messages. Toxic messages are marked with a hazard icon. Colored and bolded words highlight recurring thematic terms (e.g., "creators," "government," "taxes," 'tech giants") whose repetition across the conversation contributes to lower entropy, reflecting linguistic convergence between agents.

[36], bootstrap goodness-of-fit, and likelihood-ratio comparisons against lognormal, truncated power-law, and exponential alternatives.

Toxicity. Toxic language is a salient feature of contentious online communities and one of our validation targets. Figure 2 provides an illustrative simulated thread in which some messages are marked with hazard icons. To compare toxicity patterns between simulation and Voat, we quantify harmful language in both corpora using a RoBERTa-based model trained on the ToxiGen benchmark [37].[2] Each text unit (root post, news-link share, or comment) receives a continuous toxicity score, interpreted as the model's probability that the content is toxic.

Semantic Similarity. Semantic similarity captures how closely two texts share meaning and vocabulary. Figure 2 illustrates this: messages that reuse terms like "creators," "government," and "taxes" yield cosine similarities of 0.72–0.73, while pairs with less thematic overlap score lower (0.45–0.5). To assess whether simulation content occupies similar semantic territory to Voat, we embed each text with a sentence-level encoder (SentenceTransformers, `all-MiniLM-L6-v2`) [38] and pair each simulation item to its nearest Voat counterpart by cosine similarity. We compute best-match scores separately for posts and for comments, and summarize with the mean, median, and counts above the designated thresholds.

[2] https://huggingface.co/tomh/toxigen_roberta

Topic analysis. To compare thematic structure between the simulation and Voat, we use thread-level topic modeling. Each thread (post and all its comments) is treated as a single document, representing the overall discussion theme and reducing noise from short replies. We fit BERTopic [39] separately on simulation threads and on a sample of Voat threads using sentence embeddings (all-MiniLM-L6-v2) with Hierarchical Density-Based Spatial Clustering of Applications with Noise (HDBSCAN) clustering; dimensionality reduction uses Uniform Manifold Approximation and Projection (UMAP) (cosine metric, random seed 42). Text is lightly cleaned (URL removal, whitespace normalization), while vectorization uses 1–2-gram features, and filters tokens to avoid very short or alphanumeric strings. For each fitted model, we retain topic labels and top words to aid interpretation, and represent each topic by a document-embedding centroid formed from up to 200 threads assigned to that topic.

Convergence entropy. We estimate convergence entropy to measure short-range stylistic alignment in simulation threads. Following accommodation theory and LM-based formulations [40, 41], an utterance is considered more convergent when it becomes more predictable given prior speech. In this information-theoretic view, lower entropy indicates stronger alignment, while higher entropy reflects more independent wording. As illustrated in Figure 2, repeated use of shared terms (e.g., "government," "taxes," "creators") increases predictability across turns, reducing entropy.

We operationalize this by extracting alternating two-speaker exchanges from reply trees and segmenting them into A–B–A–B chains (minimum length 3). From these, we construct ordered message pairs at different distances and distinguish between interpersonal pairs (different speakers) and intrapersonal pairs (same speaker baseline), as shown in Figure 2. Interpersonal pairs capture cross-agent alignment, while intrapersonal pairs reflect within-speaker consistency. The entropy is computed at the token level, with tokens extracted using a BERT encoder (`bert-base-uncased`). For each token in x, we compute its maximum cosine similarity to any token in y, and map these values to log-probabilities via a Normal kernel centered at 1 ($\sigma = 0.3$). Convergence entropy is then defined as:

$$H(x;y) = -\sum_i \exp(\ell_i)\,\ell_i$$

where ℓ_i are per-token log-probabilities.

We report entropy per token (H/T) and compare interpersonal and intrapersonal distributions, treating all comparisons as exploratory without formal significance tests. Additionally, for an external baseline, we compare against the relative convergence entropy reported by [41] for GPT-4o mini ($\mu = 0.2827 \pm 0.0002$ bits/token).

4 Results

4.1 User Activity

Across 30 independent runs, we observe steady increases over time in posts/day, comments/day, and unique active users/day. Day-to-day post and comment volumes can fluctuate because local agent decisions can trigger or dampen reply cascades, and user activity is inherently stochastic and not directly controllable; nonetheless, the resulting volumes remain within the same order of magnitude across runs and relative to Voat. Table 5 shows key metrics with 99% confidence intervals against the 30 matched Voat comparison windows: root-post volume, unique users, and daily active users overlap with Voat, while comments and average thread size remain higher in the simulations. Mean toxicity also sits above the Voat benchmark and is discussed separately below. SI Sections S6–S7 and S13 report the full benchmark statistics and the associated power analysis.

Table 5 Overall statistics for the Voat simulation (v/technology) vs. matched Voat comparison windows from MADOC. Simulation values are means with 99% t-distribution CIs from 30 runs; Voat values are means with 99% t-distribution CIs from 30 matched 30-day comparison windows.

Metric	**Simulation [99% CI]**	**Voat [99% CI]**	**Overlap**
Root posts (threads)	593 [577, 610]	569 [495, 642]	✓
Comments	904 [880, 927]	733 [601, 865]	–
Users (unique)	610 [595, 625]	591 [505, 677]	✓
Avg thread size	2.53 [2.48, 2.57]	2.25 [2.14, 2.36]	–
Mean toxicity	0.143 [0.135, 0.151]	0.119 [0.108, 0.129]	–
Daily active users	37.3 [36.6, 38.0]	32.7 [27.7, 37.6]	✓

The distribution of root posts per user is strongly right-skewed with a long upper tail (Figure 3). The simulation is more tightly concentrated around the low-activity mode, while Voat spreads much more mass into the extreme-participation tail. Formal discrete tail fits reported in SI Section S8.4 show that the simulated participation tail usually admits a power-law fit only above $x_{\min} = 2$, but a truncated power law fits better in all 30 runs, consistent with the bounded action-budget design. The empirical Voat participation tail is far more concentrated by distribution-free metrics (median top-1% share 30.4% versus 5.1%), yet only 9 of 30 windows support a pure power-law fit, indicating a heavier but more heterogeneous winner-take-most pattern across windows. Overall activity volumes remain of the same order of magnitude across the synthetic and real Voat settings, and both produce short threads (≈ 2 interactions on average). Interactions per active user remain low ($\approx$ 1–1.3), indicating brief daily engagement.

4.2 Network Analysis

Under the matched 30-window Voat benchmark, the simulated and real Voat graphs are both sparse and strongly right-skewed, but the upper-degree tails differ more sharply than log-log inspection alone suggests. Average degree is close (2.72 vs. 2.31; Table 6), while the simulation produces more nodes and edges, higher density (1.6×) and clustering (4.6×), and a smaller LCC share (66.5% vs. 85.3%). Formal fits in SI Section S8.4 show that 28 of 30 Voat windows are compatible with a power-law upper tail above $x_{\min} = 2$ (median $\alpha = 2.18$), compared with only 5 of 30 simulation runs; in most simulations, lognormal or truncated alternatives fit better and the fitted tail begins much farther out ($x_{\min} = 6$). Distribution-free concentration

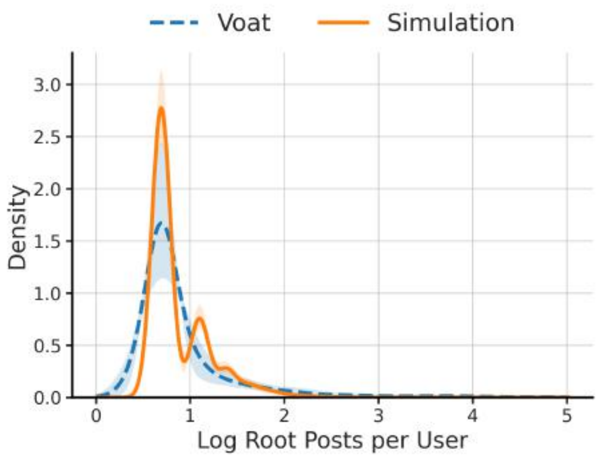

Fig. 3 KDE of log root posts per user (computed as log(1 + posts)): simulation (30 runs) vs. 30 matched 30-day Voat comparison windows. Curves show the mean density; shaded bands show the 5th–95th percentile range across runs/samples. Both corpora are strongly right-skewed, but the simulation has a sharper low-activity mode whereas Voat retains much more mass in the extreme participation tail. Formal tail-shape fits are reported in SI Section S8.4.

Table 6 Network analysis. Simulation values are means with 99% t-distribution CIs from 30 runs; Voat values are from 30 matched 30-day comparison windows.

Metric	Simulation [99% CI]	Voat [99% CI]	Ratio
Panel A: Interaction network descriptors			
Nodes	610 [595, 625]	486 [413, 560]	1.3×
Edges	831 [810, 851]	568 [464, 672]	1.5×
Avg degree	2.72 [2.66, 2.78]	2.31 [2.22, 2.39]	1.2×
Clustering coefficient	0.017 [0.015, 0.020]	0.004 [0.003, 0.005]	4.6×
Density	0.010 [0.010, 0.011]	0.007 [0.006, 0.007]	1.6×
LCC share	66.5% [65.7, 67.3]	85.3% [82.9, 87.7]	0.8×
Panel B: Core-periphery analysis (LCC)			
LCC nodes	406 [395, 416]	414 [352, 476]	1.0×
Core nodes	80 [75, 84]	22 [17, 26]	3.7×
Core % of LCC	19.6% [18.6, 20.7]	5.1% [4.2, 6.1]	3.8×
Core density	0.070 [0.065, 0.075]	0.100 [0.060, 0.140]	0.7×
Core-periphery density	0.020 [0.019, 0.021]	0.055 [0.040, 0.069]	0.4×

metrics point in the same direction: the top 1% of Voat nodes hold a median 20.3% of total degree versus 7.2% in simulation. The curve comparison makes the mismatch more specific: Voat puts more mass on degree-1 users and in the extreme right tail, whereas the simulation is elevated through the low-to-mid degree range. This

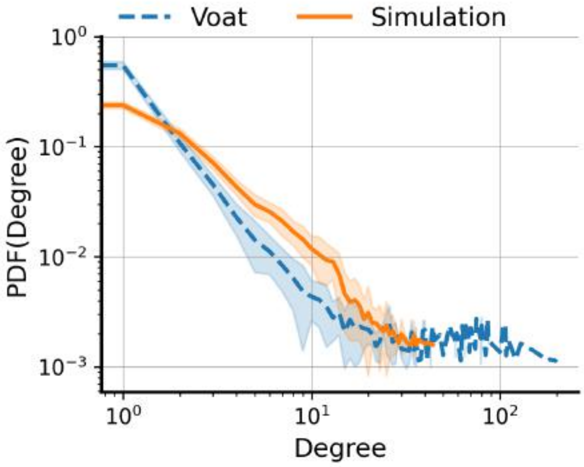

Fig. 4 Degree distribution (log-log) for the 60 networks in the main benchmark: 30 simulation runs and 30 matched 30-day Voat comparison windows. Both distributions are heavy-tailed, but formal fits in SI Section S8.4 show that a clean power-law upper tail is typical for Voat windows and uncommon in simulation. Voat places more mass on isolates and extreme hubs, whereas the simulation is more concentrated in the low-to-mid degree range.

indicates participation inequality in both corpora, but with weaker hub consolidation in the simulation. Because visibility is mediated by a popularity-plus-recency slate, exposure is coupled to feedback and can plausibly alter hub consolidation and clustering relative to purely chronological exposure [42, 43]. Despite non-overlapping CIs for clustering and density, both networks exhibit the same qualitative structure: sparse, heavy-tailed, with clear participation heterogeneity. Additional weighted-degree, repeated-interaction, hub-concentration, and formal tail-shape diagnostics are reported in SI Sections S8.1–S8.4.

Both datasets yield robust non-empty cores, confirming core-periphery structure in both simulation and Voat despite different core sizes. LCC sizes are essentially matched (406 vs. 414 nodes on average, with overlapping 99% CIs; Table 6), but the core share is much larger in the simulation (19.6% vs. 5.1% of the LCC). Core density is of the same order of magnitude in both datasets, with the real Voat core somewhat denser (0.100 vs. 0.070), while the core–periphery coupling remains markedly lower in the simulation (0.020 vs. 0.055), indicating a tighter, more strongly coupled hub set in the empirical network (Figure 5). Visually, the left-hand Voat panel concentrates a relatively small red core near the center, while the right-hand simulation panel spreads many more core nodes across a broader central region. Repeated interactions are also less frequent in simulation (5.90% vs. 8.70% of edges), reinforcing the view that the simulated network is structurally too diffuse even when its largest component is the right size. For visualization, Figure 5 shows the simulation–Voat pair with the smallest aggregate network-metric distance under the matched Voat benchmark, while Figure 7 shows the run with the highest mean comment-to-comment embedding cosine across

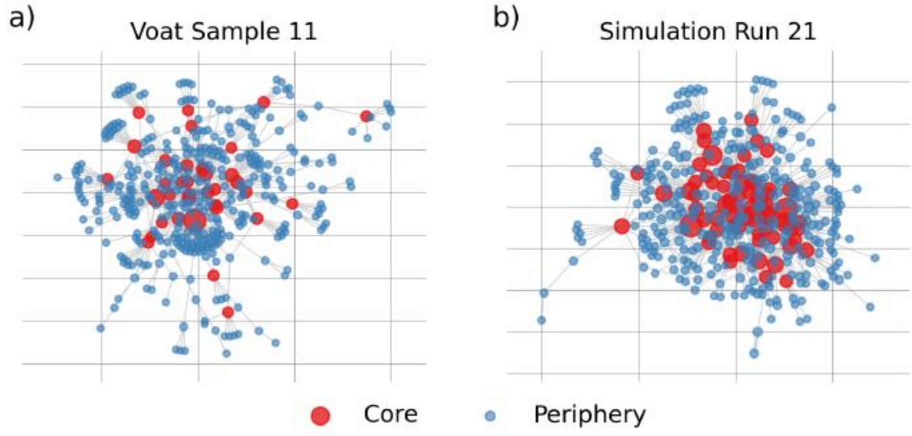

Fig. 5 Core–periphery structure on the largest connected component for the closest-matching pair under the matched Voat benchmark: Voat window 11 (left) vs. simulation run 21 (right). Red nodes indicate core members; blue nodes indicate periphery. Node sizes are scaled by weighted degree.

the 30 simulation runs. The key finding is structural: both networks exhibit clear core-periphery organization.

4.3 Toxicity Analysis

Toxicity distributions are broadly similar in shape (heavy near-zero mass with a positive tail), but against the Voat comparison windows the simulation is clearly more toxic overall: mean toxicity is 0.143 [0.135, 0.151] (99% CI) compared to Voat's 0.119 [0.108, 0.129], with non-overlapping intervals. Stratifying by content layer changes the interpretation of this mismatch. Simulated root posts/news items have mean toxicity 0.116 [0.107, 0.124], far above real Voat root submissions (0.0307 [0.0265, 0.0348]), whereas simulated comments are less toxic than Voat comments (0.161 [0.151, 0.170] vs. 0.189 [0.173, 0.205]). Comments are still more toxic than posts within the simulation (1.39×), so the posts-to-comments ordering is preserved, but the main discrepancy is not uniformly elevated comment toxicity; it is that toxicity is shifted upward into the root-post layer. Additional layer-specific benchmark statistics, the local one-at-a-time robustness panel, and the depth-shuffle permutation check are reported in SI Sections S9.1, S9.2, and S10. Within that separate 10-day setup, a neutral-persona variant reduces mean toxicity by 46.7% and the share of items above 0.5 by 51.5%, whereas a no-politics variant produces only modest shifts with overlapping intervals. Taken together, these results indicate that toxicity is sensitive to persona construction more broadly, not solely to the political-leaning field; comments/day, topic coverage, and convergence entropy remain close to baseline in the neutral-persona variant.

In both simulation and real Voat, comments are more toxic than root submissions. However, the layer contrast is much steeper in the empirical data. The simulation therefore captures the direction of the posts-to-comments gradient while misallocating

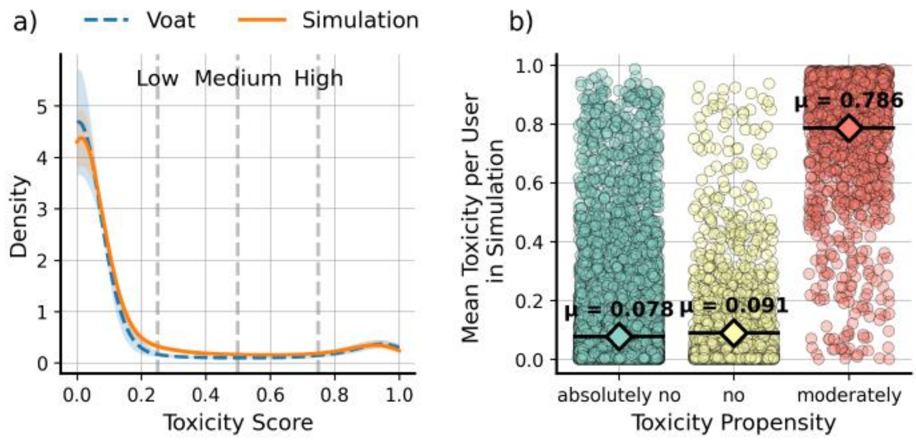

Fig. 6 Toxicity analysis. (a) KDE of item-level toxicity scores pooled across the 30 simulation runs and the 30 matched Voat comparison windows used in the main benchmark. (b) Simulation-only mechanism check: mean toxicity per user stratified by toxicity propensity trait across 30 runs. Diamonds mark group means.

its magnitude, overproducing toxic openings and underproducing the more toxic reply layer seen in Voat. A depth-shuffle permutation test reported in SI Section S9.2 yields Spearman $\rho = 0.122$, which falls inside the permutation null 95% interval [0.121, 0.127] ($p = 0.896$), indicating that this apparent depth pattern is explained by the post/comment split rather than by within-thread escalation.

Stratifying by agent propensity level confirms that the toxicity ladder mechanism produces the intended behavioral gradient (Figure 6b). Agents assigned "moderately toxic" propensity produce higher mean toxicity per user than those labeled "no toxicity," who in turn exceed "absolutely no toxicity" agents. This ordering is consistent across all 30 runs and demonstrates that toxicity variation is not merely an artifact of the base model's tendencies but follows from designed persona traits. The finding strengthens the mechanistic interpretation: agents carry norm-guided dispositions that shape content generation in predictable ways.

Figure 2 shows an adversarial exchange in which toxic messages (marked with hazard icons) co-occur with repeated thematic terms as agents adopt contrasting positions on shared content. The figure therefore illustrates confrontational language and lexical reuse within a thread, not a measured escalation effect.

4.4 Text Analysis

We compare thread-level topics discovered from simulation threads (582 threads per run; 24.2 topics on average [99% CI: 23.1, 25.3]) to topics extracted from a sample of 10,000 Voat threads (140 topics). Using sentence embeddings (all–MiniLM–L6–v2), we form topic centroids ($\leq$200 threads/topic) and compute cosine similarity between simulation and Voat centroids, retaining matches at or above 0.50. Coverage is

Table 7 Selected thread-level topic matches between simulation and Voat (MADOC). Values are cosine similarities between topic centroids (all–MiniLM–L6–v2); threshold 0.50. Representative subset shown (run01); SI Sections S12.1 and S12.2 report the full thread-level topic statistics and the complete run01 match list.

Simulation topic	Closest Voat topic	Cos
Big Tech regulation & data privacy	Data privacy & breaches	0.82
Platform speech (BitChute/censorship)	Copyright & TPP	0.74
Energy, solar & EVs	Tesla, solar & electric energy	0.75
Media bias & news	Trump, politics & media	0.73
Open source & Linux	Linux & Windows (desktop)	0.73
Gaming PCs & hardware	AMD, Intel & Ryzen CPUs	0.72
Privacy software (Proton/Apple)	Apple, iPhone & repair	0.71
AI ethics (Bostrom)	Artificial intelligence & humanity	0.69

Table 8 Embedding similarity between simulation and Voat (nearest neighbor by cosine). Values are means with 99% CIs from 30 runs.

Pair	Mean [99% CI]	Median [99% CI]
Post → post	0.607 [0.605, 0.609]	0.612 [0.609, 0.614]
Comment → comment	0.573 [0.566, 0.580]	0.568 [0.560, 0.576]

near-complete: 99.6% of simulation topics have at least one Voat match. The top 1 match per simulation topic yields mean cosine 0.687 [0.680, 0.693] across 30 runs. SI Sections S11.1–S11.2 and S12.1–S12.2 report the alternative embedding visualizations, full topic statistics, and complete run01 topic list for the same semantic comparison.

Core technology themes transfer well at the thread level: privacy/security, energy and EVs, AI discourse, and platform/Big Tech themes show consistent alignment, with best pairs ranging from 0.69 to 0.82 (Table 7). Notably, the aligned themes closely mirror the agent interest catalog in Table 3 (Social Media & Online Platforms; Internet Policy & Regulation; Artificial Intelligence; Electric Vehicles & Transportation; Software Development; Clean Energy & Sustainability; Cybersecurity & Privacy; Big Tech; Space Technology; Open Source Projects), consistent with persona interests and link seeding shaping the discussion mix. Taken together, these results support content validity on core tech themes.

Embedding similarity (nearest–neighbor)

We complement topic matching with an item-level nearest-neighbor analysis. Using all-MiniLM-L6-v2 embeddings, each simulation text (posts and comments analyzed separately) is paired to its closest Voat counterpart by cosine similarity. Across 30 runs, posts show moderate-to-good alignment (mean cosine 0.607 [0.604, 0.609]) while comments are somewhat lower (0.573 [0.566, 0.580]).

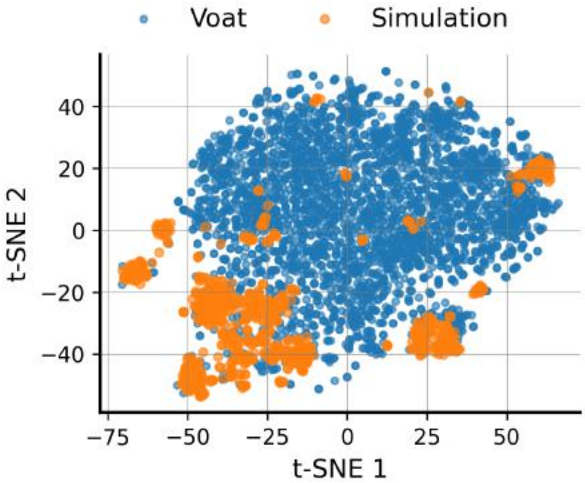

Fig. 7 t-SNE projection of comment embeddings for the simulation run with highest mean comment similarity (run11) against the full Voat comment corpus, using all-MiniLM-L6-v2 embeddings and a cosine metric. Even in this best-matching run, the simulation forms several compact clusters around the edges of the broader Voat cloud, indicating moderate proximity but clear residual separation. For context, the run reaches mean cosine 0.606 for posts and 0.598 for comments.

Cosine similarities above 0.5 correspond to human-judged similarity scores indicating topical relatedness, based on our STS-B calibration (see Methods, Embedding similarity). Posts align more closely than comments, consistent with topical alignment for news-sharing behavior and more varied commentary styles. A two-dimensional t-SNE projection (perplexity 80; cosine) of the best-matching comment run makes the residual mismatch visible: the simulated comments occupy several compact clusters around the margins of the broader Voat cloud rather than collapsing into a single shared manifold (Figure 7). The visual fit is therefore consistent with moderate semantic proximity, but not with full distributional overlap. SI Sections S11.1 and S11.2 provide a UMAP view and a side-by-side UMAP/t-SNE comparison for the same selected comment run.

4.4.1 Convergence entropy

We quantify stylistic alignment within A-B alternating reply chains using convergence entropy H (lower values indicate higher convergence). Across 30 runs, mean entropy per token is 0.275 [0.270, 0.280] (99% CI), which falls below the GPT-4o mini baseline of 0.2827 bits/token reported by [41] (Figure 8a). This indicates greater stylistic convergence in simulation threads than in the external benchmark. Figure 8b shows that most individual runs fall below this baseline, confirming the pattern is robust across replications.

Crucially, this convergence is a consequence of threaded discussion structure, not stylistic persona adaptation. Entropy rises monotonically with turn distance: H

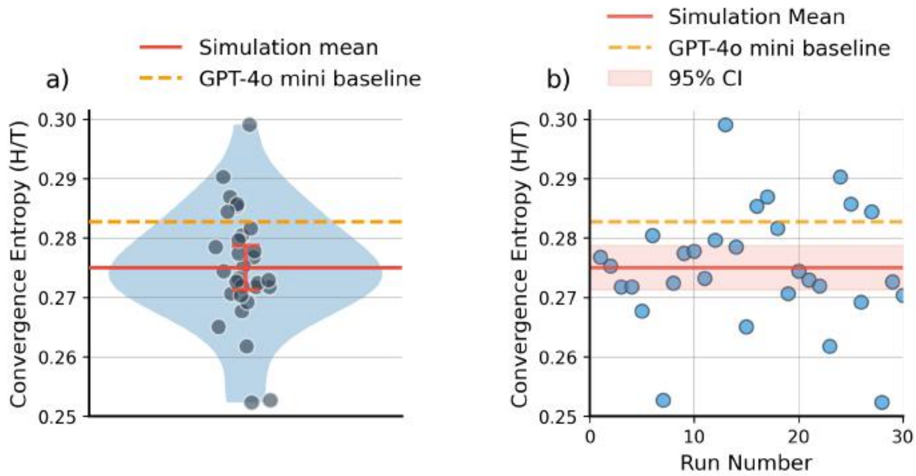

Fig. 8 Convergence entropy analysis with benchmark comparison. (a) Violin plot of entropy per token (H/T) across 30 simulation runs; the simulation mean (red line) falls below the GPT-4o mini baseline (orange dashed). (b) Run-by-run entropy per token with a descriptive 95% band around the simulation mean; most runs fall below the external baseline, indicating greater stylistic convergence (lower is more convergent). This band is a visualization aid and distinct from the 99% t-based benchmark intervals used elsewhere in the paper.

increases from 0.272 [0.267, 0.277] at lag 1 to 0.279 [0.272, 0.286] at lag 2 and 0.287 [0.278, 0.297] at lag 3, then plateaus at lag 4+ (0.287 [0.272, 0.302], n = 13). This pattern exactly traces the configured context window (K = 3): as prior turns drop out of context, entropy rises; once all context is lost, it plateaus. Interpersonal pairs show marginally lower entropy (0.273) than intrapersonal pairs (0.279), but the lag-driven decay dominates both. There is no evidence of persistent stylistic convergence between agent personas; the accommodation effect is purely local, mediated by the architectural context window rather than any form of stylistic learning or identity alignment.

5 Discussion

This study addresses a central gap in the generative agent-based modeling literature: the lack of rigorous, replicated validation against empirical data (Figure 1). Where prior work has relied primarily on subjective believability judgments or single-run demonstrations [8, 9], we provide quantitative comparison with matched empirical samples, uncertainty quantification through 30 independent replications, and explicit tracing of divergences to architectural choices. This positions our work within calls for operational validity, the requirement that simulations capture underlying mechanisms of target systems, not merely surface features [8, 10].

Our standard is operational validity: simulated aggregate distributions and meso-level structures should resemble those of the reference community at comparable scales, without one-to-one reproduction of specific users or texts. Using 99% t-based confidence intervals from 30 replications and 30 matched 30-day Voat windows, we find partial but uneven evidence for this alignment. Root-post volume, unique users, daily active users, and LCC size overlap with Voat, while comment volume, average thread size, mean toxicity, and most global network statistics do not. Given the current replication depth, these overlaps should be read as coarse-scale agreement rather than close quantitative equivalence; the power analysis in SI Section S13 shows that smaller differences remain difficult to detect at $\alpha = 0.01$. The closest fit is therefore at the level of community scale and activity rhythms: daily trajectories remain plausible (Table 5), threads are short (Table 5), and participation remains strongly right-skewed with a long upper tail (Figure 3). Network structure remains in the right regime but systematically shifted, with average degree about 1.2× the empirical value, density 1.6×, and clustering 4.6× (Table 6); the tail-shape analysis in SI Section S8.4 further shows that empirical degree windows are much closer to a clean power-law regime than the simulated ones. Content still aligns semantically: topics show near-complete coverage (99.6%; Table 7), embedding similarities remain moderate-to-good (0.61 posts, 0.57 comments; Table 8; Figure 7), and short-range stylistic accommodation is present and decays with lag. Run-average H/T also remains below the GPT-4o mini baseline reported by [41] (Figure 8). Taken together, these results show that Y Social reproduces scale and thematic coverage more convincingly than interaction structure, toxicity allocation, or persistent conversational coupling.

Despite this broad alignment, several divergences point to specific mechanisms. Although LCC sizes are essentially matched, the simulated core is much larger (19.6% vs. 5.1% of LCC) and more diffuse, with weaker core–periphery coupling (0.020 vs. 0.055) and fewer repeated interactions (5.90% vs. 8.70%) than Voat (Table 6; Figure 5). This is consistent with narrow per-round activity ranges, simplified feedback and visibility rules, and stateless dialogue that dampen hub consolidation and sustained pairwise exchange. Toxicity also diverges in a specific layer-dependent way. Overall toxicity is higher in simulation (0.143 vs. 0.119), but the excess is concentrated in the root-post layer: simulated root submissions are about 3.8× as toxic as empirical Voat roots, while simulated comments are only about 0.85× as toxic as empirical Voat comments. Both corpora still show more toxic comments than root submissions, but the empirical contrast is much steeper. This points to persona calibration, opening-post prompts, and link seeding that encourage overly confrontational starts, even as the reply process underproduces the more toxic reply layer seen in Voat. Both the diffuse core and the lag-limited convergence are expected consequences of a stateless, per-action design where appropriateness is local and memory is absent.

A recurring concern in LLM-based social simulation is circularity: models trained on toxic online discourse may simply reproduce that toxicity regardless of platform design [8]. We do not dispute that LLMs carry cultural patterns, including toxic ones, from their training data; indeed, this is precisely the mechanism that makes norm-guided simulation possible. We do not claim that toxicity emerges from platform dynamics; rather, it is prompted via persona-level propensity and scaffolded by an uncensored base model. Our contribution is narrower: toxicity is structured by persona traits and platform architecture rather than deployed indiscriminately, but the comparison to Voat shows that its magnitude is misplaced across content layers. The posts–comments gradient (comments more toxic than posts) appears in both simulation and Voat, yet the depth-shuffle permutation test indicates that this pattern is explained by the post/comment split rather than by within-thread escalation. This is consistent with the stateless design: agents have no long-range memory, so tone does not accumulate across reply depth. The K=3 convergence-entropy signature separately confirms that stylistic accommodation tracks the architectural context window. At the same time, this comparison makes the remaining limitation explicit: simulated root submissions are far too toxic, while simulated comments do not fully reproduce the harsher reply layer seen in Voat. The safer conclusion is therefore narrower: persona traits and platform scaffolding structure *where* toxicity appears, but only imperfectly. The broader 10-condition local OAT robustness panel in SI Section S10 shows that these absolute levels are strongly calibration-sensitive in a targeted way: neutralizing persona framing moves toxicity the most, temperature has weak local effects, and budget/CPR/churn settings mainly perturb activity and network structure rather than toxicity itself. The remaining mismatch therefore appears tunable rather than fundamental, even if identifying a configuration that improves toxicity while preserving the full 30-day Voat fit remains future work.

As emphasized in the introductory sections, this is a machine-to-machine baseline built on the "logic of appropriateness": agents act from norms and roles under short, stateless context. As a result, identity formation and long-range alignment are out of scope; we focus on short-range behavior and medium-scale structure rather than motives or psychology. Several measurements are proxies with familiar caveats (e.g., domain shift for the toxicity model, approximate embedding thresholds and 2D maps), and the fixed link catalog intentionally shapes topical exposure. Taken together, the results show that placing LLM agents in a realistic platform with simple, transparent rules can recover familiar platform patterns, but findings should be interpreted as *structural resemblance at the right scale, not literal replication*.

5.1 Limitations and Future Work

Three control challenges remain central for scaling this approach. First, agent behavior remains sensitive to prompt wording, context selection, and model idiosyncrasies, so "validity" is always conditional on a documented prompting protocol [44]. Second, multi-agent interaction can exhibit coherence failures (e.g., role drift or identity instability) that accumulate with horizon length, even when individual turns look locally plausible [45, 46]. Third, our stateless design deliberately avoids long-horizon memory and identity scaffolds, which improves interpretability of short-range effects but limits the class of long-range phenomena the simulation can represent. These constraints motivate a staged program of extensions where memory is introduced only when it measurably improves operational validity under the same validation panel.

This benchmark is intentionally conservative. v/technology is small, shallow-threaded, and relatively low-volume, making it a favorable first test for stateless agents. Larger or more heterogeneous communities would likely amplify exactly the mismatches already visible here, especially hub consolidation, repeated interactions, and long-range conversational carryover. We therefore interpret the present results as evidence of validity in a tractable small-community regime, not as evidence that the same architecture would validate unchanged on larger Reddit-scale communities.

Relatedly, our use of an uncensored base model should be read as a realism choice for a contentious forum setting rather than a policy statement. Preference-based alignment can induce sycophancy and suppress disagreement, which would bias a conflict-oriented simulation toward cooperation and niceness [47–49]. A natural next step is an ablation that holds the platform and validation panel fixed while varying model families (uncensored vs. instruction-tuned vs. anti-sycophancy-tuned) to quantify tradeoffs between safety, conflict realism, and structural validity.

Looking ahead, we prioritize a simple, evidence-based roadmap. First, test alternative feed variants—pure recency, pure popularity, or a "controversial" ranking (balanced ups/downs)—to probe whether different recommendation strategies consolidate the core or shift toxicity dynamics relative to the current popularity-weighted baseline. Second, widen or replace the truncated Zipf activity distribution (or test alternative heavy-tailed forms) to better capture participation heterogeneity. These steps should increase fidelity while preserving reproducibility. For substantially higher fidelity, introducing agent memory will be crucial; this study makes clear the limits of a memoryless approach and motivates future work on lightweight, per-thread memory and longer-horizon state. Longer horizons may also require explicit controls against entropy drift in multi-agent populations.

Beyond Voat's v/technology, the same operational-validation panel can in principle be transferred to other communities, but transfer of validity is empirical rather than automatic. One would update the link catalog (or content source), re-tune personas to the local context, and reuse the same evaluation axes (daily activity trajectories and thread size/depth distributions, network core–periphery, toxicity by content type, topics/embeddings, convergence), then re-establish the benchmark against community-specific data. This keeps cross-setting comparisons interpretable because the standard remains structural resemblance at comparable scales, not one-to-one replication. For larger or denser communities, however, we would expect stronger demands on persistence, repeated interaction, and long-range memory than the present stateless design can support.

The platform-faithful setup also enables practical "what-if" experiments. Researchers can vary feed rules (recency vs. popularity vs. controversial), moderation policies, or action menus and quantify shifts in the same structural terms. The same panel extends naturally to mixed human–machine studies by injecting or signaling agent presence while tracking activity, network concentration, toxicity by content type, semantic coverage, and convergence. Interpreted through operational validity, these experiments identify levers that measurably change platform-level patterns and provide a reproducible, falsifiable baseline for future improvements. In sum, Y Social with norm-guided LLM agents offers a transparent testbed for cumulative, empirical research on online social network dynamics.

Declarations

Ethics approval and consent to participate

No human participants were involved in this study. Generated content was produced with a base, less-aligned model under safeguards and filtered for research use only. The link catalog for seeding content is derived from public Voat data; no live RSS ingestion is used, and all experiments run in a closed environment. We do not use third-party generation or scoring APIs (e.g., commercial LLM endpoints or Perspective API) to avoid alignment restrictions that suppress toxic content and to ensure reproducibility; all inference uses local open models with fixed seeds and documented preprocessing.

Consent for publication

Not applicable.

Availability of data and material

The full workflow (simulation configuration, prompts, fixed URL catalog, analysis scripts, and model references) is organized for reproducibility and open access. Empirical calibration and validation samples are drawn from the Multi-Platform Aggregated Dataset of Online Communities (MADOC), which provides standardized data and FAIR (Findable, Accessible, Interoperable, Reusable) access via Zenodo (DOI: 10.5281/zenodo.15690964) [50]. Simulation results and Python code are available on GitHub: https://github.com/atomashevic/voat-simulation. The modified Y Social client used in this study is available at: https://github.com/atomashevic/Y Client-Reddit. Caution is advised when accessing or reusing released artifacts: they include offensive/toxic content and may reflect biases present in the source data and model outputs; handle, quote, and redistribute responsibly.

Competing interests

The authors declare that they have no competing interests.

Funding

This research was financially supported by the Science Fund of the Republic of Serbia, Prizma program (grant No. 7416).

Authors' contributions

A.T., D.C., S.M., S.Mal., M.A., A.V., B.S., D.V., A.B., and M.M.D. contributed to the study conceptualization and methodology. A.T. led software development, formal analysis, investigation, data curation, visualization, and wrote the original draft. D.C. contributed to software development, investigation, data curation, visualization, and manuscript review and editing. S.M., S.Mal., M.A., B.S., and A.B. contributed to data curation and manuscript review and editing. A.V. contributed to data curation, visualization, and manuscript review and editing. D.V. contributed to data curation, resources, and manuscript review and editing. A.B. contributed resources and provided supervision. M.M.D. provided supervision, managed project administration, acquired funding, and contributed to manuscript review and editing. All authors reviewed and approved the final manuscript.

Acknowledgements

We performed analyses on the Paradox V cluster at the Scientific Computing Laboratory, National Center of Excellence for the Study of Complex Systems, Institute of Physics Belgrade.

List of Abbreviations

ABM	Agent-Based Model
API	Application Programming Interface
CI	Confidence Interval
ECDF	Empirical Cumulative Distribution Function
HDBSCAN	Hierarchical Density-Based Spatial Clustering of Applications with Noise
KDE	Kernel Density Estimation
LCC	Largest Connected Component
LLM	Large Language Model
MADOC	Multi-platform Aggregated Dataset of Online Communities
MCMC	Markov Chain Monte Carlo
MDL	Minimum Description Length
RSS	Really Simple Syndication
SBM	Stochastic Block Model
SD	Standard Deviation
t-SNE	t-distributed Stochastic Neighbor Embedding
UMAP	Uniform Manifold Approximation and Projection
URL	Uniform Resource Locator

References

[1] Cinelli, M., De Francisci Morales, G., Galeazzi, A., Quattrociocchi, W., Starnini, M.: The echo chamber effect on social media. Proceedings of the National Academy of Sciences of the United States of America **118**(9), 2023301118 (2021) https://doi.org/10.1073/pnas.2023301118

[2] Avalle, M., Di Marco, N., Etta, G., Sangiorgio, E., Alipour, S., Bonetti, A., Alvisi, L., Scala, A., Baronchelli, A., Cinelli, M., Quattrociocchi, W.: Persistent interaction patterns across social media platforms and over time. Nature (2024) https://doi.org/10.1038/s41586-024-07229-y

[3] Pandita, S., Garg, K., Zhang, J., Mobbs, D.: Three roots of online toxicity: disembodiment, accountability, and disinhibition. Trends in cognitive sciences (2024)

https://doi.org/10.1016/j.tics.2024.06.001

[4] Neuman, W.R., Marcus, G.E., MacKuen, M.B.: The affective resonance of norm-violation rhetoric in social media. In: Research Handbook on Social Media and Society, pp. 161–180. Edward Elgar Publishing, Cheltenham, UK (2024). https://doi.org/10.4337/9781800377059.00023 . http://dx.doi.org/10.4337/9781800377059.00023

[5] Mimizuka, K., Brown, M.A., Yang, K.-C., Lukito, J.: Post-post-api age: Studying digital platforms in scant data access times. Journal of the ACM **37**(4), 111 (2025) https://doi.org/10.48550/arXiv.2505.09877 . arXiv:2505.09877; DSA Article 40

[6] Anthis, J.R., Liu, R., Richardson, S.M., Kozlowski, A.C., Koch, B., Evans, J.A., Brynjolfsson, E., Bernstein, M.: LLM social simulations are a promising research method. ArXiv **abs/2504.02234**, 2504–02234 (2025) https://doi.org/10.48550/arXiv.2504.02234

[7] Vezhnevets, A.S., Agapiou, J.P., Aharon, A., Ziv, R., Matyas, J., Duéñez-Guzmán, E.A., Cunningham, W.A., Osindero, S., Karmon, D., Leibo, J.Z.: Generative agent-based modeling with actions grounded in physical, social, or digital space using Concordia. arXiv [cs.AI] (2023) https://doi.org/10.48550/arXiv.2312.03664 [cs.AI]

[8] Larooij, M., T"ornberg, P.: Do large language models solve the problems of agent-based modeling? a critical review of generative social simulations. arXiv [cs.MA] (2025) https://doi.org/10.48550/arXiv.2504.03274 2504.03274

[9] Li, C., Wang, J., Wang, Y., Zhao, H.: A Survey on the Application of Large Language Models in Agent-Based Modeling and Simulation. Humanities and Social Sciences Communications **11**, 1–15 (2024)

[10] Adornetto, C., Mora, A., Hu, K., Garcia, L.I., Atchade-Adelomou, P., Greco, G., Pastor, L.A.A., Larson, K.: Generative agents in agent-based modeling: Overview, validation, and emerging challenges. IEEE transactions on artificial intelligence **PP**(99), 1–20 (2025) https://doi.org/10.1109/tai.2025.3566362

[11] Lin, Z.: Six fallacies in substituting large language models for human participants. Advances in Methods and Practices in Psychological Science **8**(3) (2025) https://doi.org/10.1177/25152459251357566

[12] Bouleimen, A., De Marzo, G., Kim, T., Pagan, N., Metzler, H., Giordano, S., Garcia, D.: The Collective Turing Test: Large Language Models Can Generate Realistic Multi-User Discussions (2025). https://doi.org/10.48550/arXiv.2511.08592 . https://arxiv.org/abs/2511.08592

[13] Mayor, E., Bietti, L.M., Bangerter, A.: Can large language models simulate spoken human conversations? Cognitive Science **49**(9) (2025) https://doi.org/10.1

111/cogs.70106

[14] Ng, L.H.X., Carley, K.M.: Are LLM-Powered Social Media Bots Realistic?, pp. 14–23. Springer, Cham (2025). https://doi.org/10.1007/978-3-032-07715-8_2 . https://doi.org/10.1007/978-3-032-07715-8_2

[15] Tsvetkova, M., Yasseri, T., Pescetelli, N., Werner, T.: A new sociology of humans and machines. Nature human behaviour **8**(10), 1864–1876 (2024) https://doi.org/10.1038/s41562-024-02001-8

[16] Brinkmann, L., Baumann, F., Bonnefon, J.-F., Derex, M., Müller, T.F., Nussberger, A.-M., Czaplicka, A., Acerbi, A., Griffiths, T.L., Henrich, J., Leibo, J.Z., McElreath, R., Oudeyer, P.-Y., Stray, J., Rahwan, I.: Machine culture. Nature human behaviour **7**(11), 1855–1868 (2023) https://doi.org/10.1038/s41562-023-01742-2

[17] Farrell, H., Gopnik, A., Shalizi, C., Evans, J.: Large ai models are cultural and social technologies. Science (Policy Forum) (2025) https://doi.org/10.1126/science.adt9819 . Science galley

[18] Park, J.S., Popowski, L., Cai, C., Morris, M.R., Liang, P., Bernstein, M.S.: Social Simulacra: Creating Populated Prototypes for Social Computing Systems. In: Proceedings of the 35th Annual ACM Symposium on User Interface Software And Technology, pp. 1–18. ACM, Bend OR USA (2022). https://doi.org/10.1145/3526113.3545616 . https://dl.acm.org/doi/10.1145/3526113.3545616 Accessed 2025-08-28

[19] Kozlowski, A.C., Evans, J.: Simulating subjects: The promise and peril of artificial intelligence stand-ins for social agents and interactions. Sociological Methods & Research **0**(0), 1–57 (2025) https://doi.org/10.1177/00491241251337316

[20] Durrheim, K., Quayle, M.: Human murmuration: Group polarisation as compression in interaction-language dynamics captured by large language models. European review of social psychology, 1–40 (2025) https://doi.org/10.1080/10463283.2025.2499332

[21] March, J.G., Olsen, J.P.: The Logic of Appropriateness. In: Goodin, R. (ed.) The Oxford Handbook of Political Science, 1st edn., pp. 478–497. Oxford University Press, Oxford, UK (2013). https://doi.org/10.1093/oxfordhb/9780199604456.013.0024

[22] Berger, P.L., Luckmann, T.: The Social Construction of Reality. Penguin Books, Harmondsworth, UK (1991)

[23] Argyle, L.P., Busby, E.C., Fulda, N., Gubler, J.R., Rytting, C., Wingate, D.: Out of One, Many: Using Language Models to Simulate Human Samples. Political Analysis **31**(3), 337–351 (2023) https://doi.org/10.1017/pan.2023.2

[24] Bao, H., Wu, S., Choi, J., Mao, Y., Evans, J.A.: Language Models Surface the Unwritten Code of Science and Society. arXiv [cs.CY] (2025) https://doi.org/10.48550/arXiv.2505.18942 [cs.CY]

[25] Epstein, J.M.: Agent-based computational models and generative social science. Complexity **4**(5), 41–60 (1999) https://doi.org/10.1002/(sici)1099-0526(199905/06)4:5<41::aid-cplx9>3.0.co;2-f

[26] Fagiolo, G., Moneta, A., Windrum, P.: A critical guide to empirical validation of agent-based models in economics: Methodologies, procedures, and open problems. Computational Economics **30**(3), 195–226 (2007) https://doi.org/10.1007/s10614-007-9104-4

[27] Guerini, M., Moneta, A.: A method for agent-based models validation. Journal of Economic Dynamics and Control **82**, 125–141 (2017) https://doi.org/10.1016/j.jedc.2017.06.001

[28] Park, J.S., O'Brien, J.C., Cai, C.J., Morris, M.R., Liang, P., Bernstein, M.S.: Generative Agents: Interactive Simulacra of Human Behavior. In: Proceedings of the 36th Annual ACM Symposium on User Interface Software and Technology, pp. 1–22 (2023). https://doi.org/10.1145/3586183.3606763

[29] Rossetti, G., Stella, M., Cazabet, R., Abramski, K., Cau, E., Citraro, S., Failla, A., Improta, R., Morini, V., Pansanella, V.: Y Social: an LLM-powered Social Media Digital Twin. arXiv [cs.AI] (2024) https://doi.org/10.48550/arXiv.2408.00818 [cs.AI]

[30] Pew Research Center: Beyond Red vs. Blue: The Political Typology. Technical report, Pew Research Center (2021). https://www.pewresearch.org/wp-content/uploads/sites/20/2021/11/PP_2021.11.09_political-typology_REPORT.pdf

[31] Mekacher, A., Papasavva, A.: "I can't keep it up." A dataset from the defunct Voat.Co news aggregator. Proceedings of the International AAAI Conference on Web and Social Media **16**, 1302–1311 (2022) https://doi.org/10.1609/icwsm.v16i1.19382

[32] Panek, E., Hollenbach, C., Yang, J., Rhodes, T.: Growth and Inequality of Participation in Online Communities. In: Proceedings of the 2017 ACM Conference on Computer Supported Cooperative Work and Social Computing, pp. 1321–1332 (2017). https://doi.org/10.1145/3097286.3097337

[33] Muchnik, L., Pei, S., Parra, L.C., Reis, S.D.S., Andrade Jr., J.S., Havlin, S., Makse, H.A.: Origins of power-law degree distribution in the heterogeneity of human activity in social networks. Scientific Reports **3**, 1783 (2013) https://doi.org/10.48550/arXiv.1304.4523 . arXiv:1304.4523

ARTICLE IN PRESS

[34] Hagberg, A.A., Schult, D.A., Swart, P.J.: Exploring network structure, dynamics, and function using NetworkX. In: Proceedings of the 7th Python in Science Conference (SciPy 2008), pp. 11–15. SciPy, Austin, Texas, USA (2008). https://doi.org/10.25080/TCWV9851

[35] Gallagher, R.J., Young, J.-G., Welles, B.F.: A clarified typology of core-periphery structure in networks. Science advances **7**(12), 9800 (2021) https://doi.org/10.1126/sciadv.abc9800

[36] Clauset, A., Shalizi, C.R., Newman, M.E.J.: Power-law distributions in empirical data. SIAM Review **51**(4), 661–703 (2009) https://doi.org/10.1137/070710111

[37] Hartvigsen, T., Gabriel, S., Palangi, H., Sap, M., Ray, D., Kamar, E.: ToxiGen: A large-scale machine-generated dataset for adversarial and implicit hate speech detection. In: Proceedings of the 60th Annual Meeting of the Association of Computational Linguistics (2022)

[38] Reimers, N., Gurevych, I.: Sentence-bert: Sentence embeddings using siamese bert-networks. In: Proceedings of the 2019 Conference on Empirical Methods in Natural Language Processing and the 9th International Joint Conference on Natural Language Processing (EMNLP-IJCNLP), pp. 3982–3992. Association for Computational Linguistics, Hong Kong, China (2019). https://doi.org/10.18653/v1/D19-1410

[39] Grootendorst, M.: BERTopic: Neural topic modeling with a class-based TF-IDF procedure. arXiv [cs.CL] (2022) https://doi.org/10.48550/arXiv.2203.05794 [cs.CL]

[40] Rosen, Z.P., Dale, R.: BERTs of a feather: Studying inter- and intra-group communication via information theory and language models. Behavior research methods **56**(4), 3140–3160 (2024) https://doi.org/10.3758/s13428-023-02267-2

[41] Chaiyakul, R., Rosen, Z.P., Dale, R.: Large language model discourse dynamics. In: Proceedings of the Annual Meeting of the Cognitive Science Society, vol. 47 (2025)

[42] Koley, G., Digrajkar, S.: A Simulation Framework for Studying Recommendation-Network Co-evolution in Social Platforms (2025). https://doi.org/10.48550/arXiv.2512.10106 . https://arxiv.org/abs/2512.10106

[43] Larooij, M., Törnberg, P.: Can we fix social media? Testing prosocial interventions using generative social simulation. arXiv [cs.SI] (2025) https://doi.org/10.48550/arXiv.2508.03385 [cs.SI]

[44] Lu, Y., Aleta, A., Du, C., Shi, L., Moreno, Y.: LLMs and generative agent-based models for complex systems research. Physics of Life Reviews **51**, 283–293 (2024) https://doi.org/10.1016/j.plrev.2024.10.013

[45] Shekkizhar, S., Cosentino, R., Earle, A., Savarese, S.: Echoing: Identity Failures when LLM Agents Talk to Each Other (2025). https://doi.org/10.48550/arXiv.2511.09710 . https://arxiv.org/abs/2511.09710

[46] Mooney, J., Woldense, J., Jia, Z.R., Hayati, S.A., Nguyen, M.H., Raheja, V., Kang, D.: Are LLM Agents Behaviorally Coherent? Latent Profiles for Social Simulation (2025). https://doi.org/10.48550/arXiv.2509.03736 . https://arxiv.org/abs/2509.03736

[47] Sharma, M., Tong, M., Korbak, T., Duvenaud, D., Askell, A., Bowman, S.R., Cheng, N., Durmus, E., Hatfield-Dodds, Z., Johnston, S.R., Kravec, S., Maxwell, T., McCandlish, S., Ndousse, K., Rausch, O., Schiefer, N., Yan, D., Zhang, M., Perez, E.: Towards Understanding Sycophancy in Language Models (2025). https://doi.org/10.48550/arXiv.2310.13548 . https://arxiv.org/abs/2310.13548

[48] Wei, J., Huang, D., Lu, Y., Zhou, D., Le, Q.V.: Simple synthetic data reduces sycophancy in large language models (2024). https://doi.org/10.48550/arXiv.2308.03958 . https://arxiv.org/abs/2308.03958

[49] Malmqvist, L.: Sycophancy in Large Language Models: Causes and Mitigations (2024). https://doi.org/10.48550/arXiv.2411.15287 . https://arxiv.org/abs/2411.15287

[50] Mitrović Dankulov, M., Tomašević, A., Maletić, S., Anđelković, M., Vranić, A., Cvetković, D., Stupovski, B., Vudragović, D., Major, S., Bogojević, A.: Multi-Platform Aggregated Dataset of Online Communities (MADOC). Proceedings of the International AAAI Conference on Web and Social Media **19**, 2529–2538 (2025) https://doi.org/10.1609/icwsm.v19i1.35954

Book of abstracts

PHOTONICA2021

VIII International School and Conference on Photonics

& HEMMAGINERO workshop

23 - 27 August 2021,

Belgrade, Serbia

Editors

Mihailo Rabasović, Marina Lekić and Aleksandar Krmpot

Institute of Physics Belgrade, Serbia

Belgrade, 2021

ABSTRACTS OF TUTORIAL, KEYNOTE, INVITED LECTURES, PROGRESS REPORTS AND CONTRIBUTED PAPERS

of

VIII International School and Conference on Photonics PHOTONICA2021

23 - 27 August 2021

Belgrade Serbia

Editors
Mihailo Rabasović, Marina Lekić and Aleksandar Krmpot

Publisher
Institute of Physics Belgrade
Pregrevica 118
11080 Belgrade, Serbia

Printed by
Serbian Academy of Sciences and Arts

Number of copies
200

ISBN 978-86-82441-53-3

CIP - Каталогизација у публикацији - Народна библиотека Србије, Београд

535(048)

621.37/.39:535(048)

621.37/.39:535]:61(048)

66.017/.018(048)

INTERNATIONAL School and Conference on Photonic (8; 2021; Beograd)

Book of abstracts / VIII International School and Conference on Photonics PHOTONICA2021 & HEMMAGINERO workshop, 23 - 27 August 2021, Belgrade, Serbia; editors Mihailo Rabasović, Marina Lekić and Aleksandar Krmpot. - Belgrade: Institute of Physics, 2021 (Belgrade: SASA). - V, 192 str.: ilustr.; 30 cm

Tiraž 200. - Bibliografija uz većinu apstrakata. - Registar.

ISBN 978-86-82441-53-3

1. Hemmaginero Workshop (2021; Beograd)

а) Оптика -- Апстракти б) Оптички материјали -- Апстракти в) Оптоелектроника -- Апстракти г) Оптоелектроника -- Биомедицина -- Апстракти д) Телекомуникације -- Апстракти

COBISS.SR-ID 44290057

Committees

Scientific Committee

- Aleksandar Krmpot, Serbia
- Aleksandra Maluckov, Serbia
- Bojan Resan, Switzerland
- Boris Malomed, Israel
- Branislav Jelenković, Serbia
- Carsten Ronning, Germany
- Concita Sibilia, Italy
- Darko Zibar, Denmark
- Dmitry Budker, Germany
- Dragan Inđin, United Kingdom
- Edik Rafailov, United Kingdom
- Francesco Cataliotti, Italy
- Giannis Zacharakis, Greece
- Goran Isić, Serbia
- Goran Mašanović, United Kingdom
- Ivana Vasić, Serbia
- Jasna Crnjanski, Serbia
- Jelena Radovanović, Serbia
- Jelena Stašić, Serbia
- Jerker Widengren, Sweden
- Jovan Bajić, Serbia
- Ljupčo Hadžievski, Serbia
- Luca Antonelli,UK
- Marco Canepari, France
- Marko Krstić, Serbia
- Marko Spasenović, Serbia
- Milan Kovačević, Serbia
- Milena Milošević, Serbia
- Milivoj Belić, Qatar
- Mirjana Novaković, Serbia
- Nikola Stojanović, Germany
- Nikola Vuković, Serbia
- Nikos Pleros, Greece
- Pavle Andjus, Serbia
- Petra Beličev, Serbia
- Sergei Turitsyn, UK
- Vladan Pavlović, Serbia
- Vladan Vuletić, USA
- Vladana Vukojević, Sweden
- Zoran Grujić, Serbia

Organizing Committee

- Marina Lekić, Institute of Physics Belgrade (Chair)
- Aleksandar Krmpot, Institute of Physics Belgrade (Co-Chair)
- Danica Pavlović , Institute of Physics Belgrade (Secretary)
- Stanko Nikolić , Institute of Physics Belgrade (Webmaster)
- Mihailo Rabasović , Institute of Physics Belgrade
- Tanja Pajić, Faculty of Biology, University of Belgrade
- Aleksandra Gočanin, Faculty of Physics, University of Belgrade
- Jadranka Vasiljević, Institute of Physics Belgrade
- Uroš Ralević, Institute of Physics Belgrade

Technical Organizer

Lufthansa City Center
Panacomp Wonderland Travel

http://www.panacomp.net/
Tel: +381 21 466 075
Tel: +381 21 466 076
Tel: +381 21 466 077

Faraday and Resonant Waves in Dipolar Cigar-Shaped Bose-Einstein Condensates

Dušan Vudragović
Scientific Computing Laboratory, Center for the Study of Complex Systems,
Institute of Physics Belgrade, University of Belgrade, Serbia
e-mail:dusan@ipb.ac.rs

Faraday and resonant density waves emerge in Bose-Einstein condensates as a result of harmonic driving of the system [1-3]. They represent nonlinear excitations and are generated due to the interaction-induced coupling of collective oscillation modes and the existence of parametric resonances. Using a mean-field variational and a full numerical approach, we study density waves in dipolar condensates at zero temperature [1], where breaking of the symmetry due to anisotropy of the dipole-dipole interaction plays an important role. We derive variational equations of motion for the dynamics of a driven dipolar system and identify the most unstable modes that correspond to the Faraday and resonant waves. Based on this, we also derive the analytical expressions for spatial periods of both types of density waves as functions of the contact and the dipole-dipole interaction strength. Finally, we compare the obtained variational results with the results of extensive numerical simulations that solve the dipolar Gross-Pitaevskii equation in 3D.

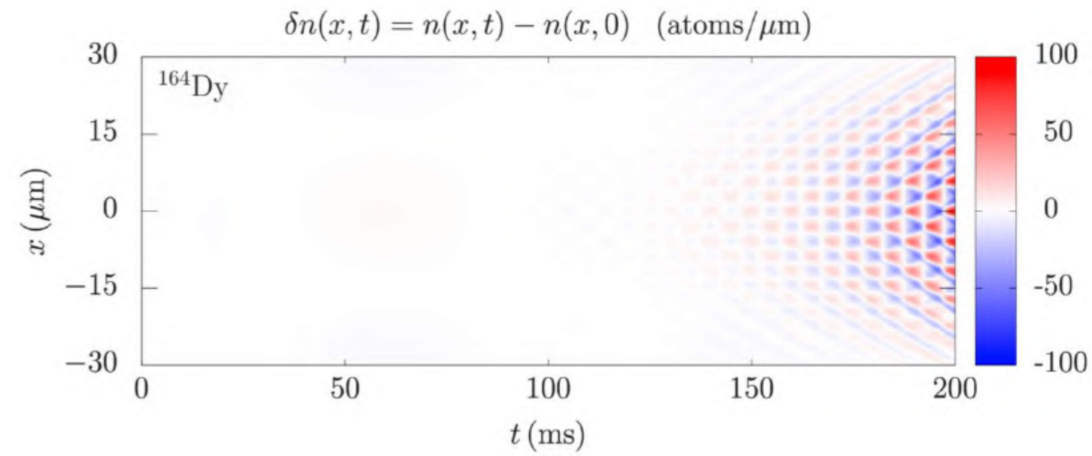

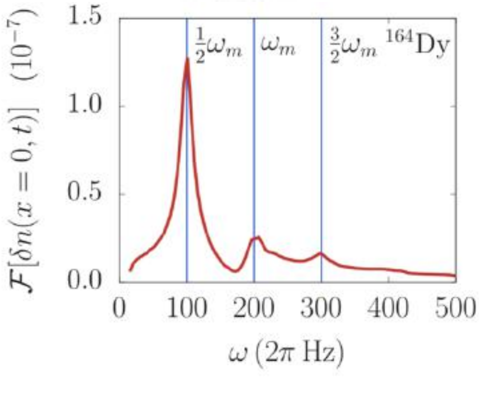

REFERENCES
[1] D. Vudragović and A. Balaž, Symmetry **11**, 1090 (2019).
[2] A. Balaž, R. Paun, A. I. Nicolin, et al., Phys. Rev. A **89**, 023609 (2014).
[3] A. Balaž and A. I. Nicolin, Phys. Rev. A **85**, 023613 (2012).

Proceedings of the Nineteenth International AAAI Conference on Web and Social Media (ICWSM 2025)

Multi-Platform Aggregated Dataset of Online Communities (MADOC)

Marija Mitrović Dankulov[1], Aleksandar Tomašević[2], Slobodan Maletić[3], Miroslav Anđelković[3], Ana Vranić[1], Darja Cvetković[1], Boris Stupovski[1], Dušan Vudragović[1], Sara Major[2], Aleksandar Bogojević[1]

[1]Institute of Physics Belgrade, University of Belgrade, Belgrade, Serbia
[2]Faculty of Philosophy, University of Novi Sad, Novi Sad, Serbia
[3]Vinča Institute of Nuclear Sciences, University of Belgrade, Belgrade, Serbia

Abstract

The Multi-platform Aggregated Dataset of Online Communities (MADOC) is a comprehensive dataset that facilitates computational social science research by providing a unified, standardized dataset for cross-platform analysis of online social dynamics. MADOC aggregates and standardizes data from four distinct platforms: Bluesky, Koo, Reddit, and Voat, spanning from 2012 to 2024. The dataset includes 18.9 million posts, 236 million comments, and data from 23.1 million unique users across all platforms, with a particular focus on understanding community dynamics, user migration patterns, and the evolution of toxic behavior across platforms. By providing standardized data structures and FAIR-compliant access through Zenodo and corresponding Python and R packages, MADOC enables researchers to conduct comparative analyses of user behavior, interaction networks, and content sentiment across diverse social media environments. The unique value of the dataset lies in its cross-platform scope, standardized structure, and rich metadata, making it particularly suitable for studying societal phenomena such as community formation, toxic behavior propagation, and user migration patterns in response to platform moderation policies.

Dataset — https://zenodo.org/records/14637314

Introduction

The proliferation of social media platforms has created diverse digital spaces where users interact, share content, and form communities. Understanding these interactions and their societal impact requires comprehensive datasets that span multiple platforms and enable comparative analyses. The Multi-platform Aggregated Dataset of Online Communities (MADOC) addresses this need by providing a standardized collection of user interactions, content, and sentiment data from four distinct platforms: Reddit, Bluesky, Koo, and Voat. Comprising 18.9 million posts and 236 million comments from 23.1 million unique users, MADOC represents one of the largest cross-platform datasets available for social media research. In an era where platform API access has become increasingly restricted—what some researchers call the "post-API era" (Poudel and Weninger 2024)—MADOC leverages existing public datasets (Baumgartner et al. 2020; Mekacher and Papasavva 2022; Failla and Rossetti 2024; Mekacher, Falkenberg, and Baronchelli 2024) to enable cross-platform research.

The dataset is structured to support various computational social science research directions:

- **Cross-platform User Behavior:** Standardized interaction data enables comparative analysis of user engagement patterns across different platform architectures and community structures (Wang, Koneru, and Rajtmajer 2024; Vranić et al. 2023).
- **Community Dynamics:** Comprehensive community-level data allows researchers to study how communities respond to major events like content moderation, user influx, or platform-wide policy changes, though individual user migration cannot be tracked across platforms due to privacy protections (Papasavva and Mariconti 2023).
- **Content and Sentiment Analysis:** Textual content, toxicity and sentiment scores facilitate research on how discourse and sentiment vary across platforms and communities.
- **Moderation Impact:** Historical data from banned communities provides insight into the effectiveness of platform moderation policies and their impact on user behavior (Cima et al. 2024).

MADOC adheres to FAIR principles (Findable, Accessible, Interoperable, and Reusable) through the following key features:

- **Findable:** The dataset is distributed through Zenodo [1] with persistent identifiers and comprehensive metadata for discovery.
- **Accessible:** All data and metadata are openly accessible through standard protocols with clear access procedures. We provide Python [2]and R [3] packages for seamless access to the dataset.
- **Interoperable:** Data is provided in standardized Apache Parquet format with a consistent schema across platforms, enabling seamless integration.
- **Reusable:** Detailed documentation of collection methodologies, processing steps, and ethical guidelines supports research reproducibility.

[1]https://zenodo.org/records/14637314
[2]https://pypi.org/project/pymadoc/
[3]https://github.com/atomashevic/rMADOC

MADOC's primary contribution is its methodologically rigorous approach to cross-platform data alignment and standardization. The dataset construction begins with a careful selection of 12 Reddit communities, with corresponding communities later identified on Voat. The first set consists of six general-interest communities (*r/funny, r/gaming, r/pics, r/videos, r/gifs, and r/technology*) that focus on mainstream topics. The second set comprises controversial communities, including four that were banned from Reddit for violating platform policies: *r/fatpeoplehate* (banned in 2015 for systematic harassment), *r/GreatAwakening* (banned in 2018 for inciting violence and promoting conspiracy theories), *r/MillionDollarExtreme* (banned in 2018 for promoting hate speech and alt-right content), and *r/CringeAnarchy* (banned in 2019 following increased hate speech after the Christchurch mosque shootings). Two additional controversial communities, while not banned, have been subjected to increased scrutiny and moderation: *r/KotakuInAction* (heavily moderated since 2014 due to its role in harassment campaigns during Gamergate) and *r/MensRights* (subject to content restrictions due to repeated incidents of coordinated harassment and anti-feminist rhetoric). These communities were chosen specifically because they represent different types of content moderation challenges: from organized harassment campaigns and hate speech to conspiracy theories and extremist content. This selection enables researchers to study both typical online interactions and potentially harmful social dynamics, particularly in communities that have faced different levels of platform enforcement (Jhaver, Chan, and Bruckman 2017). The selection is strategic: it allows us to analyze how community-level behavior, content patterns, and discourse evolve before and after significant events such as platform bans, content restrictions, or influxes of new users. While individual users cannot be tracked across platforms due to privacy protections and ethical considerations, the dataset captures aggregate changes in community characteristics, sentiment, and content patterns during periods of user migration and community restructuring.

Data Collection and Processing

Data Sources

MADOC aggregates and standardizes data from four distinct social media platforms: Reddit, Voat, Bluesky, and Koo.

For Reddit, we utilized the Pushshift.io dataset (Baumgartner et al. 2020), which encompasses submissions and comments from 2006 to 2020. From this extensive collection, we focused on 12 subreddits: six in the general-interest category, and six controversial.

The Voat dataset (Mekacher and Papasavva 2022), spanning from 2013 to the platform's shutdown in 2020, provides a complete archive of the platform's content. We extracted data from twelve subverses that directly correspond to our selected Reddit communities, maintaining the same naming convention (e.g., v/funny corresponding to r/funny).

For Bluesky, we incorporated a comprehensive dataset containing over 4 million accounts (81% of registered users) and their complete posting activity (235M posts) from March 2023 to March 2024 (Failla and Rossetti 2024). Similarly, we used the existing Koo dataset (Mekacher, Falkenberg, and Baronchelli 2024) which encompasses 1.4 million users, 72 million posts, and 75 million comments, spanning from January 2020 to September 2023 . This platform's inclusion is particularly valuable as it represents perspectives from the Global South, with a predominantly Indian user base.

Data Processing and Standardization

A key challenge in creating MADOC was aligning content across platforms with different organizational structures. While Reddit and Voat organize content into topic-specific communities (subreddits and subverses), Bluesky and Koo lack such explicit topic segregation. To address this, we developed a systematic content alignment process using Latent Dirichlet Allocation (LDA) topic modeling (Blei, Ng, and Jordan 2003; Maier et al. 2018). The detailed methodology of this process is described in the next section.

The dataset standardization process consists of four main components. First, we implemented comprehensive data cleaning procedures. These include deduplication of entries while preserving temporal precedence, conversion of all date and time related fields to UNIX timestamps, standardization of text encoding and character sets, and cleaning of URLs to remove formatting artifacts. For Bluesky and Koo, we implemented additional URL extraction from content fields, separating embedded links from the main text while preserving both components. To account for the presence of bots on Reddit and Voat—programmed to post, comment automatically, or respond to specific prompts — we implemented a "bot removal" procedure. These bots often include the phrase "I am a bot" in their posts or comments. Therefore, we screened users whose interactions (posts and comments) contained this phrase. If more than 70% of a user's interactions included "I am a bot," they were removed from our dataset. The 70% threshold was chosen after analyzing the number of users flagged as bots across various detection thresholds (ranging from 40% to 100%) for all communities. We observed a sharp decrease in flagged users at 70% for in every community, indicating it as the most suitable threshold for identifying bots across all communities.

Second, we standardized interaction types across platforms. All interactions were classified as either posts, comments, or reposts (the latter only for Bluesky and Koo). Posts are submissions on Reddit and Voat and tweet-like posts on Koo and Bluesky. Comments include submission comments on Reddit and Voat and replies to posts on Koo and Bluesky.

For Voat comments, we had only parent information linking posts and first-level comments (excluding comments on comments). This is because the original Voat dataset does not contain complete information about comment-to-comment relationships. To maintain a consistent network structure across platforms, we preserved only first-level replies and comments, excluding nested conversations. This standardization required careful validation of parent-child relationships in threaded discussions, particularly for platforms like Reddit and Voat where deep conversation trees are common. We kept comments that had no parent informa-

Metric	Reddit	Voat	Bluesky	Koo
Time span	2014-2020	2013-2020	2023-2024	2020-2023
Total interactions	247.6M	1.2M	2.8M	4.3M
Posts	14.5M	0.4M	0.9M	3.1M
Comments	233.1M	0.8M	0.9M	1.2M
Unique users	22.6M	0.1M	0.2M	0.2M
Avg. posts per user	2.7	8.5	14.4	23.0
Avg. comments per user	11.6	7.8	6.2	10.6
Mean VADER sentiment	0.063	0.011	0.088	0.054
% with URLs	10.3%	31.8%	4.5%	11.6%

Table 1: Platform-level statistics for MADOC. The dataset covers different time periods for each platform, reflecting their operational histories and data availability.

tion, because they relate to posts which have been deleted or banned from the platform. While we acknowledge that the depth of reply trees on Reddit and Voat is a distinctive feature of these platforms compared to Bluesky and Koo, our decision to include only level-1 comments was driven by the limitations of the Voat source data and the need for cross-platform standardization. Researchers specifically interested in examining conversation depth and structure should refer to the original datasets, as this aspect of platform comparison is outside MADOC's primary focus on content and community-level analysis.

The absence of parent information is noticeable on Reddit where, due to increased content-moderation, bans, and user migrations, original post-to-comment relationships are not always preserved. The most extreme case is r/fatpeoplehate subreddit, where all posts are missing because the content was banned.

For sentiment analysis, we applied two complementary approaches using lexicon and rule-based models: VADER (Hutto and Gilbert 2014) and TextBlob. VADER is specifically attuned to social media text and provides context-aware sentiment scoring, which accounts for elements like punctuation, capitalization, and modifiers. TextBlob offers a more generalized polarity assessment based on pattern analysis and provides a useful alternative perspective. Both sentiment scores range from -1 (negative) to 1 (positive), allowing researchers to compare and validate sentiment patterns using multiple methodologies. Additionally, we included TextBlob's subjectivity score, which ranges from 0.0 (objective) to 1.0 (subjective), measuring the degree to which text expresses personal opinions, emotions, or judgments versus factual information.

Additionally, we used the ToxiGen RoBERTa model (Hartvigsen et al. 2022) to detect subtle forms of implicit toxicity and hate speech in the content. Although Perspective API is widely considered the standard for toxicity detection, its rate limits were a significant limiting factor given the size of our dataset, and thus utilizing a fully open-source model like ToxiGen better supports reproducibility and aligns with open science principles. The ToxiGen model was specifically trained on adversarial examples of implicit hate speech targeting minority groups, making it particularly well-suited for detecting toxic content that might evade traditional detection methods. The toxicity_toxigen field provides a normalized score from 0.00 (non-toxic) to 1.00 (toxic), enabling researchers to analyze toxicity patterns across different platforms and communities.

For the initial release, we restricted the dataset to English-language content. For Koo, which serves a predominantly multilingual user base (Mekacher, Falkenberg, and Baronchelli 2024), we implemented additional language filtering steps to ensure reliable sentiment and toxicity analysis results.

Fourth, we implemented privacy protection measures. All post and user identifiers across all platforms are pseudonymized using UUID-based hashing, which maintains referential integrity while preventing casual re-identification. The only personally identifiable information is the content of the posts along with the timestamp of the post. However, this information was already present in the original datasets, so our pseudonymization makes it harder to reconstruct the original content in comparison with the original datasets. We deliberately chose not to attempt cross-platform profile matching (identifying the same users across different platforms), both because some source datasets already contained pseudonymized usernames making such matching technically infeasible, and because such matching would raise significant privacy concerns by potentially enabling re-identification of users across platforms.

This approach maintains the network structure and enables research on user behavior patterns while protecting user privacy through pseudonymization.

The resulting dataset follows a standardized schema across all platforms, with the structure detailed in Table 2.

To facilitate efficient data access and analysis, we store the dataset in Apache Parquet format, with separate files for each community (subreddit/subverse) while Koo and Bluesky are stored in a single file. This modular organization enables researchers to easily load specific subsets of the data while maintaining the ability to perform cross-platform analyses. The standardized schema ensures that files can be seamlessly combined (concatenated) across platforms and communities, allowing flexible dataset construction based on research needs. For example, researchers can combine all controversial communities across platforms, merge specific platform pairs for comparative analysis, or create custom subsets based on temporal or content criteria. The standardized structure also allows for the construction of interaction networks where nodes represent users and edges represent their interactions through posts and replies, enabling comparative analysis of community structures across platforms.

Topic Analysis and Selection of Posts

To enable cross-platform content analysis, we developed a systematic approach for identifying thematically similar content across platforms with different organizational structures. While Reddit and Voat organize content into topic-specific communities (subreddits and subverses), Koo and Bluesky lack explicit topic segregation. We employed Latent Dirichlet Allocation (LDA) topic modeling (Blei, Ng, and Jordan 2003; Maier et al. 2018) to extract characteristic keywords from Reddit and Voat communities, which were then used to identify related content on Koo and Bluesky.

For each community pair (subreddit and corresponding subverse), we created a combined corpus by merging posts and their first-level comments from both platforms. Each document in the corpus represents a post with its comments, preprocessed by removing mentions, hyperlinks, non-alphanumeric characters, converting to lowercase, removing stopwords, and lemmatizing. We excluded words appearing in more than 99% of documents following (Maier et al. 2018) and filtered-out documents with fewer than 20 or more than 2000 words to ensure LDA performance (Tang et al. 2014).

Due to platform size disparities, we implemented a balanced sampling strategy based on document volume:

- For communities with similar document counts (<10,000): Created nine balanced samples of 20,000 documents (10,000 from each platform)
- For communities with 10,000-20,000 Voat documents: Created five samples matching Voat's volume with Reddit documents
- For communities with <10,000 Voat documents: Created five samples of 20,000 Reddit documents plus all Voat documents

We determined the optimal number of topics for each community by maximizing coherence scores, then extracted the top 20 words per topic across all samples. The resulting keyword lists were filtered to retain only the least frequent third of English words (Norvig 2009) to improve topic specificity.

For content alignment, we applied two filtering criteria to Koo and Bluesky posts:

- Basic filter: Documents containing at least one community keyword
- Strict filter: Documents containing at least two different community keywords

It is important to note that our topic modeling approach does not attempt to align the structural differences between platforms (as Reddit and Voat have explicit community structures while Koo and Bluesky do not), but rather ensures topical equivalence across platforms. Without this filtering method, we would be left with massive, unstructured Bluesky and Koo datasets with no meaningful way to conduct comparative analysis with the community-structured data from Reddit and Voat. This approach allows researchers to compare content discussing similar themes regardless of the underlying platform architecture, maintaining consistent thematic scope while acknowledging the fundamental differences in how these platforms organize user interactions.

The topic modeling analysis revealed distinct linguistic patterns characteristic of each community, providing strong validation for our cross-platform content alignment approach. For general-interest communities, the extracted keywords closely matched their intended focuses. For example, r/gaming exhibited gaming-specific terminology (e.g., "pokemon", "hack"), while r/technology contained science and technology terms (e.g., "solar", "nasa", "electricity").

The topic modeling also revealed distinct linguistic patterns in communities focused on specific social discussions. For instance, r/MensRights showed a concentration of legal and family-related terminology ("father", "parent", "judge"). Communities focused on political discourse showed distinctive patterns. The r/GreatAwakening community, which centered on conspiracy theories before its ban in 2018, featured high frequencies of governance-related terms ("congress", "campaign", "election", "truth"). Similarly, r/KotakuInAction, which emerged during the GamerGate controversy (Jhaver, Chan, and Bruckman 2017) and focused on media criticism, developed its own specialized vocabulary around content moderation and journalistic practices. These distinctive vocabulary patterns proved particularly valuable for identifying thematically similar content on platforms lacking explicit community structures.

The topic modeling analysis also revealed patterns of problematic language usage across platforms. We observed systematic variations in the frequency and context of inflammatory rhetoric, derogatory terms, and exclusionary language. These patterns were particularly pronounced in communities that were eventually subject to platform moderation actions. This shows that the sampling strategy we used is effective in recognizing the specific language employed by communities on Voat.

These results demonstrate the robustness of our topic modeling and keyword filtering methodology for cross-platform content alignment. The approach successfully captures both explicit topical focus (through technical and domain-specific terminology) and implicit community characteristics (through platform-specific linguistic patterns), enabling meaningful comparative analyses across diverse social media environments.

Dataset Statistics

MADOC provides a comprehensive view of user interactions across four distinct platforms, with data spanning multiple years and interaction types. Table 1 presents the key statistics for each platform, including temporal coverage, interaction counts, and user activity metrics. [4]

The platform-level statistics reveal significant differences in scale and user behavior across platforms. Reddit dominates in terms of total interactions (247.6M) and user base

[4]The most recent version of the key statistics table for each platform, including TextBlob sentiment and subjectivity as well as ToxiGen toxicity scores is available at https://zenodo.org/records/14637314

(22.6M), being orders of magnitude larger than the other platforms. However, smaller platforms show higher per-user engagement rates, with Koo users averaging 23.0 posts per user compared to Reddit's 2.7. Voat shows notably higher URL sharing (31.8% of posts) compared to other platforms (4.5-11.6%), suggesting a stronger focus on external content sharing. Sentiment analysis reveals that Bluesky has the most positive average sentiment (0.088), while Voat shows the lowest (0.011), potentially reflecting differences in community norms and content moderation approaches.

For Reddit and Voat, where content is organized into topic-specific communities, we provide detailed statistics for each community pair in Table 3. These statistics enable direct comparisons between equivalent communities across the two platforms.

The community-level comparison between Reddit and Voat reveals several interesting patterns. First, there is a clear scale difference, with Reddit communities typically being 100-1000 times larger than their Voat counterparts. For instance, r/funny has 5.5M users compared to v/funny's 20K. Second, sentiment patterns show that general-interest communities (e.g., gaming, pics) tend to maintain positive sentiment scores on both platforms, with Reddit generally showing more positive values. In contrast, controversial communities exhibit negative sentiment scores across both platforms, with some communities like MensRights showing particularly negative values (Reddit: -0.076, Voat: -0.162). The absence of posts in Reddit's r/fatpeoplehate while having 1.4M comments reflects the community's ban during the data collection period, providing an interesting case study of community dynamics around platform moderation actions.

For Bluesky and Koo, which lack explicit community structures, we provide statistics based on the keyword filtering approach described in previous section. Using the basic filtering criteria (one keyword match), we identified 910,376 posts and 932,545 comments from Bluesky, and 3,083,191 posts and 1,180,449 comments from Koo that align with the topics of the Reddit/Voat communities. With the strict filtering criteria (two keyword matches), these numbers reduce to 114,431 posts and 322,193 comments for Bluesky, and 249,983 posts and 138,418 comments for Koo, respectively.

It is important to note that the MADOC dataset is constantly being updated and expanded with new metrics. Some metrics, particularly for larger platforms like Reddit, are still being processed and will be available only in the most recent versions of the dataset. As our analysis progresses, we incorporate additional sentiment analysis models, toxicity measures, and other relevant metrics. These continuous updates ensure that researchers have access to the most comprehensive and up-to-date data for their analyses. While this paper presents a snapshot of its current state, we encourage researchers to refer to the latest version of the dataset, including the most recent metrics and statistics, at the Zenodo repository: https://zenodo.org/records/14637314.

Limitations

Our dataset production approach has several limitations. First, the choice of Reddit communities, especially the non-controversial ones, was arbitrary and based on the 20 most active general-interest communities which existed on both Reddit and Voat. In the next versions of the dataset, we aim to include more Reddit-Voat community pairs.

Second, the LDA topic modeling approach was not cross-validated by performing topic modeling again on the filtered communities to verify alignment between the communities. It is important to note that traditional cross-validation is not applicable in our case due to the fundamental structure of our methodology. The content from Koo and Bluesky was filtered based on a union of keywords extracted from multiple community-specific topics from Reddit and Voat, resulting in inherently overlapping topics and combined keyword sets that cannot be meaningfully validated through conventional methods. We also limited our evaluation to selecting models based on coherence scores without exploring alternative topic modeling configurations or parameters. This lack of systematic evaluation may affect the quality and representativeness of the extracted keywords used for cross-platform content alignment. Future versions of the dataset will address these limitations by developing specialized validation techniques better suited to our cross-platform alignment approach.

Third, we introduce multiple text analysis metrics in this version of the dataset: VADER sentiment scores, TextBlob sentiment polarity, and ToxiGen toxicity scores. This combination provides researchers with complementary perspectives on content sentiment and toxicity. The ToxiGen model is specifically designed to detect subtle forms of implicit toxicity and hate speech that might evade traditional detection methods. Future versions will provide an even more comprehensive overview of posts' sentiment and toxicity using additional approaches (other RoBERTa-based models, transformer-based sentiment analysis, etc.).

Fourth, the time spans of collected data vary significantly across platforms (2014-2020 for Reddit, 2013-2020 for Voat, 2023-2024 for Bluesky, and 2020-2023 for Koo), which introduces challenges in studying long-term trends across all platforms simultaneously. However, this temporal misalignment is unavoidable given the historical reality of platform lifecycles—Bluesky did not exist during the period of Reddit-Voat migrations, making perfect temporal alignment impossible. Rather than viewing this as a limitation, researchers can leverage these different time periods to study how similar communities and content patterns manifest in different platform eras, from early alternative platforms like Voat to newer decentralized networks like Bluesky. The dataset particularly excels at enabling thematic comparisons across platforms regardless of temporal overlap, focusing on how similar discourses evolve in different platform environments and moderation contexts.

Finally, while we have aggregated a substantial amount of data, there may be gaps in our collection due to the limitations of archival sources and API restrictions. Some content might have been deleted or modified before collection, and we cannot guarantee complete coverage of all interactions that occurred on the platform.

Conclusion

In this work, we present MADOC, a comprehensive cross-platform dataset comprising 18.9 million posts and 236 million comments from 23.1 million unique users across four distinct social media platforms: Reddit, Voat, Bluesky, and Koo. The dataset spans from 2012 to 2024 and represents one of the largest standardized collections of cross-platform social media interactions. We combine data from multiple sources and implement standardization procedures to ensure consistency and comparability across platforms.

The dataset's unique value lies in its standardized structure and rich metadata, which facilitate various types of computational social science research. The inclusion of both mainstream and alternative platforms, along with comprehensive historical data on banned communities, makes MADOC particularly valuable for studying platform governance, content moderation, and user migration patterns. Our careful curation process and adherence to FAIR principles ensure the dataset's accessibility and reusability while maintaining privacy protections through pseudonymization protocols.

We envision MADOC enabling several important research directions: First, researchers can use it to study how content moderation policies affect user behavior and community dynamics across different platform architectures. Second, the dataset's temporal breadth supports longitudinal analyses of how online discourse and community norms evolve over time and across platforms. Third, the standardized sentiment scores and content features facilitate comparative studies of how platform design influences user interactions and content toxicity.

Beyond these immediate applications, we believe that MADOC will contribute to a broader understanding of online social phenomena. The dataset can help answer questions about community formation, user activity patterns, and the propagation of both harmful and benevolent narratives across platform boundaries. For computational researchers, it provides a rich testbed for developing and evaluating natural language processing models, particularly in areas like toxic content detection, cross-platform user behavior prediction, and community dynamics modeling.

Through this work, we aim to support both quantitative and qualitative research into online social dynamics. We encourage researchers to use MADOC responsibly, considering the ethical implications discussed in this paper, and to build upon our methodology for future cross-platform dataset development. To facilitate easy adoption, we provide Python (pyMADOC) and R (rMADOC) packages with command-line interfaces that enable selective downloading of data by platform or community. As social media continues to evolve and fragment across multiple platforms, we believe standardized cross-platform datasets like MADOC will become increasingly valuable for understanding and improving online social spaces.

Acknowledgments

This research was financially supported by the Science Fund of the Republic of Serbia, Prizma program (grant No. 7416). Data processing was performed on the PARADOX-IV supercomputing facility at the Scientific Computing Laboratory, National Center of Excellence for the Study of Complex Systems, Institute of Physics Belgrade.

Claude 3.5 Sonnet LLM was used in preparation of this manuscript, for table generation, text editing and LaTeX formatting.

References

Baumgartner, J.; Zannettou, S.; Keegan, B.; Squire, M.; and Blackburn, J. 2020. The Pushshift Reddit Dataset. *Proceedings of the International AAAI Conference on Web and Social Media*, 14(1): 830–839.

Blei, D. M.; Ng, A. Y.; and Jordan, M. I. 2003. Latent dirichlet allocation. *Journal of Machine Learning Research*, 3: 993–1022.

Cima, L.; Trujillo, A.; Avvenuti, M.; and Cresci, S. 2024. The Great Ban: Efficacy and Unintended Consequences of a Massive Deplatforming Operation on Reddit. *arXiv [cs.SI]*.

Failla, A.; and Rossetti, G. 2024. "I'm in the Bluesky Tonight": Insights from a year worth of social data. *PloS one*, 19(11): e0310330.

Hartvigsen, T.; Gabriel, S.; Palangi, H.; Sap, M.; Ray, D.; and Kamar, E. 2022. ToxiGen: A large-scale machine-generated dataset for adversarial and implicit hate speech detection. *arXiv [cs.CL]*.

Hutto, C.; and Gilbert, E. 2014. VADER: A parsimonious rule-based model for sentiment analysis of social media text. *Proceedings of the International AAAI Conference on Web and Social Media*, 8(1): 216–225.

Jhaver, S.; Chan, L.; and Bruckman, A. 2017. The view from the other side: The border between controversial speech and harassment on Kotaku in Action. *arXiv [cs.OH]*.

Maier, D.; Waldherr, A.; Miltner, P.; Wiedemann, G.; Niekler, A.; Keinert, A.; Pfetsch, B.; Heyer, G.; Reber, U.; Häussler, T.; Schmid-Petr, H.; and Adam, S. 2018. Applying LDA topic modeling in communication research: Toward a valid and reliable methodology. *Communication Methods and Measures*, 12: 93–118.

Mekacher, A.; Falkenberg, M.; and Baronchelli, A. 2024. The Koo dataset: An Indian microblogging platform with global ambitions. *arXiv [cs.SI]*.

Mekacher, A.; and Papasavva, A. 2022. "I can't keep it up." A dataset from the defunct Voat.Co news aggregator. *arXiv [cs.SI]*.

Norvig, P. 2009. Natural Language Corpus Data. In Segaran, T.; and Hammerbacher, J., eds., *Beautiful Data*, 219–242. O'Reilly Media, Inc. ISBN 9780596157111.

Papasavva, A.; and Mariconti, E. 2023. Waiting for Q: An Exploration of QAnon Users' Online Migration to Poal in the Wake of Voat's Demise. arxiv:2302.01397.

Poudel, A.; and Weninger, T. 2024. Navigating the Post-API dilemma | Search Engine Results Pages present a biased view of social media data. *arXiv [cs.IR]*.

Tang, J.; Meng, Z.; Nguyen, X.; Mei, Q.; and Zhang, M. 2014. Understanding the Limiting Factors of Topic Modeling via Posterior Contraction Analysis. In Xing, E. P.; and Jebara, T., eds., *Proceedings of the 31st International Conference on Machine Learning*, volume 32 of *Proceedings of Machine Learning Research*, 190–198. Bejing, China: PMLR.

Vranić, A.; Tomašević, A.; Alorić, A.; and Mitrović Dankulov, M. 2023. Sustainability of Stack Exchange Q&A communities: the role of trust. *EPJ Data Science*, 12(1).

Wang, X.; Koneru, S.; and Rajtmajer, S. 2024. The failed migration of academic Twitter. *arXiv [cs.SI]*.

Paper Checklist

1. For most authors...
   (a) Would answering this research question advance science without violating social contracts, such as violating privacy norms, perpetuating unfair profiling, exacerbating the socio-economic divide, or implying disrespect to societies or cultures? Yes, our research advances science by providing a standardized dataset for studying online social dynamics while implementing strong privacy protections and ethical safeguards as detailed in the Ethical Considerations section.
   (b) Do your main claims in the abstract and introduction accurately reflect the paper's contributions and scope?
   (c) Do you clarify how the proposed methodological approach is appropriate for the claims made? This is a dataset paper, it does not make specific claims.
   (d) Do you clarify what are possible artifacts in the data used, given population-specific distributions? We have addressed questions like these in Ethical Considerations section.
   (e) Did you describe the limitations of your work? Yes, we discuss limitations including arbitrary community selection, LDA topic modeling validation, sentiment analysis scope, and data collection gaps in the Limitations section.
   (f) Did you discuss any potential negative societal impacts of your work? We have addressed this in the Ethical Considerations section.
   (g) Did you discuss any potential misuse of your work? We have addressed this in Ethical Considerations section.
   (h) Did you describe steps taken to prevent or mitigate potential negative outcomes of the research, such as data and model documentation, data anonymization, responsible release, access control, and the reproducibility of findings? Yes, we have implemented extensive measures including pseudonymization, clear documentation, usage tracking, and FAIR principles as detailed in the Ethical Considerations section.
   (i) Have you read the ethics review guidelines and ensured that your paper conforms to them?
2. Additionally, if your study involves hypotheses testing...
   (a) Did you clearly state the assumptions underlying all theoretical results?
   (b) Have you provided justifications for all theoretical results?
   (c) Did you discuss competing hypotheses or theories that might challenge or complement your theoretical results?
   (d) Have you considered alternative mechanisms or explanations that might account for the same outcomes observed in your study?
   (e) Did you address potential biases or limitations in your theoretical framework?
   (f) Have you related your theoretical results to the existing literature in social science?

(g) Did you discuss the implications of your theoretical results for policy, practice, or further research in the social science domain?

3. Additionally, if you are including theoretical proofs...
   (a) Did you state the full set of assumptions of all theoretical results?
   (b) Did you include complete proofs of all theoretical results?
4. Additionally, if you ran machine learning experiments...
   (a) Did you include the code, data, and instructions needed to reproduce the main experimental results (either in the supplemental material or as a URL)?
   (b) Did you specify all the training details (e.g., data splits, hyperparameters, how they were chosen)?
   (c) Did you report error bars (e.g., with respect to the random seed after running experiments multiple times)?
   (d) Did you include the total amount of compute and the type of resources used (e.g., type of GPUs, internal cluster, or cloud provider)?
   (e) Do you justify how the proposed evaluation is sufficient and appropriate to the claims made?
   (f) Do you discuss what is "the cost" of misclassification and fault (in)tolerance?
5. Additionally, if you are using existing assets (e.g., code, data, models) or curating/releasing new assets, **without compromising anonymity**...
   (a) If your work uses existing assets, did you cite the creators? Yes, we cited Pushshift.io, Voat dataset, Bluesky dataset, and Koo dataset creators.
   (b) Did you mention the license of the assets? Yes, we mentioned CC0 for Reddit Pushshift and CC BY 4.0 International for Voat, Bluesky, and Koo datasets.
   (c) Did you include any new assets in the supplemental material or as a URL? Yes, we provided the Zenodo URL for the dataset.
   (d) Did you discuss whether and how consent was obtained from people whose data you're using/curating? No, because we aggregated publicly available datasets.
   (e) Did you discuss whether the data you are using/curating contains personally identifiable information or offensive content? Yes, we explicitly discuss both PII handling and the presence of offensive content in the Ethical Considerations section.
   (f) If you are curating or releasing new datasets, did you discuss how you intend to make your datasets FAIR? Yes, we discuss FAIR principles implementation including findability through Zenodo, accessibility through standard protocols, interoperability through standardized formats, and reusability through documentation.
   (g) If you are curating or releasing new datasets, did you create a Datasheet for the Dataset? Partially. The paper itself serves as a comprehensive datasheet covering motivation, composition, collection process, preprocessing, uses, distribution, and maintenance. Additionally, these is a detailed README file in the Zenodo repository.
6. Additionally, if you used crowdsourcing or conducted research with human subjects, **without compromising anonymity**...
   (a) Did you include the full text of instructions given to participants and screenshots?
   (b) Did you describe any potential participant risks, with mentions of Institutional Review Board (IRB) approvals?
   (c) Did you include the estimated hourly wage paid to participants and the total amount spent on participant compensation?
   (d) Did you discuss how data is stored, shared, and deidentified?

Ethical Considerations

The MADOC dataset raises several important ethical considerations that we have addressed throughout its development and release. Our approach to these considerations is guided by the principles of responsible data science and research ethics, with particular attention to privacy protection, content handling, and potential misuse prevention.

The dataset is created through aggregation of existing, publicly available datasets, and we have taken extensive measures to enhance privacy protections beyond those present in the source data. We have not introduced any new sources of personally identifiable information (PII). Instead, all user identifiers are pseudonymized using UUID-based hashing, which maintains referential integrity while preventing casual re-identification. Platform-specific identifiers have been standardized and pseudonymized to prevent cross-platform user tracking. The only retained potentially identifying information is post content and timestamps, which were already public in the source datasets.

The aggregation of data complies with the existing licenses of previously published datasets, where licensing information is available (Reddit Pushshift under CC0; Voat, Bluesky, and Koo under CC BY 4.0 International). The MADOC dataset is released under CC BY 4.0 International License to ensure broad accessibility while maintaining attribution requirements.

The dataset includes offensive content present in post and comment text, URLs attached to posts, and community names and descriptions, which may be harmful to some users. However, the inclusion of this content is necessary for several important research purposes: enabling cross-platform studies of toxic and hateful content propagation, understanding the effectiveness of different moderation approaches, studying community dynamics around controversial topics, and analyzing patterns of harmful behavior across platforms. This content is particularly valuable for researchers studying the evolution and spread of harmful narratives across different social media environments.

We acknowledge several potential risks of misuse of this dataset, including: use of the data to train harmful AI models or content generation systems, analysis aimed at identifying vulnerable communities or users, attempts to re-identify users across platforms, and exploitation of toxic content patterns for harassment. To mitigate these risks, we have implemented several safeguards. These include clear documentation of appropriate use cases and research guidelines, strict pseudonymization protocols that make re-identification significantly more difficult, release through established academic repository (Zenodo) with usage tracking, and detailed metadata and documentation following FAIR principles.

Despite these risks, we believe the dataset provides significant value for legitimate research purposes. It enables understanding of cross-platform content moderation effectiveness, studying community migration patterns and their impact, developing better detection systems for harmful content, and improving platform design to promote healthier online interactions. We encourage researchers using MADOC to carefully consider these ethical implications in their work and to implement appropriate safeguards in their research designs. Following standard ethical guidelines and making no attempt to re-identify users, we have focused on creating a resource that balances research utility with responsible data stewardship.

Field	**Description**
post_id	Unique identifier for the interaction, anonymized to prevent reconstruction of original URLs
publish_date	UNIX timestamp of the interaction (seconds since epoch)
user_id	Anonymized identifier of the content creator, consistent across all interactions from the same user
parent_id	Identifier of the parent post for comments/replies, NA for original posts
parent_user_id	Identifier of the parent post's creator, NA for original posts
content	Textual content of the interaction, with URLs extracted
url	External URLs referenced in the content, multiple URLs separated by '|'
language	Detected language code (currently 'English' for all entries)
interaction_type	Type of interaction: 'POST', 'COMMENT', or 'REPOST'
platform	Source platform: 'reddit', 'voat', 'bluesky', or 'koo'
community	Community identifier (subreddit/subverse name), NA for Bluesky/Koo
sentiment_vader	VADER sentiment score ranging from -1 (negative) to 1 (positive)
sentiment_textblob	TextBlob sentiment polarity score ranging from -1 (negative) to 1 (positive)
subjectivity_textblob	TextBlob subjectivity score ranging from 0.0 (objective) to 1.0 (subjective)
toxicity_toxigen	ToxiGen toxicity score ranging from 0.00 (non-toxic) to 1.00 (toxic)
strict_filter	Whether content matches strict keyword filtering criteria (TRUE/FALSE)

Table 2: Structure of the MADOC dataset. Each row represents a single interaction (post, comment, or repost) with the fields standardized across all platforms.

Community	Reddit				Voat			
	Posts	**Comments**	**Users**	**Avg. Sent.**	**Posts**	**Comments**	**Users**	**Avg. Sent.**
funny	4.2M	57.6M	5.5M	0.056	47K	97K	20K	0.001
gaming	2.9M	41.4M	4.1M	0.114	29K	41K	12K	0.093
pics	2.4M	49.5M	4.9M	0.075	15K	24K	9K	0.037
videos	3.1M	33.7M	3.2M	0.054	45K	41K	14K	-0.037
gifs	449K	20.6M	2.8M	0.051	8K	14K	6K	0.029
technology	848K	10.9M	1.3M	0.055	35K	49K	19K	0.029
fatpeoplehate	0	1.4M	79K	0.011	75K	279K	22K	0.002
GreatAwakening	67K	848K	26K	0.079	103K	222K	12K	0.016
MillionDollarExtreme	69K	1.2M	28K	0.008	7K	14K	3K	0.000
CringeAnarchy	195K	6.3M	342K	-0.031	1K	2K	1K	-0.038
KotakuInAction	128K	6.7M	146K	-0.029	3K	5K	2K	-0.028
MensRights	148K	3.0M	185K	-0.076	2K	2K	1K	-0.162

Table 3: Community-level statistics for Reddit and Voat. The first six rows show general-interest communities, while the last six show controversial communities. Average sentiment scores range from -1 (negative) to 1 (positive).

Lecture Notes in Computer Science 16061

Founding Editors

Gerhard Goos
Juris Hartmanis

The series Lecture Notes in Computer Science (LNCS), including its subseries Lect
Notes in Artificial Intelligence (LNAI) and Lecture Notes in Bioinformatics (LNB
has established itself as a medium for the publication of new developments in comp
science and information technology research, teaching, and education.

LNCS enjoys close cooperation with the computer science R & D community,
series counts many renowned academics among its volume editors and paper authors,
collaborates with prestigious societies. Its mission is to serve this international comn
nity by providing an invaluable service, mainly focused on the publication of confere
and workshop proceedings and postproceedings. LNCS commenced publication in 197

Ivan Lirkov · Svetozar Margenov
Editors

Large-Scale Scientific Computations

15th International Conference, LSSC 2025
Sozopol, Bulgaria, June 16–20, 2025
Revised Selected Papers

Springer

Editors
Ivan Lirkov
Bulgarian Academy of Sciences
Sofia, Bulgaria

Svetozar Margenov
Bulgarian Academy of Sciences
Sofia, Bulgaria

ISSN 0302-9743 ISSN 1611-3349 (electronic)
Lecture Notes in Computer Science
ISBN 978-3-032-22220-6 ISBN 978-3-032-22221-3 (eBook)
https://doi.org/10.1007/978-3-032-22221-3

This Springer imprint is published by the registered company Springer Nature Switzerland AG
The registered company address is: Gewerbestrasse 11, 6330 Cham, Switzerland

Preface

The 15th International Conference on Large-Scale Scientific Computations (LSS
2025) was held in Sozopol, Bulgaria, June 16–20, 2025. The conference was o
nized by the Institute of Information and Communication Technologies at the Bulgar
Academy of Sciences and MIV Consult Ltd. in cooperation with the Center of E
lence in Informatics and Information and Communication Technologies, and Sozop
municipality.

The plenary invited speakers and lectures were:

– Pavel Bochev, Data-Driven Compact Models for Devices and Circuits: a Syste
  Identification Approach for Non-intrusive Reduced-Order Modeling of Normal an
  Radiation Environments in Microelectronics
– Ulrich Langer, State-Based Numerical Solution of PDE-constrained Optimal Contr
  Problems
– Kent-Andre Mardal, Mathematical Challenges of Modeling the Fluid Flow of t
  Brain—Brain Clearance, Sleep and Dementia
– Markus Melenk, High-Order Methods for Fractional Diffusion
– Marcus Sarkis, Adaptive LOD BDDC for Elliptic Problems with Rough Coefficie
– Panayot Vassilevski, Interpolation Spaces, Fractional Order Operators, and Scales
  Multilevel Decompositions
– Gabriel Wittum, Parallel Adaptive Simulation of Processes from Science a
  Engineering

The success of the conference and the present volume are the outcome of the
efforts of many partners from various institutions and organizations. First, we would
to thank all the members of the Scientific Committee for their valuable contributi
forming the scientific face of the conference, as well as for their help in revie
contributed papers. We especially thank the organizers of the special sessions. We
also grateful to the staff involved in the local organization.

Traditionally, the purpose of the conference is to bring together scientists work
with large-scale computational models in natural sciences and environmental and ind
trial applications, as well as specialists in the field of numerical methods and algori
for modern high-performance computers. The invited lectures reviewed some of t
most advanced achievements in the field of numerical methods and their efficient ap
cations. The conference talks were presented by researchers from academic institutio
and practical industry engineers including applied mathematicians, numerical analyst
and computer experts. The general theme for LSSC 2025 was "Large-Scale Scient
Computing" with a particular focus on the organized special sessions.

The special sessions and organizers were:

– Numerical Methods: Analysis and Computations, In memory of Raytcho Lazarov–
  Svetozar Margenov and Panayot Vassilevski
– Mathematical and Numerical Modeling of Multiphysics Problems—Ivan Yotov

– Variational Analysis and Optimal Control—Mikhail Krastanov and Vladimir Velio
– Space-Time Methods for PDE-Based Simulation and Optimization—Ulrich Lange and Thomas Wick
– Numerical Methods for Nonlocal Problems—Markus Faustmann and Markus Melen
– Fractional Operators and Multi-Physics—Timo Koch, Miroslav Kuchta, Kent-Andre Mardal, and Ludmil Zikatanov
– Recent Advances in Computational and Applied Poromechanics—Markus Bause Johannes Kraus, and Maria Lymbery
– Mathematics and Algorithms for Predictive Digital Twins (DT) —Pavel Bochev, Iri Tezaur, and Paul Kuberry
– Adaptive and Robust Domain Decomposition Methods—Marcus Sarkis
– Applications of Metaheuristics to Large-Scale Problems—Stefka Fidanova anc Gabriel Luque
– Large-Scale Models: from Life Sciences to Climate Research—Ivan Dimov ar Nevena Ilieva
– HPC and HPDA: Algorithms and Applications—Aneta Karaivanova, Todor Guro and Emanouil Atanassov
– Numerical Solvers and Preconditioners for Differential Equations—Fabio Durastant and Mariarosa Mazza
– Porous Media Flow and Transport—Gabriel Wittum

About 150 participants from all over the world attended the conference represent some of the strongest research groups in the field of advanced large-scale scientific c puting. For the conference proceedings in total 69 papers were received. The organi of the special sessions managed the reviewing process in their sessions. Following initial single-blind review phase by reviewers in which submissions received an aver of two reviews each, the special session organizers provided a recommendation for e paper. Following a final revision of the papers the editors of the volume made their decision about the acceptance of the papers. This process resulted in the publicatio 58 papers by authors from 15 countries.

The next international conference on LSSC will be organized in June 2027.

February 2026

Ivan Lirkov
Svetozar Margenov

Organization

Program Committee Chair

Svetozar Margenov	Institute of Information and Communication Technologies, BAS, Bulgaria

Scientific Committee

Lidia Aceto	Università del Piemonte Orientale, Italy
Emanouil Atanassov	Institute of Information and Communication Technologies, BAS, Bulgaria
Markus Bause	Helmut Schmidt University, Hamburg, Germany
Pavel Bochev	Sandia National Laboratories, USA
Ivan Dimov	Institute of Information and Communication Technologies, BAS, Bulgaria
Markus Faustmann	TU Wien, Austria
Stefka Fidanova	Institute of Information and Communication Technologies, BAS, Bulgaria
Ivan Georgiev	Institute of Information and Communication Technologies, BAS, Bulgaria
Todor Gurov	Institute of Information and Communication Technologies, BAS, Bulgaria
Stanislav Harizanov	Institute of Information and Communication Technologies, BAS, Bulgaria
Oleg Iliev	Fraunhofer ITWM, Germany
Nevena Ilieva	Institute of Information and Communication Technologies, BAS, Bulgaria
Aneta Karaivanova	Institute of Information and Communication Technologies, BAS, Bulgaria
Mikhail Krastanov	Institute of Mathematics and Informatics, BAS, Bulgaria
Johannes Kraus	University of Duisburg-Essen, Germany
Paul Kuberry	Sandia National Laboratories, USA
Miroslav Kuchta	Simula Research Laboratory, Norway
Ulrich Langer	Johannes Kepler University Linz, Austria
Ivan Lirkov	Institute of Information and Communication Technologies, BAS, Bulgaria
Gabriel Luque	University of Málaga, Spain

Maria Lymbery	University of Duisburg-Essen, Germany
Kent-Andre Mardal	University of Oslo, Norway
Svetozar Margenov	Institute of Information and Communication Technologies, BAS, Bulgaria
Markus Melenk	TU Wien, Austria
Maya Neytcheva	Uppsala University, Sweden
Marcus Sarkis	Worcester Polytechnic Institute,USA
Irina Tezaur	Sandia National Laboratories, USA
Panayot Vassilevski	Portland State University, USA
Vladimir Veliov	TU Vienna, Austria
Thomas Wick	Leibniz University Hannover, Germany
Gabriel Wittum	King Abdullah University of Science and Technology, Saudi Arabia
Ivan Yotov	University of Pittsburgh, USA
Ludmil Zikatanov	Pennsylvania State University, USA
Zahari Zlatev	Aarhus University, Denmark

Contents

High-performance data analytics for analysis of collective trust dynamics

Darja Cvetković[1][0000-0002-3649-719X], Sara Major[2][0009-0008-7901-5489], Aleksandar Tomašević[2][0000-0003-4863-6051], Slobodan Maletić[3][0000-0001-7642-8271], Miroslav Anđelković[3][0000-0002-4449-8934], Ana Vranić[1][0000-0002-8729-654X], Boris Stupovski[1][0009-0009-5610-0012], Dušan Vudragović[1][0000-0001-5735-3198], Aleksandra Alorić[1][0000-0002-7278-599X], Aleksandar Bogojević[1][0000-0001-6850-6786], and Marija Mitrović Dankulov[1][0000-0002-8484-3501]

[1] Institute of Physics Belgrade, Univeristy of Belgrade, Pregrevica 118, 11080 Belgrade, Serbia
[2] Faculty of Philosophy, University of Novi Sad, Serbia
[3] Vinča Institute of Nuclear Sciences, University of Belgrade, Serbia
mitrovic@ipb.ac.rs

Abstract. Trust is a fundamental force that binds society together, yet the emergence and evolution of collective trust in social groups remain insufficiently understood. With over two billion active users engaging online, vast amounts of data provide an opportunity to analyze trust formation at a large scale. In this work, we integrate high-performance data analytics of empirical data to investigate how the structure of social networks influences trust dynamics. We aim to uncover key network properties that drive collective trust by leveraging complex network theory and novel topological methods. We explain our approach in details and apply it to one of the closed social groups in Stack Exchange networks. Our results show that while this group had relatively large and well connected core, typical for sustainable communities, the dynamics of collective trust was a good indicator of its dissolution. We illustrate how different types of structures contribute to the dynamics of the number of active users and the role of collective trust in the sustainability of online social groups.

Keywords: collective trust · social networks · data analysis

1 Introduction

In recent years, there has been a growing concern over the apparent decrease in trust among the general public towards various social and political institutions, as well as the mass media. The decline in trust in public institutions has been attributed to a variety of factors, including economic insecurity, perceptions of poor or corrupt government performance. Decrease of trust in mass media [9] has also been linked to this broader trend, with individuals becoming more skeptical of the information they receive from traditional media outlets. While trust in these traditional institutions has been declining, trust in social media platforms and online communities has seen a notable increase. Studies show that private online groups, community-driven platforms (e.g., Reddit, X), and interest-based forums are increasingly trusted as sources of information. A 2022 Edelman Trust Barometer survey [1] found that nearly 60% of respondents trusted people in online communities more than government officials or journalists. This reflects a shift toward peer-driven information ecosystems where trust is built through personal interactions and shared experiences.

Trust in traditional social groups was built through shared identity, frequent face-to-face interactions, and mutual aid, reinforcing a sense of community [12]. Rituals, traditions, and social norms helped maintain cohesion, while trusted leaders and elders provided stability. Interdependence in daily life made trust essential, and kinship ties further strengthened social bonds. Accountability was ensured through reputation and informal enforcement, fostering long-term relationships based on reliability and reciprocity. Unlike traditional social groups, online social groups are large, diverse, and often lack the close-knit, face-to-face interactions that historically built trust [3]. Instead of relying on shared identity and direct reciprocity, online communities establish trust through shared interests, transparency in communication, and active participation in discussions. Members of social groups also signal the trustworthy individuals by communicating with them [13]. Online social groups exhibit an emergence of collective or social trust [11].

Clearly, online social groups have become integral to modern social life, fostering connections, information sharing, and collective action [8]. However, the dynamics of collective trust within these online groups are complex and multifaceted, with important implications for their cohesion, influence, and long-term sustainability [11]. The structure of the social network underlying an online group can significantly shape the dynamics of collective trust [11]. For instance, the presence of influential "social media influencers" or hubs within the network can affect the flow of information and the formation of trust between members. These prominent individuals have the power to steer conversations, popularize certain worldviews, and establish themselves as trusted sources of information, potentially influencing the beliefs and behaviors of the larger collective [5].

In this manuscript we present a high-performance data analysis framework that enables study of evolution of structure of social networks and dynamics of collective trust within the online social groups. The abundance of detailed data about the structure and interactions within online social networks has enabled researchers to study the emergence and dynamics of collective trust, evolution of networks topology and their complex connection. We base our framework on tools and methods from complex networks theory, computer science and sociology. The framework enables analysis of collective trust in online social groups. Using advanced computational techniques we examine interaction patterns and reputation dynamics, and identify trustworthy members, detect anomalies, and predict the evolution of trust within online communities.

The structure of the paper is the following. We describe data and present methodology in the Section 2 and then demonstrate it in Section 3 on Stack Exchange *Startups* community. We give brief conclusion in Section 4.

2 Methodology

2.1 Data

Social media platforms have become ubiquitous in our daily lives, with billions of users worldwide generating vast troves of data that offer unprecedented insights into human behavior, social dynamics, and cultural trends. This wealth of information has the potential to unlock groundbreaking discoveries, but also presents a unique set of challenges that researchers must navigate with care [7].

One of the key advantages of social media data is their ability to capture real-time, large-scale interactions between individuals across diverse geographic and demographic boundaries [7]. This data can be leveraged to study complex phenomena, such as the spread of information, the emergence of online communities, and the impact of social media on mental health and well-being. While these platforms have different purposes, and as a consequence, the obtain data can be of different structure, the interactions are always asynchronous, textual and are used to convey information, opinion and sentiment. This enables us to standardize the data structure and enable cross-platform analysis.

We follow the data structure described in the Multi-Platform Aggregated Dataset of Online Communities [7]. The dataset is structured with each row representing a single interaction with fields include a pseudonymized identifier of the content creator, post id, a parent post identifier, the content's text, URLs, interaction type, the platform of origin. Type of interaction depends on the platform. For instance, *post* and *comment* are for platforms like Reddit and Voat, *question*, *answer* and *comment* for Stack Exchange, and *post*, *comment* and *repost* for Koo and BlueSky platform.

2.2 Complex networks structure

Social networks have become an integral part of our daily lives, and the study of their structure has become increasingly important in various fields, including sociology, psychology, and computer science. Social networks can be understood as a collection of individuals or organizations connected by a set of relationships, such as friendship, kinship, or shared interests [10]. Mathematically, social networks are represented by complex networks or graphs, where individuals and organizations are represented by nodes and the connections between them are represented by edges [2]. Depending on interaction symmetricity we can distinguish between directed graphs, where the links between nodes have a direction from, and undirected graphs, where the links are reciprocal. If all interactions have the same importance, we use unweighted graphs; if interactions have different weights, we use weighted graphs [2]. If individuals or organizations are of different types where interactions are only allowed between nodes of different types we have multipartite networks, otherwise networks are monopartite [2]. To represent a social network with interactions of different type we use multiplex networks.

The field of complex networks theory focuses on understanding the structure and dynamics of these social networks, including the roles and behaviors of individual actors, the patterns of relationships, and the overall network properties. Crucial to this field is the examination of network topology on local, mesoscopic and global level. On local level, we examine the distribution of nodes' connections or a local cohesiveness of immediate neighborhood of a node. On mesoscopic level we examine community or core-periphery structure, while on global level we analyze properties like network diameter, average path length, degree distribution and centralization [10]. Understanding the structure of social networks can provide valuable insights into a wide range of social phenomena, such as information diffusion, opinion formation, and the spread of diseases [10]. For example, studies have shown that the structure of social networks can influence the spread of information and the adoption of new technologies [10].

In the case of our data, we are interested in the structure and dynamics of social networks between users of a certain platform, where interactions are of the same importance. Thus, we map our data onto unweighted, monopartite, undirected social network G [2]. The link exists between two users, i and j, if they interacted on a question or a posts. We are interested in the evolution of structural properties of this network over time. For these reasons we consider aggregates of the data for certain time window and map these data onto networks. The choice of time window will depend on different factors, including the temporal span of available data, the expected evolution speed of the network, and the specific objectives of the study.

We focus on local cohesiveness and how it evolves during time in a social group. Local cohesiveness can be measured using different metrics, but the most common one is clustering coefficient of a node. The clustering coefficient of a node is a measure of the degree to which the neighbors of that node tend to be connected to each other. Clustering coefficient can also be aggregated on the network level to give the average clustering coefficient of the entire network, which indicates the overall tendency of nodes to form tightly-knit groups. The clustering coefficient c_i of the node i equals $c_i = \frac{e_i}{\frac{q_i}{2}(q_i-1)}$, where e_i is the number of edges existing between neighbors of node i, while q_i is the number of neighbors of node i and $\frac{q_i}{2}(q_i - 1)$ is number of possible links between them. The clustering coefficient can take values between 0 and 1, where 0 is typical for tree-like structure, while 1 corresponds to fully connected neighborhood. We want to follow the evolution of the network properties over time, which means that the number of nodes, edges and clustering coefficient are changing over time.

The concept of core-periphery structure has been extensively studied in various fields, including sociology, economics, and network science. In the context of social networks, the core-periphery structure refers to the organization of nodes (individuals, groups, or organizations) into a central, densely connected core and a peripheral set of nodes that are less connected to the core [4]. This structural pattern has important implications for understanding of structure and dynamics of social networks. We study the evolution of core-periphery structure of network in online social groups. Specifically, we determine core periphery structure of each network, analyze the structure of core, and the connectivity within the core and between core and periphery.

To detect core-periphery structure we use adaptation of stochastic block model (SBM). This approach models the network structure as a block matrix with blocks representing different groups, allowing us to identify core and periphery nodes in the network. Using SBM model we search for the optimal values of parameters p and θ for which our model is the most probable one to produce our network. Here p is a two dimensional symmetric matrix with the following constraint $0 < p_{22} < p_{12} < p_{11} < 1$, where p_{22} and p_{11} are probabilities of connections between nodes in network periphery and core, respectively, and p_{12} probability of connections between a pair of nodes belonging to two different groups. The element i of vector θ can take values 1 and 2 and indicates the node's group membership. The most probable model for a network G maximizes likelihood

$$P(G|p,\theta) = \prod_{i<j} p_{\theta_i\theta_j}^{A_{ij}} (1 - p_{\theta_i\theta_j})^{1-A_{ij}}, \tag{1}$$

where A_{ij} is the element of adjacency matrix whose value is equal 1 if the nodes i and j are connected, and 0 otherwise. We fit the model using Metropolis-within-Gibbs algorithm and following the procedure given in [4]. We use described approach to determine core-periphery structure of network in each instance, and analyze the size and stability of the core. We also measure the evolution of number of links within the core and between core and periphery per node.

2.3 Dynamic reputation model

The concept of reputation has gained significant attention in various fields, including economics, sociology, and computer science. As the digital landscape continues to evolve, the notion of reputation has become increasingly dynamic, driven by the emergence of web-based platforms and social media. Researchers have explored the factors that contribute to the formation and management of online reputation, particularly in the context of social e-commerce.

Here we use reputation as a proxy of trustworthiness of users in a social group. Specifically, we use Dynamic Interaction Based Reputation Model (DIBRM) to estimate the evolution of trustworthiness of users over time [6]. The model assumes that the reputation of the user increases with each activity and decreases if the user is inactive. The highest reputation growth occurs after bursts of activity followed by short inactivity periods. We use discrete time to determine the reputation of the user on daily basis. The user's reputation on day n T_n is calculated based on her reputation on day $n-1$ and contribution of activity to reputation I_n using the following formula

$$T_n = T_{n-1}\beta^{\Delta_n} + I_n \ , \tag{2}$$

Here β is the forgetting factor and together with Δ_n determines the velocity of reputational decay. Δ_n is the number of periods between two different interactions and is equal $\Delta_n = \frac{t_n - t_{n-1}}{t_a}$ is the number of periods between the two successive interactions, while t_a time window represents the maximum time spent by the user to make a meaningful contribution. The value of parameter t_a depends on a platform type, but our experiments show that for social media platforms $t_a = 2$. The reputation contribution I_n is calculated based on

$$I_n = I_{bn} + I_{cn} = I_{bn}(1 + \alpha(1 - \frac{1}{S_n - 1})) \ , \tag{3}$$

where α s the weight of the cumulative part, I_{bn} contribution of single activity to reputation and S_n is number of sequential activities. $I_n = 0$ if the user is not active at time t_n. We chose the following values of parameters: $\beta = 0.96$, $I_{bn} = 1$, and $\alpha = 2$, see [11] for more details.

3 Example

To demonstrate our approach we analyze the first 180 days of the Stack Exchange closed group *Startups*. Stack Exchange is a network of Question and Answers (*Q&A*) social groups covering a wide range of topics. In these groups users can ask and answer questions, as well comment question and answers. Each of these activities is mapped onto a network and is represented as a link. If user i answers or comments question, or accepts or comments answer of user j, we create a link between user i and j. We disregard multiple interactions and direction of interaction. We only consider interactions within the time window of 30 days, and slide this window to cover the first 180 days of groups existence. This way we obtain 150 networks and analyze their properties using our approach to study the evolution of social network structure and dynamics of reputation in *Startups* social group. The *Startups* group was dedicated to topics related to startups. After launch it struggled to attract and maintain the necessary community engagement during its beta phase, which led to its closure.

Figure 1 shows the results of our analysis. Average clustering coefficient, shown in Fig. 1 (a), fluctuates over the first 100 days, and then it exhibits slow decrease. Social networks, compared to biological and technological networks, have relatively high value of clustering coefficient, thus it is not surprising that we observe relatively high cohesion in this social group. However, the steady decrease of clustering coefficient in the last 60 days of our observation period indicates that local neighborhoods of nodes became less and less connected. The number of nodes in the core exhibits large fluctuations during first 100 days with around 45 nodes in the core on average (see Fig. 1 (b)). Again, we see a drop in the average core size to approximately 35 nodes in the last 60 days, indicating the decrease in community stability. This is further confirmed by the decrease of number of links between users in the core per user, Fig. 1 (c), and number of links between users the core and periphery, Fig. 1 (d).

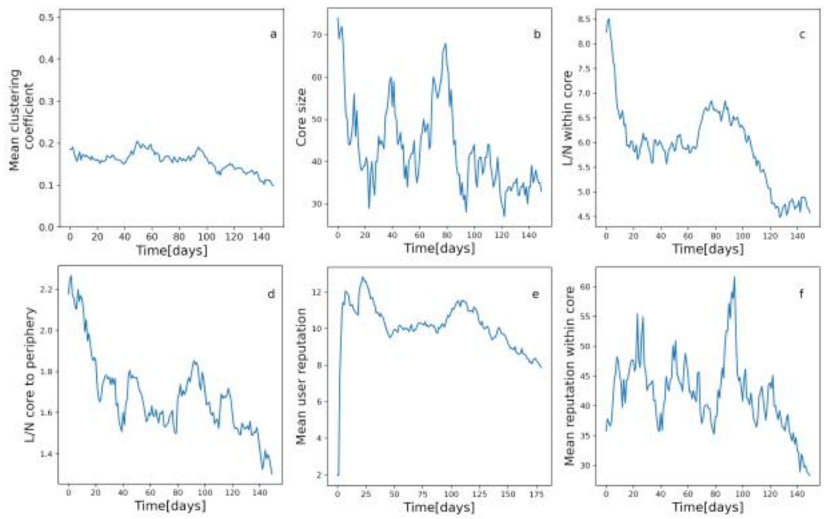

Fig. 1. (top panel) Evolution of clustering (a), core size (b), number of links among users within the core averaged over number of users (c), number of links among between core and periphery users averaged over number of users (d), average dynamical reputation of all users (e) and users within the core (f) of social network for *Startups* social group for the first 180 days of it existence.

Average user reputation (Fig. 1 (e)) and average reputation of users in the core (Fig. 1 (f)) show that users in the core have three times higher reputation than the average user in the social group. This is observed in other communities, both closed and active ones [11], but in active communities the average reputation of core users either grows or remains steady over the period od 180 days while in closed communities we see decrease at the end of this period. The decrease of average reputation in the whole group and within the core was an indicator that the group will be eventually closed.

4 Conclusion

In this paper we presented the high-performance data analytics approach for studying collective trust dynamics in online social groups. The approach is based on methods and tools from complex network theory, computer science and sociology and can be used for studying collective trust dynamics in various online social groups. We demonstrated our approach on *Startups* social group from Stack Exchange *Q&A* network. Our results show that at the beginning the group gained momentum with relatively large core size, and relatively high connectivity in the core and between core and periphery, comparable to still active communities [11]. However, the value and dynamics of collective trust resembled more to one observed in closed communities [11]. The same approach can be applied to other online social groups [7] to study other phenomena and characteristics of social groups, besides their sustainability.

Acknowledgments. This research was financially supported by the Science Fund of Republic of Serbia, 7416, Topology-derived methods for the analysis of collective trust dynamics - CTRUST. The work of M.M.D. and V.D. is also supported by the EUROHPC JU through the project EUROCC4SEE, Grant Agreement No. 101191697. Data processing was performed on PARADOX-IV supercomputing facility at the Scientific Computing Laboratory, National Center of Excellence for the Study of Complex Systems, Institute of Physics Belgrade.

Competing interests. The authors declare no competing interests.

References

1. Barometer, E.T.: Edelman trust barometer. Retrieved March **24**, 2021 (2021)
2. Boccaletti, S., Latora, V., Moreno, Y., Chavez, M., Hwang, D.U.: Complex networks: Structure and dynamics. Physics reports **424**(4-5), 175–308 (2006)
3. Donath, J.: Signals in social supernets. Journal of computer-mediated communication **13**(1), 231–251 (2007)
4. Gallagher, R.J., Young, J.G., Welles, B.F.: A clarified typology of core-periphery structure in networks. Science advances **7**(12), eabc9800 (2021)
5. Huang, C.C., Liang, W.Y., Chen, P.A., Chan, Y.C.: Identification of opinion leaders and followers—a case study of green energy and low carbons. Applied Sciences **10**(23), 8416 (2020)
6. Melnikov, A., Lee, J., Rivera, V., Mazzara, M., Longo, L.: Towards dynamic interaction-based reputation models. In: 2018 IEEE 32nd international conference on Advanced Information Networking and Applications (AINA). pp. 422–428. IEEE (2018)
7. Mitrović Dankulov, M., Tomašević, A., Maletić, S., Anđelković, M., Vranić, A., Cvetković, D., Stupovski, B., Vudragović, D., Major, S., Bogojević, A.: Multiplatform aggregated dataset of online communities (madoc). arXiv e-prints pp. arXiv–2501 (2025)
8. Oliver, P.E., Marwell, G.: Whatever happened to critical mass theory? a retrospective and assessment. Sociological Theory **19**(3), 292–311 (2001)
9. Perry, J., et al.: Trust in public institutions: Trends and implications for economic security (2021)
10. Sen, P., Chakrabarti, B.K.: Sociophysics: an introduction. OUP Oxford (2014)
11. Vranić, A., Tomašević, A., Alorić, A., Dankulov, M.M.: Sustainability of stack exchange q&a communities: the role of trust. EPJ Data Science **12**(1), 4 (2023)
12. Whitehouse, H., Lanman, J.A.: The ties that bind us: Ritual, fusion, and identification. Current Anthropology **55**(6), 674–695 (2014)
13. Zou, Q., Park, E.G.: Trust and trust building of virtual communities in the networked age. In: Handbook of Research on Emerging Developments in Data Privacy, pp. 300–328. IGI Global Scientific Publishing (2015)

Lecture Notes in Computer Science 16061

The series Lecture Notes in Computer Science (LNCS), including its subseries Lect Notes in Artificial Intelligence (LNAI) and Lecture Notes in Bioinformatics (LNB has established itself as a medium for the publication of new developments in comp science and information technology research, teaching, and education.

LNCS enjoys close cooperation with the computer science R & D community, series counts many renowned academics among its volume editors and paper authors, collaborates with prestigious societies. Its mission is to serve this international comn nity by providing an invaluable service, mainly focused on the publication of confere and workshop proceedings and postproceedings. LNCS commenced publication in 197

Ivan Lirkov · Svetozar Margenov
Editors

Large-Scale Scientific Computations

15th International Conference, LSSC 2025
Sozopol, Bulgaria, June 16–20, 2025
Revised Selected Papers

Springer

Editors
Ivan Lirkov
Bulgarian Academy of Sciences
Sofia, Bulgaria

Svetozar Margenov
Bulgarian Academy of Sciences
Sofia, Bulgaria

ISSN 0302-9743 ISSN 1611-3349 (electronic)
Lecture Notes in Computer Science
ISBN 978-3-032-22220-6 ISBN 978-3-032-22221-3 (eBook)
https://doi.org/10.1007/978-3-032-22221-3

This Springer imprint is published by the registered company Springer Nature Switzerland AG
The registered company address is: Gewerbestrasse 11, 6330 Cham, Switzerland

Preface

The 15th International Conference on Large-Scale Scientific Computations (LSS
2025) was held in Sozopol, Bulgaria, June 16–20, 2025. The conference was o
nized by the Institute of Information and Communication Technologies at the Bulgar
Academy of Sciences and MIV Consult Ltd. in cooperation with the Center of Ex
lence in Informatics and Information and Communication Technologies, and Sozop
municipality.

The plenary invited speakers and lectures were:

– Pavel Bochev, Data-Driven Compact Models for Devices and Circuits: a Syste
Identification Approach for Non-intrusive Reduced-Order Modeling of Normal an
Radiation Environments in Microelectronics
– Ulrich Langer, State-Based Numerical Solution of PDE-constrained Optimal Contr
Problems
– Kent-Andre Mardal, Mathematical Challenges of Modeling the Fluid Flow of t
Brain—Brain Clearance, Sleep and Dementia
– Markus Melenk, High-Order Methods for Fractional Diffusion
– Marcus Sarkis, Adaptive LOD BDDC for Elliptic Problems with Rough Coefficie
– Panayot Vassilevski, Interpolation Spaces, Fractional Order Operators, and Scales
Multilevel Decompositions
– Gabriel Wittum, Parallel Adaptive Simulation of Processes from Science ar
Engineering

The success of the conference and the present volume are the outcome of the
efforts of many partners from various institutions and organizations. First, we would
to thank all the members of the Scientific Committee for their valuable contributi
forming the scientific face of the conference, as well as for their help in revie
contributed papers. We especially thank the organizers of the special sessions. We
also grateful to the staff involved in the local organization.

Traditionally, the purpose of the conference is to bring together scientists work
with large-scale computational models in natural sciences and environmental and ind
trial applications, as well as specialists in the field of numerical methods and algori
for modern high-performance computers. The invited lectures reviewed some of t
most advanced achievements in the field of numerical methods and their efficient ap
cations. The conference talks were presented by researchers from academic institutio
and practical industry engineers including applied mathematicians, numerical analysts
and computer experts. The general theme for LSSC 2025 was "Large-Scale Scient
Computing" with a particular focus on the organized special sessions.

The special sessions and organizers were:

– Numerical Methods: Analysis and Computations, In memory of Raytcho Lazarov–
Svetozar Margenov and Panayot Vassilevski
– Mathematical and Numerical Modeling of Multiphysics Problems—Ivan Yotov

– Variational Analysis and Optimal Control—Mikhail Krastanov and Vladimir Velio
– Space-Time Methods for PDE-Based Simulation and Optimization—Ulrich Lange and Thomas Wick
– Numerical Methods for Nonlocal Problems—Markus Faustmann and Markus Melen
– Fractional Operators and Multi-Physics—Timo Koch, Miroslav Kuchta, Kent-Andre Mardal, and Ludmil Zikatanov
– Recent Advances in Computational and Applied Poromechanics—Markus Bause Johannes Kraus, and Maria Lymbery
– Mathematics and Algorithms for Predictive Digital Twins (DT) —Pavel Bochev, Iri Tezaur, and Paul Kuberry
– Adaptive and Robust Domain Decomposition Methods—Marcus Sarkis
– Applications of Metaheuristics to Large-Scale Problems—Stefka Fidanova and Gabriel Luque
– Large-Scale Models: from Life Sciences to Climate Research—Ivan Dimov ar Nevena Ilieva
– HPC and HPDA: Algorithms and Applications—Aneta Karaivanova, Todor Gurov and Emanouil Atanassov
– Numerical Solvers and Preconditioners for Differential Equations—Fabio Durastante and Mariarosa Mazza
– Porous Media Flow and Transport—Gabriel Wittum

About 150 participants from all over the world attended the conference represent some of the strongest research groups in the field of advanced large-scale scientific c puting. For the conference proceedings in total 69 papers were received. The organi of the special sessions managed the reviewing process in their sessions. Following initial single-blind review phase by reviewers in which submissions received an avera of two reviews each, the special session organizers provided a recommendation for e paper. Following a final revision of the papers the editors of the volume made their decision about the acceptance of the papers. This process resulted in the publicatio 58 papers by authors from 15 countries.

The next international conference on LSSC will be organized in June 2027.

February 2026

Ivan Lirkov
Svetozar Margenov

Organization

Program Committee Chair

Svetozar Margenov	Institute of Information and Communication Technologies, BAS, Bulgaria

Scientific Committee

Lidia Aceto	Università del Piemonte Orientale, Italy
Emanouil Atanassov	Institute of Information and Communication Technologies, BAS, Bulgaria
Markus Bause	Helmut Schmidt University, Hamburg, Germany
Pavel Bochev	Sandia National Laboratories, USA
Ivan Dimov	Institute of Information and Communication Technologies, BAS, Bulgaria
Markus Faustmann	TU Wien, Austria
Stefka Fidanova	Institute of Information and Communication Technologies, BAS, Bulgaria
Ivan Georgiev	Institute of Information and Communication Technologies, BAS, Bulgaria
Todor Gurov	Institute of Information and Communication Technologies, BAS, Bulgaria
Stanislav Harizanov	Institute of Information and Communication Technologies, BAS, Bulgaria
Oleg Iliev	Fraunhofer ITWM, Germany
Nevena Ilieva	Institute of Information and Communication Technologies, BAS, Bulgaria
Aneta Karaivanova	Institute of Information and Communication Technologies, BAS, Bulgaria
Mikhail Krastanov	Institute of Mathematics and Informatics, BAS, Bulgaria
Johannes Kraus	University of Duisburg-Essen, Germany
Paul Kuberry	Sandia National Laboratories, USA
Miroslav Kuchta	Simula Research Laboratory, Norway
Ulrich Langer	Johannes Kepler University Linz, Austria
Ivan Lirkov	Institute of Information and Communication Technologies, BAS, Bulgaria
Gabriel Luque	University of Málaga, Spain

Maria Lymbery	University of Duisburg-Essen, Germany
Kent-Andre Mardal	University of Oslo, Norway
Svetozar Margenov	Institute of Information and Communication Technologies, BAS, Bulgaria
Markus Melenk	TU Wien, Austria
Maya Neytcheva	Uppsala University, Sweden
Marcus Sarkis	Worcester Polytechnic Institute,USA
Irina Tezaur	Sandia National Laboratories, USA
Panayot Vassilevski	Portland State University, USA
Vladimir Veliov	TU Vienna, Austria
Thomas Wick	Leibniz University Hannover, Germany
Gabriel Wittum	King Abdullah University of Science and Technology, Saudi Arabia
Ivan Yotov	University of Pittsburgh, USA
Ludmil Zikatanov	Pennsylvania State University, USA
Zahari Zlatev	Aarhus University, Denmark

Contents

Adaptive and Robust Domain Decomposition Methods

Applications of Metaheuristics to Large-Scale Problems

HPC and HPDA: Algorithms and Applications

Numerical Solvers and Preconditioners for Differential Equations

Porous Media Flow and Transport

Fractional Differential Problems: Theoretical Aspects, Algorithms and Applications

Contributed Papers

Parallel algorithm for solving dipolar Gross-Pitaevskii equation

Dušan Vudragović[1 [0000-0001-5735-3198]], Vladimir Lončar[1,2], and Antun Balaž[1 [0000-0002-5435-1688]]

[1] Institute of Physics Belgrade, University of Belgrade, Serbia
[2] Massachusetts Institute of Technology, United States of America

Abstract. There are several numerical methods available for solving the dipolar Gross-Pitaevskii equation, focusing on both the ground state properties and the non-stationary dynamics of a Bose-Einstein condensate. These methods can be categorized into three main types: finite difference, split-step, and spectral methods. In this paper, we present our numerical algorithm for solving the dipolar Gross-Pitaevskii equation, which combines the split-step method with the semi-implicit Crank-Nicolson approach. To calculate the ground state of the system, we use imaginary time propagation starting from an arbitrary initial state. In contrast, the dynamics of the system are determined through real-time propagation from a given initial wave function. We also present various parallelization strategies, aimed at both shared memory and distributed memory systems, with a particular focus on heterogeneous computing platforms.

Keywords: Crank-Nicolson method · Gross-Pitaevskii equation · Bose-Einstein condensates

1 Introduction

The presence of nonlinear terms in equations that describe physical systems often leads to novel phenomena. However, understanding these phenomena requires careful and detailed analysis, as intuition based on linear equations is insufficient for predicting the system's behavior. From an experimental standpoint, this necessitates the development and refinement of specialized methods tailored to specific phenomena. Additionally, it is often necessary to establish or further enhance analytical or numerical approaches to solve the relevant equations. In the case of a Bose-Einstein condensate (BEC) with dipole-dipole interactions, nonlinearity arises from two sources: contact interaction and the dipole-dipole interaction between the atoms in the condensate, while the behavior of the system is described by the dipolar Gross-Pitaevskii equation (GPE)

$$\begin{aligned} i\hbar\frac{\partial}{\partial t}\psi(\mathbf{r},t) = \Bigg[& -\frac{\hbar^2}{2m}\nabla^2 + U(\mathbf{r},t) + g|\psi(\mathbf{r},t)|^2 \\ & + \int d\mathbf{r}'\,\psi^*(\mathbf{r}',t)U_{\mathrm{dd}}(\mathbf{r}-\mathbf{r}',t)\psi(\mathbf{r}',t)\Bigg]\psi(\mathbf{r},t)\,. \end{aligned} \tag{1}$$

In the above equation, also known as the nonlinear Schrödinger equation, $U(\mathbf{r},t)$ represents the potential of the magneto-optical trap that confines the atoms in the condensate, g denotes the contact interaction coupling constant, $U_{\mathrm{dd}}(\mathbf{r})$ is the potential of the dipole-dipole interaction between the atoms, while $\psi(\mathbf{r},t)$ is the wave function of the condensate.

Various numerical methods have been developed in the literature to solve the GPE. Some of these methods focus on calculating the properties of the ground state [1–4], while others concentrate on the dynamics governed by the time-dependent GPE [5–13]. Additionally, there are several methods that can provide numerical solutions for both the ground state and the non-stationary dynamics of a BEC [5–13]. These methods can be categorized into several types, including finite difference methods, split-step methods, and spectral methods.

A finite difference method involves the discretization of both space and time. When working with the dipolar GPE, this discretization is typically carried out using different schemes: forward, backward, or central difference schemes for time derivatives, along with a second-order central difference scheme for spatial derivatives. In these methods, a forward difference scheme in time is referred to as an explicit method, while a backward difference approach is known as an implicit method. The central difference scheme in time incorporates aspects of both and is called a semi-implicit algorithm, specifically the Crank-Nicolson semi-implicit algorithm. In all our implementations, we used the Crank–Nicolson semi-implicit algorithm. This approach expresses the space derivatives as averages of their finite difference approximations in the present and future time steps, making the Crank-Nicolson scheme unconditionally stable.

The split-step method involves dividing the time evolution in each time step into several sub-steps. This corresponds to separating the Hamiltonian that governs the dynamics of the system into different components. Each component is then used to evolve the wave function independently. Typically, it is implemented by splitting the Hamiltonian, $\hat{H} = \hat{T} + \hat{V}$, into two parts: the kinetic energy part, $\hat{T}$, and the potential energy part, $\hat{V}$. For our GPE eq. 1, potential energy component includes the trap potential and nonlinear terms that account for both contact and dipole-dipole interactions.

To implement the splitting of the Hamiltonian and calculate the system's time evolution, we use the Baker-Campbell-Hausdorff lemma, also known as the Zassenhaus formula

$$e^{\Delta t(\hat{\mathcal{O}}_1+\hat{\mathcal{O}}_2)} = e^{\Delta t\hat{\mathcal{O}}_1}\, e^{\Delta t\hat{\mathcal{O}}_2}\, e^{-\frac{\Delta t^2}{2}[\hat{\mathcal{O}}_1,\hat{\mathcal{O}}_2]} e^{\frac{\Delta t^3}{6}(2[\hat{\mathcal{O}}_2,[\hat{\mathcal{O}}_1,\hat{\mathcal{O}}_2]]+[\hat{\mathcal{O}}_1,[\hat{\mathcal{O}}_1,\hat{\mathcal{O}}_2]])}\dots \quad (2)$$

where time step is denoted by Δt. The Zassenhaus formula provides a way to express the exponential of the sum of two operators $\hat{\mathcal{O}}_1$ and $\hat{\mathcal{O}}_2$, which generally do not commute, as a product of their individual exponentials along with additional terms that include quadratic and higher-order contributions of the parameter Δt. When Δt is small, we can ignore these higher-order terms and utilize the splitting formula, which for the time evolution of the Hamiltonian $\hat{H} = \hat{T} + \hat{V}$ gives

$$e^{-\frac{i}{\hbar}\hat{H}\Delta t} = e^{-\frac{i}{\hbar}(\hat{T}+\hat{V})\Delta t} = e^{-\frac{i}{\hbar}\hat{T}\Delta t}\, e^{-\frac{i}{\hbar}\hat{V}\Delta t} + \mathcal{O}(\Delta t^2)\,. \quad (3)$$

Thus, we introduce an error similar to that caused by the finite difference scheme employed to approximate time derivatives.

Spectral methods involve expressing the solution to the GPE as a linear combination of orthonormal special functions in a suitably chosen basis. This approach reformulates the original equation into a set of equations that determine the coefficients of the wave function expansion in the selected basis. For example, using a plane-wave basis yields the most common spectral decomposition of the wave function.

Our numerical algorithm to solve the GPE combines the split-step approach with the semi-implicit Crank-Nicolson method [14–16]. To calculate the ground state of the system, we propagate in imaginary-time [2–4] starting from an arbitrary initial state. For the system's dynamics, we use real-time propagation from a specified initial wave function. The corresponding codes that implement the algorithm solve the GPE in three physical dimensions. In the implementation, we rescaled variables to eliminate physical units, leading us to the following form of the GPE

$$\begin{aligned} i\,\frac{\partial\psi(\mathbf{r};t)}{\partial t} = \Bigg[&-\frac{\nabla^2}{2} + U(\mathbf{r};t) + 4\pi N a_s\,|\psi(\mathbf{r};t)|^2 \\ &+ 3N a_{\mathrm{dd}} \int d\mathbf{r}'\,U_{\mathrm{dd}}(\mathbf{r}-\mathbf{r}';t)\,|\psi(\mathbf{r}';t)|^2 \Bigg]\psi(\mathbf{r};t)\,, \end{aligned} \tag{4}$$

which is derived from the GPE eq. 1 by selecting a reference frequency and expressing all other physical variables in units defined using this frequency. The parameter a_s represents the s-wave scattering length, a_{dd} denotes the dipolar length, which measures the strength of dipole-dipole interactions, and N is the number of atoms in the condensate.

2 Algorithm

The split-step semi-implicit Crank-Nicolson method allow us to divide the Hamiltonian into the non-derivative ($\hat{H}_0$) and derivative ($\hat{H}_1$, $\hat{H}_2$, $\hat{H}_3$) parts

$$\hat{H}_0 = U(\mathbf{r};t) + 4\pi N a_s\,|\psi(\mathbf{r};t)|^2 + 3N a_{\mathrm{dd}} \int d\mathbf{r}'\,U_{\mathrm{dd}}(\mathbf{r}-\mathbf{r}';t)\,|\psi(\mathbf{r}';t)|^2\,, \tag{5}$$

$$\hat{H}_1 = \frac{\partial^2}{\partial x^2}\,,\quad \hat{H}_2 = \frac{\partial^2}{\partial y^2}\,,\quad \hat{H}_3 = \frac{\partial^2}{\partial z^2}\,, \tag{6}$$

which transforms our dipolar GPE (4) into four sequential partial differential equations

$$i\,\frac{\partial\psi(\mathbf{r};t)}{\partial t} = \hat{H}_j\,\psi(\mathbf{r};t)\,,\quad j=0,1,2,3\,, \tag{7}$$

which are solved one after the other in the algorithm.

Starting from a preceding solution $\psi^n(\mathbf{r})$, obtained in the previous complete time step, the time evolution with respect to $\hat{H}_0$ in the current time step yields an intermediate solution $\psi^{n+1/4}(\mathbf{r})$ of eq. 7 for $j=0$. The superscript $1/4$ denotes that this is a first of four sub-steps in the current time iteration. Since $\hat{H}_0$ has no derivatives, the solution can be written exactly as

$$\psi^{n+1/4}(\mathbf{r}) = e^{-i\hat{H}_0\Delta t}\,\psi^n(\mathbf{r}) \equiv \hat{\mathcal{P}}(\hat{H}_0)\,\psi^n(\mathbf{r})\,. \tag{8}$$

From this intermediate solution, using the semi-implicit Crank-Nicolson scheme, the time propagation of the wave function continues and is calculated by solving the series of partial differential equations,

$$\begin{aligned} i\,\frac{\psi^{n+2/4}(\mathbf{r}) - \psi^{n+1/4}(\mathbf{r})}{\Delta t} &= \frac{1}{2}\,\hat{H}_1\left[\psi^{n+2/4}(\mathbf{r}) + \psi^{n+1/4}(\mathbf{r})\right]\,, \\ i\,\frac{\psi^{n+3/4}(\mathbf{r}) - \psi^{n+2/4}(\mathbf{r})}{\Delta t} &= \frac{1}{2}\,\hat{H}_2\left[\psi^{n+3/4}(\mathbf{r}) + \psi^{n+2/4}(\mathbf{r})\right]\,, \\ i\,\frac{\psi^{n+1}(\mathbf{r}) - \psi^{n+3/4}(\mathbf{r})}{\Delta t} &= \frac{1}{2}\,\hat{H}_3\left[\psi^{n+1}(\mathbf{r}) + \psi^{n+3/4}(\mathbf{r})\right]\,. \end{aligned} \tag{9}$$

On the left-hand side, partial derivatives in time are estimated by a two-point formula, and on the right-side, the wave function is averaged over the current and the future time sub-step, which is a characteristic for the finite-difference semi-implicit Crank–Nicolson method. Eq. 9 have a formal solution that propagates the wave function to the next intermediate solution,

$$\begin{aligned} \psi^{n+2/4}(\mathbf{r}) &= \frac{1 - i\hat{H}_1\Delta t/2}{1 + i\hat{H}_1\Delta t/2}\,\psi^{n+1/4}(\mathbf{r}) \equiv \hat{\mathcal{P}}(\hat{H}_1)\,\psi^{n+1/4}(\mathbf{r})\,, \\ \psi^{n+3/4}(\mathbf{r}) &= \frac{1 - i\hat{H}_2\Delta t/2}{1 + i\hat{H}_2\Delta t/2}\,\psi^{n+2/4}(\mathbf{r}) \equiv \hat{\mathcal{P}}(\hat{H}_2)\,\psi^{n+2/4}(\mathbf{r})\,, \\ \psi^{n+1}(\mathbf{r}) &= \frac{1 - i\hat{H}_3\Delta t/2}{1 + i\hat{H}_3\Delta t/2}\,\psi^{n+3/4}(\mathbf{r}) \equiv \hat{\mathcal{P}}(\hat{H}_3)\,\psi^{n+3/4}(\mathbf{r})\,. \end{aligned} \tag{10}$$

Flowchart of the algorithm for solving the dipolar GPE is illustrated in Fig. 1. Using the parameters specified in the configuration input file, the algorithm in the very first step generates an initial wave function or reads its values from the external file. This is represented by the operator $\hat{\mathcal{I}}$, which will initialize the wave function matrix to be propagated within the main loop of the algorithm. In the case of imaginary-time propagation, most frequently, the initial wave function will be generated in the form of a predefined Gaussian, or if it is explicitly defined in the input file, it will be populated by the values from the external file. For real-time propagation, the initial wave function is always read from the external file. Usually, it is a wave function obtained from previous calculation, either in imaginary- or real-time propagation.

Using the initial wave function, the algorithm in N equal time steps Δt propagates the wave function. Each time step consists of four sub-steps, which are implemented using the operators $\hat{\mathcal{P}}(\hat{H}_0)$, $\hat{\mathcal{P}}(\hat{H}_1)$, $\hat{\mathcal{P}}(\hat{H}_2)$, $\hat{\mathcal{P}}(\hat{H}_3)$. After each step, the operator $\hat{\mathcal{M}}$ calculates the relevant physical quantities. In the case of imaginary-time propagation, there is an additional operation in which we normalize the wave function to 1 using the operator $\hat{\mathcal{N}}$. After the main loop is finished, the simulation saves the wave function for further use (operator $\hat{\mathcal{E}}$).

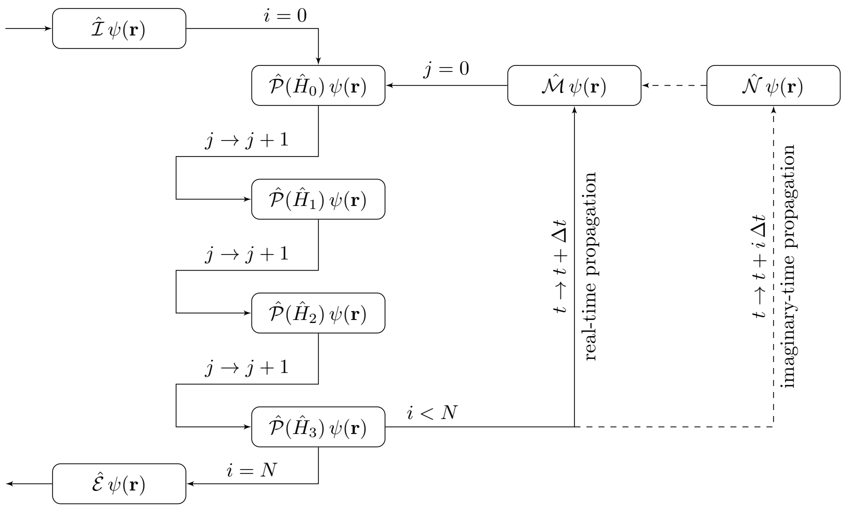

Fig. 1. Flowchart of the algorithm for solving the dipolar GPE. The operator $\hat{\mathcal{I}}$ is responsible for the initialization of the wave function matrix. Propagation of the wave function is done in four sub-steps using operators $\hat{\mathcal{P}}(\hat{H}_0)$, $\hat{\mathcal{P}}(\hat{H}_1)$, $\hat{\mathcal{P}}(\hat{H}_2)$, $\hat{\mathcal{P}}(\hat{H}_3)$. The operator $\hat{\mathcal{M}}$ calculates physical quantities of the system, and the operator $\hat{\mathcal{E}}$ saves the wave function for further use. In the case of imaginary-time propagation, the operator $\hat{\mathcal{N}}$ normalizes the wave function.

3 Parallelization and optimization

We developed an algorithm to solve the fully anisotropic three-dimensional dipolar GPE, building on our previous work [6, 7]. The initial program for the contact-interaction GPE was written in Fortran [5]. We subsequently rewrote this program in C and parallelized it using the Open Multi-Processing (OpenMP) [8–10, 13]. After that, we produced additional programs that include both contact and dipole-dipole interactions in both C and Fortran [11, 12]. Our numerical results show excellent agreement with recent experimental findings on dipolar BECs of atoms such as ^{52}Cr, ^{164}Dy, and ^{168}Er [17]. By parallelizing our programs, we were able to take full advantage of all available processors/cores on a shared memory computer, achieving efficiency of $70-90\%$ compared to ideal performance.

Fig. 2 depicts the speedup (circles) and efficiency (triangles) of execution times for both imaginary-time (left panel) and real-time (right panel) propagation, in relation to the number of CPU cores used. The speedup $S\,(N_{\mathrm{c}})$ is determined by comparing the execution time of a simulation run on a single CPU core with that of a simulation using N_{c} cores. Efficiency is defined as $S\,(N_{\mathrm{c}})\,/N_{\mathrm{c}}$, representing the ratio of the experimentally measured speedup to the ideal speedup, which is equal to N_{c}.

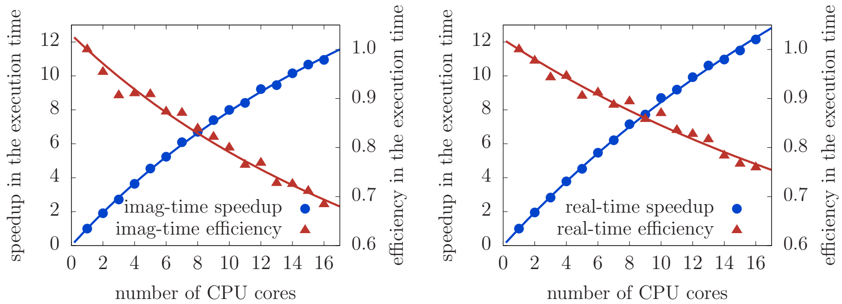

Fig. 2. Speedup (circles) and efficiency (triangles) of the algorithm for solving the dipolar GPE during imaginary-time (left) and real-time (right) propagation as a function of the number of utilized CPU cores.

Due to the inherent memory limitations of a single computer, we have developed a distributed memory algorithm [9, 10, 13] utilizing the Message Passing Interface (MPI) alongside a previous shared memory approach. To enhance the performance of hybrid implementations, we optimize the parameters that dictate data and workload distribution using a genetic algorithm. Testing was conducted with varying numbers of cluster nodes, ranging from 4 to 32, resulting in measured speedups between 11 and 16.5. The corresponding speedup and efficiency graphs are presented in the first row of Fig. 3, demonstrating that speedup increases linearly with the number of nodes, while efficiency remains relatively stable, fluctuating between $40 - 60\%$. This indicates that OpenMP/MPI programs offer significant advantages for solving problems with large grid sizes.

We have also developed CUDA/MPI programs [11, 12], and their performance is shown in the second row of Fig. 3. For 32 nodes, the observed speedup ranges from 9 to 10, with efficiency levels between $30-40\%$. While this efficiency is somewhat lower compared to the OpenMP/MPI programs - due to the complexities of the memory hierarchy in a multi-GPU system spread across multiple cluster nodes - the speedup still reflects a linear trend. This makes CUDA/MPI programs a strong candidate for deployment on GPU-enabled computer clusters. Additionally, these programs utilize minimal CPU resources (up to one CPU core), allowing the same cluster nodes to be available for other CPU-intensive simulations.

4 Conclusions

In this paper, we presented a numerical algorithm for solving the GPE. This algorithm combines the split-step method with the semi-implicit Crank-Nicolson approach. Additionally, we provided results from scalability testing of our parallel programs, which demonstrate their efficiency when executed on parallel computer clusters. The highest speedup we achieved was on a shared memory

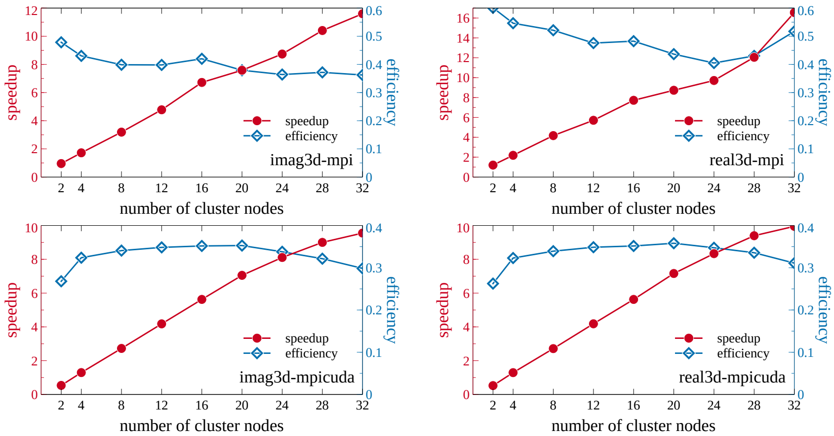

Fig. 3. Speedup (circles) and efficiency (diamonds) of the hybrid OpenMP/MPI (first row) and CUDA/MPI (second row) algorithms for solving the dipolar GPE during imaginary-time (left column) and real-time (right column) propagation as a function of the number of utilized cluster nodes.

computer, where the corresponding code can be effectively utilized up to a certain spatial discretization limit, which depends on the available memory of the specific node. For larger spatial meshes, we developed OpenMP/MPI code, which achieves a linear speedup as the number of nodes increases. For GPU-enabled computer clusters, we released CUDA/MPI programs. Although their efficiency is somewhat lower compared to the OpenMP/MPI programs, the speedup still shows a linear trend.

Acknowledgments. This work has been supported by the Institute of Physics Belgrade through a grant from the Ministry of Science, Technological Development, and Innovations of the Republic of Serbia. It was also funded by the EuroHPC Joint Undertaking through the EuroCC4SEE project, under Grant Agreement No. 101191697. All computer simulations were conducted on the PARADOX supercomputing facility at the Scientific Computing Laboratory of the Institute of Physics Belgrade, University of Belgrade, Serbia.

Competing interests. The authors declare no competing interests.

References

1. Bao, W., Tang, W.: Ground-state solution of Bose–Einstein condensate by directly minimizing the energy functional. J. Comput. Phys. **187**, 230 (2003)
2. Chiofalo, M. L., Succi, S., Tosi, M. P.: Ground state of trapped interacting Bose-Einstein condensates by an explicit imaginary-time algorithm. Phys. Rev. E **62**, 7438 (2000)

3. Lehtovaara, L., Toivanen, J., Eloranta, J.: Solution of time-independent Schrödinger equation by the imaginary time propagation method. J. Comput. Phys. **221**, 148 (2007)
4. Cerimele, M. M., Chiofalo, M. L., Pistella, F.: Numerical solution of the stationary Gross–Pitaevskii equation: tests of a combined imaginary-time-marching technique with splitting. Nonlinear Anal. Theory Methods Appl. **47**, 3345 (2001)
5. Muruganandam, P., Adhikari, S. K.: Fortran programs for the time-dependent Gross-Pitaevskii equation in a fully anisotropic trap. Comput. Phys. Commun. **180**, 1888 (2009)
6. Vudragović, D., Vidanović, I., Balaž, A., Muruganandam, P., Adhikari, S. K.: C Programs for solving the time-dependent Gross-Pitaevskii equation in a fully anisotropic trap. Comput. Phys. Commun. **183**, 2021 (2012)
7. Kumar, R. K., Young-S., Luis E., Vudragović, D., Balaž, A., Muruganandam, P., Adhikari, S. K.: Fortran and C programs for the time-dependent dipolar Gross-Pitaevskii equation in an anisotropic trap. Comput. Phys. Commun. **195**, 117 (2015)
8. Young-S., Luis E., Vudragović, D., Muruganandam, P., Adhikari, S. K., Balaž, A.: OpenMP Fortran and C programs for solving the time-dependent Gross-Pitaevskii equation in an anisotropic trap. Comput. Phys. Commun. **204**, 209 (2016)
9. Young-S., Luis E., Muruganandam, P., Adhikari, S. K., Lončar, V., Vudragović, D., Balaž, A.: OpenMP GNU and Intel Fortran programs for solving the time-dependent Gross-Pitaevskii equation. Comput. Phys. Commun. **220**, 503 (2017)
10. Satarić, B., Slavnić, V., Belić, A., Balaž, A., Muruganandam, P., Adhikari, S. K.: Hybrid OpenMP/MPI programs for solving the time-dependent Gross–Pitaevskii equation in a fully anisotropic trap. Comput. Phys. Commun. **200**, 411 (2016)
11. Lončar, V., Balaž, A., Bogojević, A., Škrbić, S., Muruganandam, P., Adhikari, S. K.: CUDA programs for solving the time-dependent dipolar Gross–Pitaevskii equation in an anisotropic trap. Comput. Phys. Commun. **200**, 406 (2016)
12. Lončar, V., Young-S., Luis E., Škrbić, S., Muruganandam, P., Adhikari, S. K., Balaž, A.: OpenMP, OpenMP/MPI, and CUDA/MPI C programs for solving the time-dependent dipolar Gross–Pitaevskii equation. Comput. Phys. Commun. **209**, 190 (2016)
13. Kumar, R. K., Lončar, V., Muruganandam, P., Adhikari, S. K., Balaž, A.: C and Fortran OpenMP programs for rotating Bose–Einstein condensates. Comput. Phys. Commun. **240**, 74 (2019)
14. Crank, J., Nicolson, P.: A practical method for numerical evaluation of solutions of partial differential equations of the heat-conduction type. P. Adv Comput Math **6**, 207 (1996)
15. Ames, W.: Numerical Methods for Partial Differential Equations 3rd Edition. Academic Press (1992)
16. Dautray, R., Lions, J.-L.: Mathematical Analysis and Numerical Methods for Science and Technology. Springer-Verlag Berlin Heidelberg (2000)
17. Vudragović, D., Balaž, A.: Faraday and Resonant Waves in Dipolar Cigar-Shaped Bose-Einstein Condensates. Symmetry **11**, 1090 (2019)

BOOK OF ABSTRACTS

In Memory of Antun Balaž

Insights into Complex Systems

Belgrade, 11-12 June 2026

Institute of Physics Belgrade

Book of Abstracts

Institute of Physics Belgrade

Editors	**Ivana Vasić, Nenad Vukmirović**
Photo in page 7 by	**Bojan Džodan**
ISBN	**978-86-82441-68-7**
Publisher	**Institute of Physics Belgrade** **Pregrevica 118** **11080 Belgrade, Serbia**
Layout	**Vladimir Stankovski**
Printed by	**GIT, Pančevo**
Number of copies	**50**
Published in	**2026.**

Book of Abstracts

In Memory of Antun Balaž – Insights into Complex Systems

Organizing Committee:

Marija Mitrović Dankulov, Institute of Physics Belgrade, Serbia
Nenad Vukmirović, Institute of Physics Belgrade, Serbia
Dušan Vudragović, Institute of Physics Belgrade, Serbia
Ivana Vasić, Institute of Physics Belgrade, Serbia
Igor Franović, Institute of Physics Belgrade, Serbia
Ana Hudomal, Institute of Physics Belgrade, Serbia

Scientific Committee:

Ivana Vasić, Institute of Physics Belgrade, Serbia
Axel Pelster, Technical University of Kaiserslautern, Germany
Alexandru Nicolin-Żaczek, Institute of Space Science, Romania
Marina Radulaški, University of California Davis, USA
Emanouil Atanassov, Bulgarian Academy of Sciences, Bulgaria

Organized by:

Scientific Computing Laboratory
Center for the Study of Complex Systems
Institute of Physics Belgrade
Pregrevica 118
11080 Belgrade, Serbia

Faraday and resonant waves in dipolar cigar-shaped Bose-Einstein condensates

Dušan Vudragović and Antun Balaž

Scientific Computing Laboratory, Center for the Study of Complex Systems,
Institute of Physics Belgrade, University of Belgrade, Serbia
E-mail: dusan@ipb.ac.rs

Faraday and resonant density waves appear in Bose-Einstein condensates due to the harmonic excitation of the system [1-3]. These nonlinear excitations result from interactions that couple collective oscillation modes and the presence of parametric resonances. Using both variational mean-field and comprehensive numerical methods, we examine density waves in dipolar condensates at zero temperature [1], where anisotropy in the dipole-dipole interaction causes symmetry breaking. We develop variational equations of motion to describe the dynamics of a driven dipolar system and identify the most unstable modes, which correspond to Faraday and resonant waves. Additionally, we derive analytical formulas for the spatial periods of these density waves as functions of contact and dipole-dipole interaction strengths. Finally, we compare these variational results with extensive numerical simulations solving the 3D dipolar Gross-Pitaevskii equation.

I would like to express my sincere gratitude to Antun Balaž for his support, inspiration, and friendship throughout the years. His guidance and influence will always remain an important part of both my scientific and personal life.

References

[1] D. Vudragović and A. Balaž, Symmetry 11, 1090 (2019).
[2] A. Balaž, R. Paun, A. I. Nicolin, et al., Phys. Rev. A 89, 023609 (2014).
[3] A. Balaž and A. I. Nicolin, Phys. Rev. A 85, 023613 (2012).

ARTIFICIAL INTELLIGENCE CONFERENCE

BOOK OF ABSTRACTS

BELGRADE, OCTOBER 9-10, 2025

PROGRAM COMMITTEE

Co-chairs:
Vladan Devedžić, SASA, Belgrade and Faculty of Organizational Sciences, University of Belgrade
Miodrag Mihaljević, SASA, Belgrade and Mathematical Institute, SASA, Belgrade
Dušan Teodorović, SASA. Belgrade

Members:
Aleksandar Kostić, SASA, Belgrade
Angelo Sifaleras, University of Macedonia, Greece
Boško Nikolić, School of Electrical Engineering, University of Belgrade
Basant Agarwal, Central University of Rajasthan, Ajmer, India
Danijela Milošević, Faculty of Technical Sciences in Čačak, University of Kragujevac
Goce Trajčevski, Iowa State University, Ames, USA
Igor Đurović, Montenegro Academy of Sciences and Arts, Podgorica, Montenegro
Jelena Jovanović, Faculty of Organizational Sciences, University of Belgrade
Jesus Medina, University of Cadiz, Cadiz, Spain
Jianxun Cui, Harbin Institute of Technology, Harbin, China
Leonid Stoimenov, Faculty of Electronic Engineering, Univeristy of Niš
Marija Mitrović Dankulov, The Institute of Physics Belgrade
Mart Laanpere, Tallinn University, Tallinn, Estonia
Michael Benedikt, University of Oxford, Oxford, UK
Mirjana Ivanović, Faculty of Sciences, University of Novi Sad
Mirko Dinulović, Faculty of Mechanical Engineering, University of Belgrade
Predrag Janičić, Faculty of Mathematics, Univeristy of Belgrade
Ranka Stanković, Faculty of Mining and Geology, University of Belgrade
Slobodan Vukosavić, Faculty of Electrical Engineering, University of Belgrade and SASA, Belgrade
Sonja Dimitrijević, "Mihajlo Pupin" Institite, Belgrade
Vladimir Srdanović, Mathematical Institute SASA, Belgrade
Weiqin Chen, Oslo Metropolitan University, Oslo, Norway
Zoran Ognjanović, Mathematical Institute SASA, Belgrade

ORGANIZING COMMITTEE

Co-chairs:
Andreja Tepavčević, Mathematical Institute SASA, Belgrade and Faculty of Sciences, University of Novi Sad
Tatjana Davidović, Mathematical Institute SASA, Belgrade

Members:
Ana Anokić, Academy of Technical and Art Applied Studies, Belgrade
Anastazia Žunić, Mathematical Institute SASA, Belgrade
Anđelka Zečević, Mathematical Institute SASA, Belgrade
Biljana Stojanović, Mathematical Institute SASA, Belgrade
Božo Vuković, Mathematical Institute SASA, Belgrade
Dejan Vukelić, Mathematical Institute SASA, Belgrade
Dragan Jočić, Mathematical Institute SASA, Belgrade
Nataša Stević, SASA, Belgrade
Petar Vranić, Mathematical Institute SASA, Belgrade
Slobodan Jelić, Faculty of Civil Engineering, Univeristy of Belgrade
Una Stanković, Mathematical Institute SASA, Belgrade
Vanja Stepanović, Faculty of Agriculture, University of Belgrade

ORGANIZERS
Department of Technical Sciences SASA, Belgrade
Mathematical Institute SASA, Belgrade
Academy Board for Artificial Intelligence, SASA, Belgrade

Large-Scale Simulation of Reddit Communities Using Multi-Agent LLM Systems

Aleksandar Tomašević[1,] Darja Cvetković[2], Sara Major[1], Slobodan Maletić[3], Miroslav Anđelković[3], Ana Vranić[2], Boris Stupovski[2], Dušan Vudragović[2], Aleksandar Bogojević[2], Marija Mitrović Dankulov[2]

[1]Faculty of Philosophy, University of Novi Sad, Novi Sad, Serbia, atomashevic@ff.uns.ac.rs
[2]Institute of Physics Belgrade, University of Belgrade, Belgrade, Serbia
[3]Vinča Institute of Nuclear Sciences, University of Belgrade, Belgrade, Serbia

Large Language Models (LLMs) present unprecedented opportunities for simulating complex online social dynamics at scale. This paper presents a comprehensive multi-agent simulation of Reddit-style technology discussion communities using an adapted version of the Y Social framework (Rossetti et al. 2024), originally designed for Twitter simulations but forked and modified for Reddit-like environments.[7] We specifically target the simulation of r/technology communities because technology topics often contain contentious subjects that are more or less politically polarizing - from Big Tech regulation to AI ethics to Elon Musk's ventures - allowing us to study how politically charged and potentially toxic conversations emerge within communities not explicitly focused on politics. Our simulation encompasses one month of activity with approximately 50,000 posts and comments generated by 7,637 unique LLM agents.

The simulation integrates real-world content through RSS feeds from 33 diverse technology news sources from TechCrunch and Wired to Fox News Technology and CNN Tech. This approach ensures that agent discussions are grounded in authentic current events rather than artificial scenarios. Simulation parameters were calibrated using data drawn from the MADOC dataset (Dankulov et al. 2025), ensuring realistic behavioral patterns and community dynamics. Each agent is powered by the uncensored Dolphin3 LLM (based on Llama 3.1 8B) and possesses detailed psychological profiles including demographic characteristics, political affiliations, Big Five personality traits, education levels, and critically, configurable toxicity propensities ranging from "absolutely no" to "extremely" toxic behavior.

Our methodology employs prompt engineering to enable agents to engage in contextually appropriate behaviors including posting original content, commenting on news articles, participating in threaded discussions, and exhibiting realistic activity patterns across 24-hour cycles. The system successfully generated conversations demonstrating sustained multi-turn interactions characteristic of real online communities. Figure 1 demonstrates key emergent properties: (left) power-law distribution in posting behavior with 7,637 agents showing patterns that mirror empirical observations from actual social media platforms, and (right) k-core network structure revealing the community's hierarchical organization, with high k-core nodes (yellow/green) forming the dense interaction core and lower k-core nodes (blue/purple) positioned at the periphery.

[7] https://github.com/atomashevic/YClient-Reddit

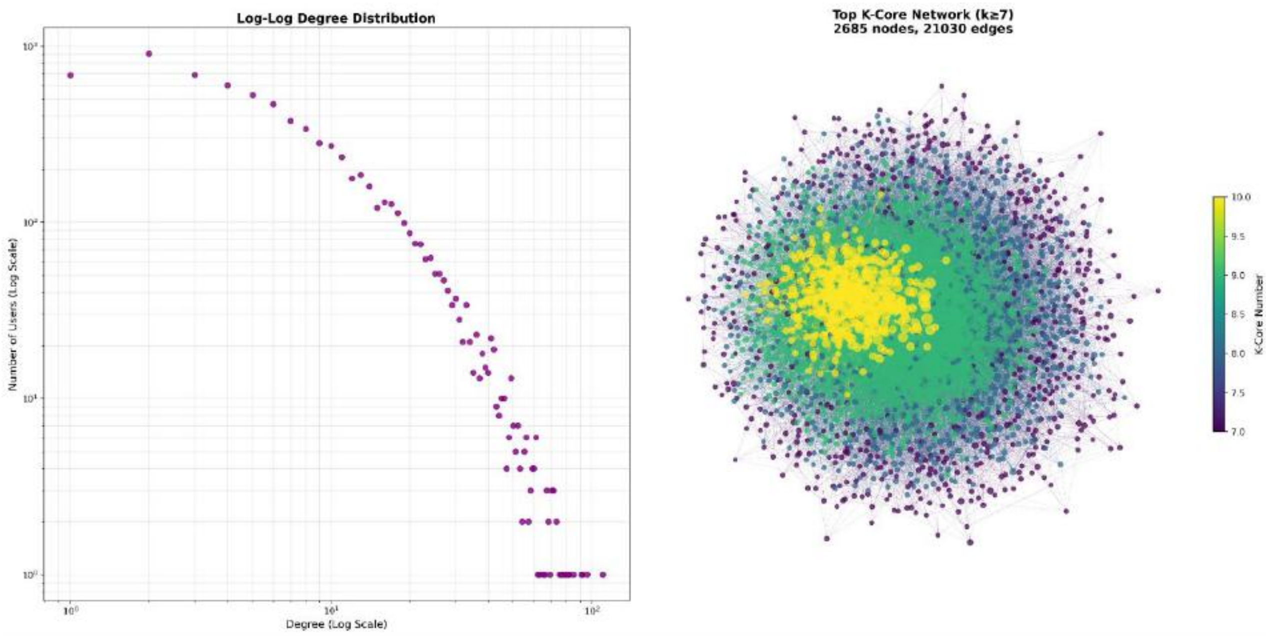

Fig. 1 Left panel: Log-log degree distribution showing power-law posting degree patterns across 7,637 agents. Right panel: Top k-core network visualization displaying emergent hierarchical community structure, where node colors represent k-core values and edges show interaction patterns between high-influence agents.

Toxicity analysis reveals compelling emergent patterns: 10.55% of content exceeded moderate toxicity thresholds (0.5), with 17.97% showing elevated toxicity levels (0.25+), closely matching empirical observations from actual technology forums. We demonstrate fidelity between our simulation and real sample of Reddit r/technology data, with both distributions exhibiting similar right-skewed patterns dominated by low-toxicity content (>80% below 0.2), comparable tail behaviors for moderate-to-high toxicity ranges and similar mean toxicity scores (0.1327 in simulated community vs. 0.1339 in real r/technology sample).

This work advances AI research in several domains: multi-agent systems capable of sustained social simulation, prompt engineering for realistic behavioral modeling, and computational social science methodologies. The framework provides researchers with a controlled environment for studying online community dynamics, testing moderation strategies, and understanding the emergence of toxic discourse patterns without ethical constraints of live platform experimentation. Our results demonstrate that LLM-based agent societies can serve as valuable digital laboratories for investigating complex social phenomena at unprecedented scale and fidelity.

Keywords: Large Language Models, Multi-Agent Systems, Social Simulation, Online Communities

References:

[1] Dankulov, M. M., Tomašević, A., Maletić, S., Anđelković, M., Vranić, A., Cvetković, D., Stupovski, B., Vudragović, D., Major, S., & Bogojević, A. (2025). Multi-Platform Aggregated Dataset of Online Communities (MADOC). In arXiv [cs.SI]. arXiv. http://arxiv.org/abs/2501.12886

[2] Rossetti, G., Stella, M., Cazabet, R., Abramski, K., Cau, E., Citraro, S., Failla, A., Improta, R., Morini, V., & Pansanella, V. (2024). Y Social: an LLM-powered Social Media Digital Twin. In arXiv [cs.AI]. arXiv. http://arxiv.org/abs/2408.00818

Table of Contents:

Innovation Center of Faculty of Mechanical Engineering

Faculty of Mechanical Engineering, University of Belgrade

Center for Business Trainings

„International Conference of Experimental and Numerical Investigations and New Technologies“

Sponsored by:

MINISTRY OF EDUCATION, SCIENCE AND TECHNICAL DEVELOPMENT

OF THE REPUBLIC OF SERBIA

Programme

and

The Book of Abstracts

29 June – 02 July 2021

Zlatibor, Serbia

„International Conference of Experimental and Numerical Investigations and New Technologies“

CNN TECH 2021

29 June – 02 July 2021

Hotel Mona, Miladina Pecinara 26, Zlatibor, Serbia

http://cnntechno.com

Programme

and

The Book of Abstracts

Organised by:

Innovation Center of Faculty of Mechanical Engineering

Faculty of Mechanical Engineering, University of Belgrade

Center for Business Trainings

Sponsored by:

Ministry of Education, Science and Technical development of the Republic of Serbia

Title:	International Conference of Experimental and Numerical Investigations and New Technologies – **CNN TECH 2021** **PROGRAMME AND THE BOOK OF ABSTRACTS**
Publisher:	Innovation Center of Faculty of Mechanical Engineering Kraljice Marije 16, 11120 Belgrade 35 tel: (+381 11) 3302-346, fax 3370364 e-mail: cnntechno@gmail.com web site: http://cnntechno.com, http://www.inovacionicentar.rs
Editors:	Dr Goran Mladenovic, Associate Professor Dr Martina Balac, Senior Scientific Researcher Dr Aleksandra Dragicevic, Scientific Researcher
Technical editor	Dr Goran Mladenovic, Associate Professor
Cover page:	Dr Goran Mladenovic, Associate Professor
Printed in:	Innovation Center of Faculty of Mechanical Engineering Kraljice Marije 16 11120 Belgrade 35 tel: (+381 11) 3302-346
Circulation:	100 copies. The end of printing: June 2021.

ISBN: 978-86-6060-077-8

“International Conference of Experimental and Numerical Investigations and New Technologies”

CNN TECH 2021

SCIENTIFIC COMMITTEE:

Milos Milosevic, Serbia (chairman)
Nenad Mitrovic, Serbia (co-chairman)
Aleksandar Sedmak, Serbia
Hloch Sergej, Slovakia
Drazan Kozak, Croatia
Nenad Gubeljak Slovenia
Monka Peter, Slovakia
Snezana Kirin, Serbia
Samardzic Ivan, Croatia
Martina Balac, Serbia
Mládková Ludmila, Czech Republic
Johanyák Zsolt Csaba, Hungary
Igor Svetel, Serbia
Aleksandra Mitrovic, Serbia
Valentin Birdeanu, Romania
Danilo Nikolic, Montenegro
Goran Mladenovic, Serbia
Bajic Darko, Montenegro
Tasko Manski, Srbija
Luis Reis, Portugal
Zarko Miskovic, Serbia
Tozan Hakan, Turkey
Nikola Momcilovic, Serbia
Traussnigg Udo, Austria
Gordana Bakic, Serbia
Katarina Colic, Serbia
Peter Horňak, Slovakia
Róbert Huňady, Slovakia
Martin Hagara, Slovakia
Jovan Tanaskovic, Serbia
Aleksa Milovanovic, Serbia
Marija Durkovic, Serbia
Tsanka Dikova, Bulgaria
Ján Danko, Slovakia
Ognjen Pekovic, Serbia
Jelena Svorcan, Serbia
Suzana Filipovic, Serbia
Darko Kosanovic, Serbia
Nebojsa Manic, Serbia
Zorana Golubovic, Serbia
Vera Pavlovic, Serbia

ORGANIZING COMMITTEE:

Nenad Mitrovic (chairman)
Milos Milosevic (co-chairman)
Aleksandar Sedmak
Martina Balac
Vesna Miletic
Igor Svetel
Goran Mladenovic
Aleksandra Mitrovic
Aleksandra Dragicevic
Zarko Miskovic
Katarina Colic
Milan Travica
Dragana Perovic
Aleksandra Joksimovic
Beti Kostadinovska Dimitrovska
Tsanka Dikova
Isaak Trajkovic
Toni Ivanov
Snezana Kirin
Igor Stankovic
Ivana Vasovic Maksimovic
Nina Obradovic
Andreja Stojic
Ivana Jevtic

THE POTENTIAL FOR FORECASTING THE PARTICULATE MATTER LEVELS IN COMPLEX URBAN ENVIRONMENT

Mirjana Perisic [1,2], Andreja Stojic[1,2*], Gordana Jovanovic[1,2], Andrej Sostaric[3], Dimitrije Maletic[1], Dusan Vudragovic[1], Svetlana Stanisic[2]

[1]Institute of Physics Belgrade, National Institute of the Republic of Serbia, University of Belgrade, 118 Pregrevica Street, 11000, Belgrade, Serbia

[2]Singidunum University, 32 Danijelova Street, Belgrade, 11000, Serbia

[3]Institute of Public Health Belgrade, 54 Despota Stefana Street, 11000, Belgrade, Serbia

Corresponding author e-mail: andreja.stojic@ipb.ac.rs

Abstract

In this study, we employed regression analysis by means of machine learning eXtreme Gradient Boosting method for estimating the relationships between particulate matter (PM_{10}) concentrations and a number of parameters including benzene, inorganic gaseous pollutants (SO_2, NO, NO_2, NOx), Global Data Assimilation System-modeled (GDAS1) meteorological parameters, as well as daily and weekend PM variations in Belgrade, Serbia. The data was provided by the Institute of Public Health Belgrade, Serbia. The successful and reliable predictions were provided with relative errors in the range from approx. 19% to 26% and correlation coefficients higher than 0.95. The lowest relative error and the highest correlation coefficient were obtained for monitoring station of rural/industrial type located in Ovca, while the highest difference between modeled and measured values were detected at urban-type monitoring stations Novi Beograd and Institute of Public Health Belgrade, both of which are exposed to traffic emissions. The modeling results were not satisfying for rural/industrial monitoring station located in Veliki Crljeni (relative error>30%, corr. coefficient<0,8), which implies that the dynamic of PM_{10} emissions at the selected monitoring site were not governed by the available data on pollutant concentrations and meteorological parameters.

Keywords

Particulate matter, air pollution forecast, machine learning

Acknowledgement

We acknowledge funding provided by the Institute of Physics Belgrade, through the grant by the Ministry of Education, Science, and Technological Development of the Republic of Serbia. This research was supported by the Science Fund of the Republic of Serbia, #GRANT No. 65241005, AI-ATLAS.

Innovation Center of Faculty of Mechanical Engineering

Faculty of Mechanical Engineering, University of Belgrade

Center for Business Trainings

CNN TECH

„International Conference of Experimental and Numerical Investigations and New Technologies“

Sponsored by:

MINISTRY OF EDUCATION, SCIENCE AND TECHNICAL DEVELOPMENT

OF THE REPUBLIC OF SERBIA

Programme

and

The Book of Abstracts

29 June – 02 July 2021

Zlatibor, Serbia

„International Conference of Experimental and Numerical Investigations and New Technologies“

CNN TECH 2021

29 June – 02 July 2021

Hotel Mona, Miladina Pecinara 26, Zlatibor, Serbia

http://cnntechno.com

Programme

and

The Book of Abstracts

Organised by:

Innovation Center of Faculty of Mechanical Engineering

Faculty of Mechanical Engineering, University of Belgrade

Center for Business Trainings

Sponsored by:

Ministry of Education, Science and Technical development of the Republic of Serbia

Title: International Conference of Experimental and Numerical Investigations and New Technologies – **CNN TECH 2021**

PROGRAMME AND THE BOOK OF ABSTRACTS

Publisher: Innovation Center of Faculty of Mechanical Engineering
Kraljice Marije 16, 11120 Belgrade 35
tel: (+381 11) 3302-346, fax 3370364
e-mail: cnntechno@gmail.com
web site: http://cnntechno.com, http://www.inovacionicentar.rs

Editors: Dr Goran Mladenovic, Associate Professor
Dr Martina Balac, Senior Scientific Researcher
Dr Aleksandra Dragicevic, Scientific Researcher

Technical editor Dr Goran Mladenovic, Associate Professor

Cover page: Dr Goran Mladenovic, Associate Professor

Printed in: Innovation Center of Faculty of Mechanical Engineering
Kraljice Marije 16
11120 Belgrade 35
tel: (+381 11) 3302-346

Circulation: 100 copies. The end of printing: June 2021.

ISBN: 978-86-6060-077-8

“International Conference of Experimental and Numerical Investigations and New Technologies”

CNN TECH 2021

SCIENTIFIC COMMITTEE:

Milos Milosevic, Serbia (chairman)
Nenad Mitrovic, Serbia (co-chairman)
Aleksandar Sedmak, Serbia
Hloch Sergej, Slovakia
Drazan Kozak, Croatia
Nenad Gubeljak Slovenia
Monka Peter, Slovakia
Snezana Kirin, Serbia
Samardzic Ivan, Croatia
Martina Balac, Serbia
Mládková Ludmila, Czech Republic
Johanyák Zsolt Csaba, Hungary
Igor Svetel, Serbia
Aleksandra Mitrovic, Serbia
Valentin Birdeanu, Romania
Danilo Nikolic, Montenegro
Goran Mladenovic, Serbia
Bajic Darko, Montenegro
Tasko Manski, Srbija
Luis Reis, Portugal
Zarko Miskovic, Serbia
Tozan Hakan, Turkey
Nikola Momcilovic, Serbia
Traussnigg Udo, Austria
Gordana Bakic, Serbia
Katarina Colic, Serbia
Peter Horňak, Slovakia
Róbert Huňady, Slovakia
Martin Hagara, Slovakia
Jovan Tanaskovic, Serbia
Aleksa Milovanovic, Serbia
Marija Durkovic, Serbia
Tsanka Dikova, Bulgaria
Ján Danko, Slovakia
Ognjen Pekovic, Serbia
Jelena Svorcan, Serbia
Suzana Filipovic, Serbia
Darko Kosanovic, Serbia
Nebojsa Manic, Serbia
Zorana Golubovic, Serbia
Vera Pavlovic, Serbia

ORGANIZING COMMITTEE:

Nenad Mitrovic (chairman)
Milos Milosevic (co-chairman)
Aleksandar Sedmak
Martina Balac
Vesna Miletic
Igor Svetel
Goran Mladenovic
Aleksandra Mitrovic
Aleksandra Dragicevic
Zarko Miskovic
Katarina Colic
Milan Travica
Dragana Perovic
Aleksandra Joksimovic
Beti Kostadinovska Dimitrovska
Tsanka Dikova
Isaak Trajkovic
Toni Ivanov
Snezana Kirin
Igor Stankovic
Ivana Vasovic Maksimovic
Nina Obradovic
Andreja Stojic
Ivana Jevtic

enterprise europe network
Business Support on Your Doorstep

THE IMPACT OF GASEOUS POLLUTANTS ON PARTICULATE MATTER DISTRIBUTION

Svetlana Stanisic[2], Mirjana Perisic[1,2], Andreja Stojic[1,2*], Andrej Sostaric[3], Dusan Vudragovic[1], Dimitrije Maletic[1], Gordana Jovanovic[1,2]

[1]Institute of Physics Belgrade, National Institute of the Republic of Serbia, University of Belgrade, 118 Pregrevica Street, 11000, Belgrade, Serbia

[2]Singidunum University, 32 Danijelova Street, Belgrade, 11000, Serbia

[3]Institute of Public Health Belgrade, 54 Despota Stefana Street, 11000, Belgrade, Serbia

*Corresponding author e-mail: andreja.stojic@ipb.ac.rs

Abstract

In this study, we used eXtreme Gradient Boosting machine learning and SHapley Additive exPlanations (SHAP) explainable artificial intelligence methods to examine the relationships between PM_{10} and other air pollutant concentrations in the urban area of Belgrade. The data was provided by the Institute of Public Health Belgrade, Serbia. As shown, the most significant relative impact of benzene levels (50%) on the increase of PM_{10} concentrations up to several tens of μg m^{-3} was recorded at the occasions when benzene concentrations exceeded 5 μg m^{-3} and the concentrations of NO_2 were low (combustion of fossil fuels). The same effect was less pronounced at higher NO_2 concentrations. Taking into consideration the relative impact of SO_2 on PM_{10} levels and the observed relationship between NO and PM_{10}, four dominant environment types that describe the PM level dynamics were distinguished. In the first-type environment, the decrease of PM_{10} levels noticed for SO_2 levels below 50 μg m^{-3} and the dominance of sources with a significant share of NO (> 120 μg m^{-3}) were attributed to traffic emissions. The ambiance recognized as type 2 with no effect on PM levels is characterized by low gaseous oxide concentrations. The third and the fourth type of environment are characterized by SO_2 values exceeding 50 μg m^{-3} and their significant impact on the increase of PM_{10} concentrations.

Keywords

particulate matter, inorganic gaseous pollutants, explainable artificial intelligence

Acknowledgement

We acknowledge funding provided by the Institute of Physics Belgrade, through the grant by the Ministry of Education, Science, and Technological Development of the Republic of Serbia. This research was supported by the Science Fund of the Republic of Serbia, #GRANT No. 65241005, AI-ATLAS.

Innovation Center of Faculty of Mechanical Engineering

Faculty of Mechanical Engineering, University of Belgrade

Center for Business Trainings

CNN TECH

„International Conference of Experimental and Numerical Investigations and New Technologies“

Sponsored by:

MINISTRY OF EDUCATION, SCIENCE AND TECHNICAL DEVELOPMENT

OF THE REPUBLIC OF SERBIA

Programme

and

The Book of Abstracts

29 June – 02 July 2021

Zlatibor, Serbia

„International Conference of Experimental and Numerical Investigations and New Technologies“

CNN TECH 2021

29 June – 02 July 2021

Hotel Mona, Miladina Pecinara 26, Zlatibor, Serbia

http://cnntechno.com

Programme

and

The Book of Abstracts

Organised by:

Innovation Center of Faculty of Mechanical Engineering

Faculty of Mechanical Engineering, University of Belgrade

Center for Business Trainings

Sponsored by:

Ministry of Education, Science and Technical development of the Republic of Serbia

Title:	International Conference of Experimental and Numerical Investigations and New Technologies – **CNN TECH 2021** **PROGRAMME AND THE BOOK OF ABSTRACTS**
Publisher:	Innovation Center of Faculty of Mechanical Engineering Kraljice Marije 16, 11120 Belgrade 35 tel: (+381 11) 3302-346, fax 3370364 e-mail: cnntechno@gmail.com web site: http://cnntechno.com, http://www.inovacionicentar.rs
Editors:	Dr Goran Mladenovic, Associate Professor Dr Martina Balac, Senior Scientific Researcher Dr Aleksandra Dragicevic, Scientific Researcher
Technical editor	Dr Goran Mladenovic, Associate Professor
Cover page:	Dr Goran Mladenovic, Associate Professor
Printed in:	Innovation Center of Faculty of Mechanical Engineering Kraljice Marije 16 11120 Belgrade 35 tel: (+381 11) 3302-346
Circulation:	100 copies. The end of printing: June 2021.

ISBN: 978-86-6060-077-8

“International Conference of Experimental and Numerical Investigations and New Technologies”

CNN TECH 2021

SCIENTIFIC COMMITTEE:

Milos Milosevic, Serbia (chairman)
Nenad Mitrovic, Serbia (co-chairman)
Aleksandar Sedmak, Serbia
Hloch Sergej, Slovakia
Drazan Kozak, Croatia
Nenad Gubeljak Slovenia
Monka Peter, Slovakia
Snezana Kirin, Serbia
Samardzic Ivan, Croatia
Martina Balac, Serbia
Mládková Ludmila, Czech Republic
Johanyák Zsolt Csaba, Hungary
Igor Svetel, Serbia
Aleksandra Mitrovic, Serbia
Valentin Birdeanu, Romania
Danilo Nikolic, Montenegro
Goran Mladenovic, Serbia
Bajic Darko, Montenegro
Tasko Manski, Srbija
Luis Reis, Portugal
Zarko Miskovic, Serbia
Tozan Hakan, Turkey
Nikola Momcilovic, Serbia
Traussnigg Udo, Austria
Gordana Bakic, Serbia
Katarina Colic, Serbia
Peter Horňak, Slovakia
Róbert Huňady, Slovakia
Martin Hagara, Slovakia
Jovan Tanaskovic, Serbia
Aleksa Milovanovic, Serbia
Marija Durkovic, Serbia
Tsanka Dikova, Bulgaria
Ján Danko, Slovakia
Ognjen Pekovic, Serbia
Jelena Svorcan, Serbia
Suzana Filipovic, Serbia
Darko Kosanovic, Serbia
Nebojsa Manic, Serbia
Zorana Golubovic, Serbia
Vera Pavlovic, Serbia

ORGANIZING COMMITTEE:

Nenad Mitrovic (chairman)
Milos Milosevic (co-chairman)
Aleksandar Sedmak
Martina Balac
Vesna Miletic
Igor Svetel
Goran Mladenovic
Aleksandra Mitrovic
Aleksandra Dragicevic
Zarko Miskovic
Katarina Colic
Milan Travica
Dragana Perovic
Aleksandra Joksimovic
Beti Kostadinovska Dimitrovska
Tsanka Dikova
Isaak Trajkovic
Toni Ivanov
Snezana Kirin
Igor Stankovic
Ivana Vasovic Maksimovic
Nina Obradovic
Andreja Stojic
Ivana Jevtic

SPATIO-TEMPORAL ANALYSIS OF MOBILITY PATTERNS IN THE CITY OF BELGRADE

Nikola Stupar[1], Ana Vranic[1], Andreja Stojic[1,2], Gordana Vukovic[1,2], Dusan Vudragovic[1], Dimitrije Maletic[1], Marija Mitrovic Dankulov[1*]

[1] Institute of Physics Belgrade, University of Belgrade, Pregrevica 118, 11080 Belgrade, Serbia

[2]Singidunum University, 32 Danijelova Street, Belgrade, 11000, Serbia

Corresponding author e-mail: mitrovic@ipb.ac.rs

Abstract

Information about human mobility is essential for sustainable development planning. It is crucial for urban and transportation planning and the role of mobility in reducing contributions of human activities in air pollution and fighting climate change. While *human* mobility patterns are typically stable over space and time, they can dramatically change due to critical events, such as earthquakes and epidemics. We still lack a detailed description and understanding of how these critical events influence mobility patterns. In this work, we combine artificial intelligence tools with tools and methods from complex network theory to study human mobility patterns in the City of Belgrade during the COVID-19. We use data about mobility in the City of Belgrade between May 2020 and January 2021 from the Facebook Data for Good dataset. The City of Belgrade is divided into 201 cells with information on the mobility before and during the crises within and between the cells. The time resolution of the data is 8 hours. We use the k-mean clustering technique to cluster the data and find five clusters with different average mobility patterns. All mobility time series have trends and cycles, but they differ between clusters. While residential and suburban area clusters have the peaks of activity during the working days, clusters including central municipalities have the peak of activity during Saturday afternoon. Our results show that different city areas react differently to COVID19 information and that this aspect has to be considered in air pollution and crisis management planning.

Keywords

mobility patterns, time series analysis, k-means clustering

Acknowledgement

We acknowledge funding provided by the Institute of Physics Belgrade, through the grant by the Ministry of Education, Science, and Technological Development of the Republic of Serbia. This research was supported by the Science Fund of the Republic of Serbia, #GRANT No. 65241005, AI-ATLAS. Numerical simulations were run on the PARADOX-IV supercomputing facility at the Scientific Computing Laboratory, National Center of Excellence for the Study of Complex Systems, Institute of Physics Belgrade.

Exploring Quantum Many-Body Physics with Ultracold Atoms and Molecules

735. WE-Heraeus-Seminar

14 Dec - 18 Dec 2020
at the Physikzentrum Bad Honnef/Germany

WILHELM UND ELSE
HERAEUS-STIFTUNG

Faraday and Resonant Waves in Dipolar Cigar-Shaped Bose-Einstein Condensates

D. Vudragović and A. Balaž

Institute of Physics Belgrade, University of Belgrade, Serbia

Faraday and resonant density waves emerge in Bose-Einstein condensates as a result of harmonic driving of the system [1-3]. They represent nonlinear excitations and are generated due to the interaction-induced coupling of collective oscillation modes and the existence of parametric resonances. Using a mean-field variational and a full numerical approach, we study density waves in dipolar condensates at zero temperature [1], where breaking of the symmetry due to anisotropy of the dipole-dipole interaction (DDI) plays an important role. We derive variational equations of motion for the dynamics of a driven dipolar system and identify the most unstable modes that correspond to the Faraday and resonant waves. Based on this, we also derive the analytical expressions for spatial periods of both types of density waves as functions of the contact and the DDI strength. Finally, we compare the obtained variational results with the results of extensive numerical simulations that solve the dipolar Gross-Pitaevskii equation in 3D.

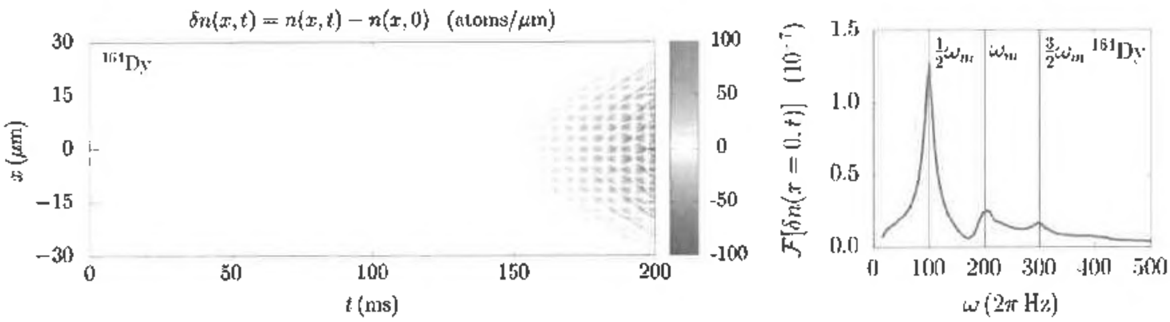

References

[1] D. Vudragović and A. Balaž, Symmetry **11**, 1090 (2019).
[2] A. Balaž, R. Paun, A. I. Nicolin, et al., Phys. Rev. A **89**, 023609 (2014).
[3] A. Balaž and A. I. Nicolin, Phys. Rev. A **85**, 023613 (2012).